STARS

Electronic Theses and Dissertations, 2004-2019

2011

Super-adiabatic Combustion In Porous Media With Catalytic Enhancement For Thermoelectric Power Conversion

Kyle Thomas Mueller
University of Central Florida

STARS Citation

SUPER-ADIABATIC COMBUSTION IN
POROUS MEDIA WITH CATALYTIC ENHANCEMENT
FOR THERMOELECTRIC POWER CONVERSION

by

KYLE THOMAS MUELLER
B.S. Georgia Institute of Technology, 2008

A thesis submitted in partial fulfillment of the requirements
for the degree of Master of Science
in the Department of Mechanical, Materials and Aerospace Engineering
in the College of Engineering and Computer Science
at the University of Central Florida
Orlando, Florida

Fall Term
2011

ABSTRACT

The combustion of ultra-lean fuel to air mixtures provides an efficient way to convert the chemical energy of hydrocarbons into useful power. Conventional burning techniques of a mixture have defined flammability limits beyond which a flame cannot self-propagate due to heat losses. Matrix stabilized porous medium combustion is an advanced technique in which a solid porous matrix within the combustion chamber accumulates heat from the hot gaseous products and preheats incoming reactants. This heat recirculation extends the standard flammability limits and allows the burning of ultra-lean fuel mixtures, conserving energy resources, or the burning of gases of low calorific value, utilizing otherwise wasted resources. The heat generated by the porous burner can be harvested with thermoelectric devices for a reliable method of generating electricity for portable electronic devices by the burning of otherwise noncombustible mixtures.

The design of the porous media burner, its assembly and testing are presented. Highly porous (~80% porosity) alumina foam was used as the central media and alumina honeycomb structure was used as an inlet for fuel and an outlet for products of the methane-air combustion. The upstream and downstream honeycomb structures were designed with pore sizes smaller than the flame quenching distance, preventing the flame from propagating outside of the central section. Experimental results include measurements from thermocouples distributed throughout the burner and on each side of the thermoelectric module along with associated current, voltage and power outputs. Measurements of the burner with catalytic coating were obtained for stoichiometric and lean mixtures and compared to the results obtained from the catalytically inert matrix, showing the effect on overall efficiency for the combustion of fuel-lean mixtures.

ACKNOWLEDGMENTS

TABLE OF CONTENTS

LIST OF FIGURES

LIST OF TABLES

CHAPTER ONE: INTRODUCTION

Matrix stabilized porous burner technology is an advanced combustion method in which a mixture of fuel and oxidizer is burned within a solid porous medium providing favorable conditions for the combustion of lean mixtures. The solid porous medium provides a method of enthalpy recirculation where the high temperature combustion products in the post flame zone heat the upstream porous solid which, in turn, preheats the incoming reactants [1,2,3,4]. The process results in a flame temperature higher than the equilibrium adiabatic value achievable by the fuel mixture; this process is called super-adiabatic combustion [5,6,7,8,9]. A porous medium with a very large surface area to volume ratio increases contact of the solid and gas, thus maximizing the heat transfer between phases [7,10,11]. A high thermal conductivity and high thermal capacity of the solid medium material facilitate the recirculation heat transfer mechanism through the solid matrix which does not exist in a typical gas burner. The heat transfer is further enhanced by the dispersion of the reactants flowing through the porous medium and the mixing due to turbulence generated by the presence of the solid medium [1,7,12]. Figure 1 shows a schematic presentation of a three section porous burner.
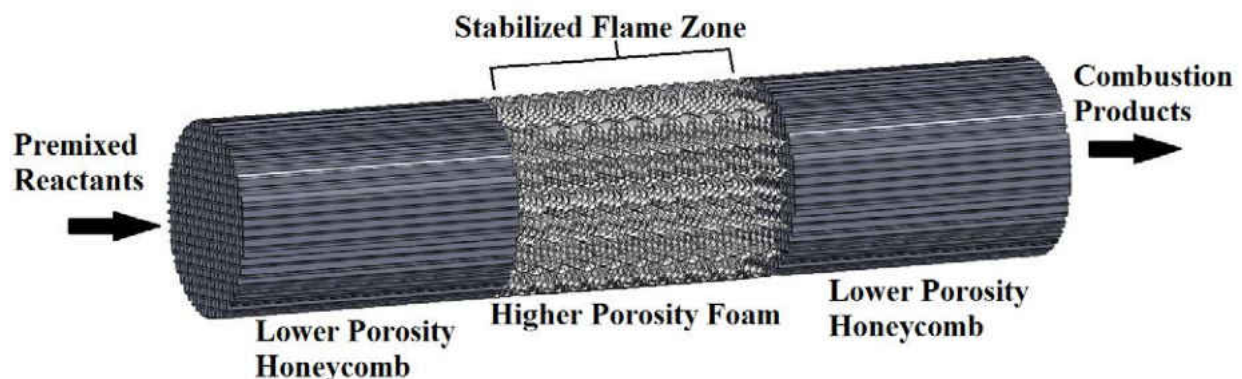
Figure 1. Schematic of a three section porous medium burner

The flame is stabilized and localized within the central high porosity section in between two lower porosity sections that serve to quench the flame if it propagates too far upstream or downstream. It is a very safe technology because the mixture is so lean that it cannot burn outside the porous medium. Among possible practical applications of porous burner technology are power generation [4,13,14,15], small scale heating purposes [16] and the utilization of gases of low calorific value, byproduct or landfill seepage gases [7,17].

Special consideration must be made to the configuration, design and material selection for the solid medium within the porous burner in order to maximize the heat transfer capabilities and avoid degradation. The porous medium should have good thermal mechanical strength and thermal shock resistance to endure creep and thermal cycling during ignition and combustion. Good heat transfer properties of the solid medium allows the burning of very lean mixtures and helps maintain a low maximum flame temperature, which helps to reduce NO_x formation, and helps keep a homogeneous temperature field over the length of the combustion zone, allowing time for CO oxidation [10,18,19,20]. The porous matrix in the burner can be catalytically inert, such as alumina, quartz or zirconia, and may be coated with a catalytically active material to help facilitate the combustion process [5,21,22]. The left hand photo in Figure 2 is a three section burner configuration with a central ceramic foam section and two outer low porosity ceramic honeycomb sections resting in a metallic casing. The right hand photo in Figure 2 is an end view of one of the honeycomb outer sections. The heat generated by the burner may be harvested to provide a source of power; one such method is by the use of thermoelectric devices.
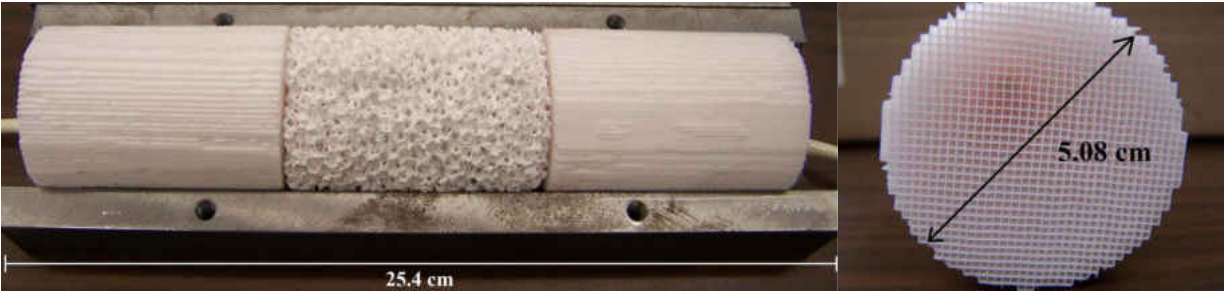
Figure 2. Three section burner configuration and honeycomb end view

Thermoelectrics operate by utilizing the Seebeck effect: a temperature gradient across two joined conducting materials will create a voltage [23]. In order to further increase the voltage and power output, the temperature gradient may be increased by increasing the hot-side temperature or decreasing the cool-side temperature across the device. Therefore, for a porous burner utilizing thermoelectric devices, the power generated can be maximized by cooling the cool-side of the device to reach the desired temperature gradient by either passive means like a heat-sink or active means like a fan or impinging jet. It is standard to connect multiple thermoelectric devices together in series to increase the voltage and power outputs although most commercially available thermoelectric devices already incorporate multiple individual thermoelectric elements [23]. A schematic of a typical commercially available thermoelectric device is provided as Figure 3, incorporating many small individual elements in series. The current burner prototype design uses an impinging jet of air to cool the cool-side of the thermoelectric device while a thin quartz plate may be placed in-between the exterior of the metallic burner casing and the hot-side of the thermoelectric module to optimize the maximum hot-side temperature to the specifications of the module and to prevent it from overheating. The use of a porous medium burner coupled with thermoelectrics has the potential to provide a reliable source of power.

3
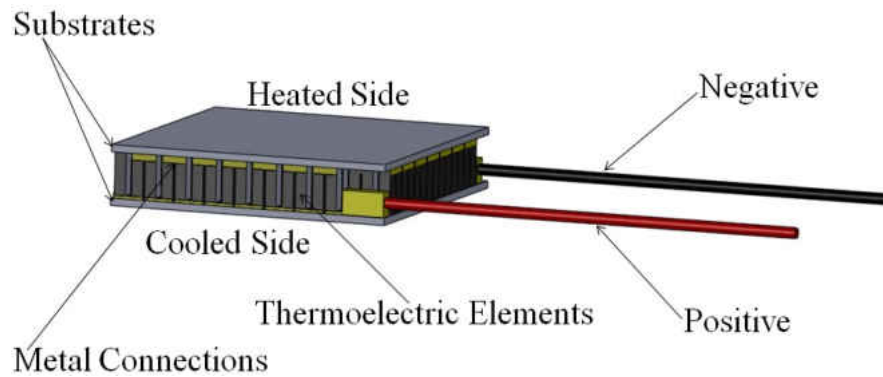
Figure 3. Diagram of a typical thermoelectric module

There have been interests in the development of new power systems for portable devices as use of these devices has been increasing significantly [24]. Hydrocarbon fuels have an exceptionally high power density over current portable power systems. Porous burner technology has a clear advantage over typical gas burners to burn these hydrocarbon fuels since the recirculation heat transfer enables leaner mixtures and low calorific value gases to be burned [1,6,25,26]. Other innovative aspects of a porous burner system over a traditional burner are an improved heat accumulation and transfer characteristics resulting in a thicker flame zone and therefore more complete and stable combustion, especially at lower temperatures [27]. A porous media burner offers lower emissions and a higher power density, up to 40 MW/m^3, with a larger dynamic power range, space utilization and wider range of inlet velocities due to a more homogeneous temperature field and superior heat feedback mechanism [10,27,28]. There is a very good potential for the powering of portable and handheld devices with a porous burner system coupled with thermoelectric modules. The use of catalysts in the porous burner is expected to improve this potential, not only by allowing the burning of leaner mixtures, but also by allowing the device to be run at lower inlet flow velocities. These two factors will extend the amount of time a porous medium burner can power a portable device with a given amount of hydrocarbon fuel.

4

CHAPTER TWO: LITERATURE REVIEW

The combustion of lean fuel and air mixtures provides an efficient way to convert the chemical energy of hydrocarbon fuels into heat. Conventional burning of a mixture has defined flammability limits beyond which a flame cannot self-propagate due to heat losses. The ability of a fuel and air mixture to maintain a self-sustained combustion reaction is largely dependent on its temperature, pressure and the heat of combustion value of the fuel. It was proposed by Weinberg and Lloyd in the 1970's that a method of heat recirculation could be used to pre-heat the incoming reactant mixture and extend the traditional flammability limits [8,9]. One common method of heat recirculation before this was simply mixing some of the hot products in with the reactant flow, increasing the inlet enthalpy but diluting the reactant mixture. Weinberg and Lloyd proposed a burner with intertwined reactant and product flows such that heat transfer could flow through the duct walls, avoiding the dilution of the reactants [8,9]. This heat recirculation method could be used to control the combustion temperature of a mixture with less dependence on the actual fuel to air ratio of the reactant flow. Weinberg and Lloyd developed a spiral burner that was able to combust a mixture at one third the normal lean flammability limit [8,9].

Hardesty in 1974 theorized that heat recirculation could be used to increase the combustion temperature in the reaction zone of a burner without producing a high final temperature [25]. Heat recirculation could be used to burn mixtures of low calorific value, below the lean flammability limit; the recirculated heat would be used to raise the temperature of lean mixtures to the point of ignition while still maintaining a relatively low peak temperature due to the low heat content of the mixture. Controlling the amount of heat recirculation effectively eliminates the dependency the flame temperature has on initial mixture stoichiometry [8,9,25]. A burner

with a counter current heat exchanger and a spiral design for the inlet and outlets with heat transport through the walls from the hot products to the reactants similar to the design used by Weinberg are both shown in Figure 4.
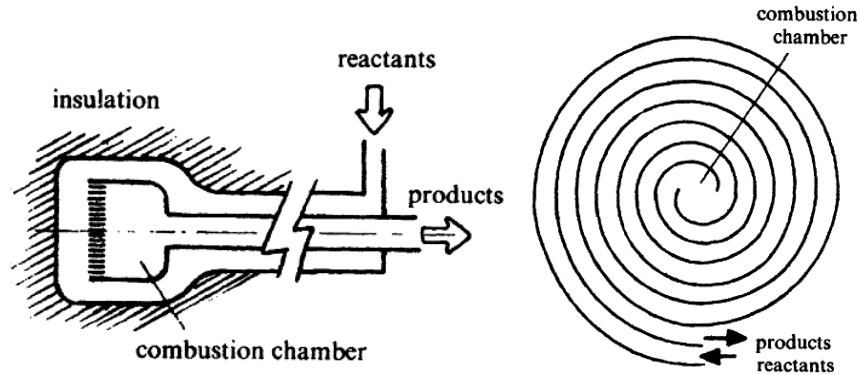
Figure 4. Counter current heat exchanger and double spiral burner [26]

Alternative to these burner configurations, another method of heat recirculation could be realized by use of a solid porous medium within the combustion chamber. This would involve two phases being present within the combustion chamber, the gaseous fuel and air mixture and the solid porous medium [17]. The advantage of this is that the porous medium, being continuously present in the combustion chamber and having a much higher thermal capacity than the gas, would absorb the heat generated by the combustion process and preheat the incoming reactant flow much more efficiently than a free flame [9]. The adiabatic flame temperature of a mixture is defined as the maximum flame temperature in an ideal scenario if all of the heat released during combustion were used to heat the product composition with no losses. A combustion process utilizing a heat recirculation method could burn mixtures at super-adiabatic conditions.

Porous media combustion has two main scenarios, surface and matrix stabilized combustion, primarily defined by the flame location in each case. With surface stabilized combustion, a flame

6

sheet is developed on the surface of a solid porous body by many small individual laminar premixed flames [29]. With matrix stabilized combustion, the combustion process takes place within the solid porous media. The two phase interaction of matrix stabilized combustion is similar to surface stabilized combustion within porous media except that it takes place within the three dimensional volume of the porous matrix rather than the two dimensional surface on the porous matrix, reducing the overall volume required for the combustion process, increasing the energy density of the burner [29]. In matrix stabilized combustion, a low porosity inlet section is used to transfer heat from the combustion chamber to the reactants and to prevent upstream ignition [29]. The low porosity inlet section has a pore diameter less than the flame quenching diameter at the operating conditions which prevents flashback from occurring, where the flame speed is higher than the mixture velocity and the flame propagates upstream [29].
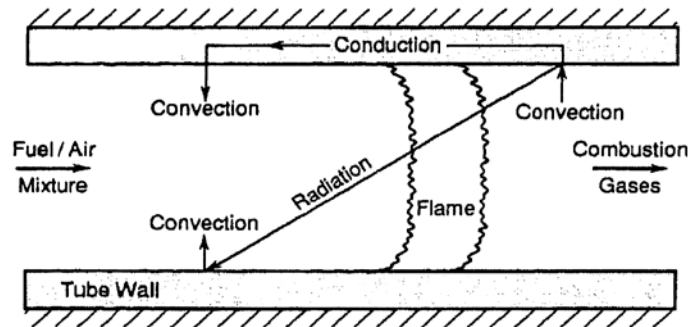
Figure 5. Illustration of the heat transport modes present within a porous medium [26]

The heat transport modes present within the porous medium are depicted in Figure 5. In matrix stabilized porous media combustion a combustion chamber normally consists of an upstream low porosity solid section and a downstream high porosity section. A fuel and air mixture enters the combustion chamber, usually premixed, and encounters the low porosity section upstream of the combustion zone. The solid structure is hotter than the reactant mixture since it accumulates heat from the central porous media within the combustion zone by

conduction and radiation. The reactant mixture is effectively preheated by the solid by convection before reaching the combustion zone. The mixture will reach ignition temperature in the combustion zone which is stabilized within the higher porosity solid media section. The combustion reaction will reach a higher temperature than the porous media downstream of the reaction and will heat that porous media by convection which then heats the upstream solid media by conduction and radiation, completing the heat recirculation cycle.

Porous medium combustion has a few notable advantages to traditional free flame combustion. The main benefit over a free flame system is a more efficient method of heat transfer from products to reactants [30]. The conduction and radiative modes of heat transfer are more significant in porous media combustion since the solid media has much better radiative properties than the gaseous phase and the convection heat transfer is improved due to an increased contact surface area with the solid media [29]. The large inner surface of the porous medium results in high heat transport between the gas phase and the porous medium, providing efficient heat recirculation [29]. The larger heat transport properties of the solid porous medium result in higher sustainable combustion speeds such that burner and heat exchanger can be about 10 times smaller in volume than conventional burner heat exchanger units for comparable thermal loads, increasing power density [29, 31]. The solid media absorbs a significant amount of heat and transports it effectively resulting in a lower peak combustion temperature and more uniform temperature field keeping NO_x and CO formation low; $C_{NOx} < 25$mg/kWh, $C_{CO} < 7$ mg/kWh for some experimental burners and stable combustion for equivalence ratios of 0.53-0.591 for CH_4 and air mixtures or as low as 0.22 for C_3H_8 in some cases [29,31]. The equivalence ratio of a combustible mixture is defined in Equation 1where n is the number of moles of the air or oxidizer and "st" is at stoichiometric ratio.

8

$$\phi = \frac{\binom{n_{air}/n_{oxidizer}}{}}{\binom{n_{air}/n_{oxidizer}}{st}} \qquad (1)$$

The high heat capacity of the porous medium ensures high combustion process stability against changes in thermal load and equivalence ratio making a porous media burner a much more stable environment for combustion than a conventional burner [29]. Porous burners therefore have wider stability limits and can operate over an extended range of firing rates when compared to conventional burners, especially at lean operation [32]. Overall, porous media burners may have higher power densities, offer higher efficiencies over a larger power dynamic range and have lower harmful emissions while minimizing heat losses [29,30].

Materials and Geometry

Overall performance of a porous media burner is governed by both the material and geometric selection [30]. Different possible geometrical configurations which can be used in the combustion chamber include a packed bed of material, open-cell ceramic foams, fiber mats, ported metals or ceramics, metal-alloy wire mesh, or lamellas [33]. Each of these configurations has a similar goal, couple a large thermal capacity with a large surface area per volume to provide maximum heat retention within the burner for recirculation. The geometrical configuration should provide good contact, conduction and convective heat transport [28]. The material chosen must be resistant to high temperatures up to 1600 °C depending on fuel type and concentration and be resistant to the oxidative or reductive atmosphere within a combustion chamber in order to be used dependably. The thermal expansion coefficient of the porous material should be low due to the large temperature gradients that exist within the burner during the heating-up and cooling-down processes. The heat transport properties of the porous materials should be well known so that high heat transports in the combustion region can be achieved and

9

optimized for a particular application. High heat transport properties of the porous media in the combustion region reduce the peak combustion temperature and yield a homogeneous temperature field, reducing pollutant emissions. High heat transport in the radial direction is advantageous to maintain a low combustion temperature while high transport in the axial direction allows for higher combustion velocities by more effectively preheating the incoming flow, allowing a reduction in burner size and increasing power density [28].
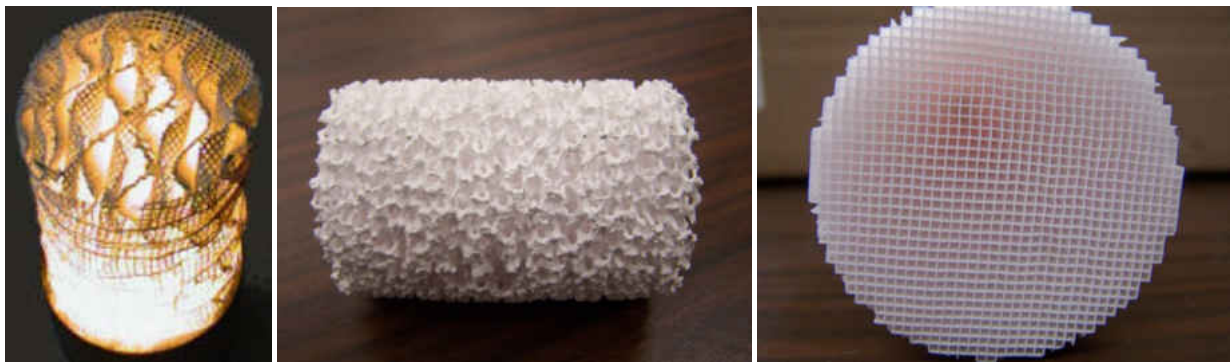
Figure 6. Lamella, reticulated foam and honeycomb structures [26]

Possible designs for the solid porous media include a reticulated foam, packed bed of material, thin wire mesh, foil or even an ordered structure such as a honeycomb [34,35,36]. Photos of a lamella, ceramic reticulated foam and honeycomb structure are shown in Figure 6. Ceramic foams have fair conduction heat transport, a long start-up time, low radiation heat transport properties, intermediate dispersion properties and a relatively high pressure drop [30]. In comparison with other porous media, foams exhibit much better convective heat transfer between solid and gas due to the large internal contact surface area. Foams are also easily manufacturable in a variety of complex shapes. Due to their rigid structure, foams allow the burner to be more flexible to the angles at which it can be operated whereas a packed bed may shift due to movement of the burner which is important if the burner is to be portable [26]. Foam

structures have a high porosity (70-90%) and may have a high optical thickness. The conductive heat transport is also good for foams due to a continuous solid structure, as opposed to packed beds where conduction is hindered between individual elements.

Wire meshes and foils have poor dispersion properties due to their high porosity and may be problematic considering thermal degradation at higher temperatures [26,30,37]. Wire meshes, however, allow for greater radiative heat transfer and due to a minimal amount of solid material, have a shorter start-up time of the burner but therefore may have poor conduction heat transport. Wire meshes and mixer-like structures have a small pressure drop and good start-up behavior due to their typical high [30].

Packed beds may be of elements such as saddles, Raschig rings and spheres. Images of the different types of packed bed geometries are presented in Figure 7 [38,39,40]. Each type can have a different porosity depending on size and shape, between 30-50% for spheres and up to 90% for saddles or Raschig rings. Packed beds may have somewhat worse heat transfer characteristics in comparison with foams due to inferior contact thermal conductivity between individual elements [1,14,35]. Packed beds of spheres may a low optical thickness, reducing radiative transport. A packed bed of material therefore makes a good geometrical configuration for use in the upstream region where the aforementioned are desired characteristics [28].

Figure 7. Packed bed geometries: saddles, Raschig rings and spheres [38,39,40]

Ceramic and metallic materials are both suitable materials, each with their own advantages. Ceramics may have high thermal conductivity and emissivity which are desired properties in the downstream section [28]. Aluminum oxide is relatively cheap, has moderate thermal conductivity and a high application temperature [28]. Aluminum oxide can be used up to about 1700 °C in air but exhibits a high thermal expansion coefficient [10]. Silicon oxide has a very high thermal conductivity, a high application temperature, lower thermal expansion, a high emissivity and excellent thermal shock behavior [28]. Silicon carbide oxidizes to SiO_2 at around 600 °C which is inert and thermally resistive with operational temperatures up to 1750 °C.

Table 1. Physical properties of different material selections [41]

Material	Specification	Mean linear thermal coefficient		Thermal conductivity	Melting point	Application temperature
		30-100 °C $10^{-6}K^{-1}$	30-600 °C $10^{-6}K^{-1}$	$Wm^{-1}K^{-1}$	°C	°C
PSZ	partly stabilized zirconoxide		9-13	1.2-3	2700	900-2400
ATI	aluminiumtitanat		5.0	1.5-3		900-1600
	cordierite, $(Mg,Fe)_2Al_4Si_5O_{18}$		1.7	3		1371
Al_2O_3	aluminiumoxide 80%	5-7	6-8	10-16		1400-1500
Al_2O_3	aluminiumoxide 86%	5.5-7.5	6-8	14-24	2050	1400-1500
Al_2O_3	aluminiumoxide 95%	5-7	6-8	16-28		1400-1500
Al_2O_3	aluminiumoxide >99%	5-7	7-8.2	19-30		1400-1700
SSN	sintered siliconntrid		2.5-3.5	15-45		1750
RBSN	reaction bound siliconnitrid		2.1-3	4-15		1100
HPSN	hot forced siliciumnitrid		3.0-3.4	15-40		1400
AIN	aluminiumnitrid	2.5-4	4.5-5	100-180		1750
SSIC	pressureless sintered siliconcarbid		4-4.8	40-120	2800[1]	1400-1750
SISIC	silicon infiltrated siliconcarbid		4.3-4.8	110-160		1380
HPSIC	hot forced siliconcarbid		3.9-4.8	80-145		1700
RSIC	recrystallized siliconcarbid	4.2	4.8	20		1600
NSIC	nitridbound siliconcarbid	4.2	4.8	14-15		1450
PS 1	iron-chromium-aluminium-alloy			13	1500	1400

1) Dissociation starts at temperatures over 2000 ˚C

Stabilized zirconium oxide has a very high application temperature, up to 2400 °C, a good thermal shock behavior, high thermal expansion but a poor thermal conductivity [28]. Most

metals cannot be used at as high temperatures but have good thermal shock resistance, mechanical strength and good conductive heat transport [30]. Metallic materials such as nickel-based and FeCrAl-alloys have an upper thermal stability limit of about 1400 °C and with high thermal capacity but lose stability at higher operational temperatures [10]. A comparison of different materials and their properties is presented in Table 1 [41].

Most of the proposed materials and geometries have been investigated and tested experimentally along with a number of studies that have focused solely on optimizing material properties and burner configurations for a particular application. Howell et. al. performed a survey on different porous media materials used in other experimental investigations. They focused on the difficulty of modeling the overall material properties of each porous media configuration. Each geometrical configuration has a complicated flow characterization and when coupled with each material's unique properties, it makes computer modeling difficult but essential to choosing an optimal configuration for any particular application. They were able to reliably predict maximum flame speeds, minimum equivalence ratio, trends of flame speed versus pore diameter and equivalence ratio and emission concentrations of CO, CO_2 and NO for different geometries [37]. Pickenäcker et. al. in 1999 surveyed and highlighted the use of different geometrical configurations including ceramic foams, lamella structures and static mixers within a burner versus the typically used packed bed of material. Their survey mostly focused on what geometries, currently being manufactured for other uses, were applicable and the individual benefits of each geometrical configuration, particularly for SiC. Since the ceramic foam is a continuous solid it exhibits very good heat transfer properties especially compared to a packed bed of spheres which has poor heat conduction between individual elements and has an open-pore structures which keep pressure losses low [10]. Babkin et. al. in 1980 and 1985 used a

packed bed and thermally reticulated polyurethane foam with a cell size of 3.8-4 mm and porosity of 97-98% to examine the basic properties of the combustion process and associated pressure increase within the combustion vessel. They concentrated mainly on the difference between low and high porosity media and determined that the rate of combustion was dependent not only on the temperature and pressure, but by the effect of the porous medium in creating a turbulent flow field [42,43].

Fu et. al. in 1998 conducted a review of conduction heat transfer literature on porous materials and developed an applicable theoretical model. Their purpose was to model different configurations of porous media to try to accurately predict the heat transfer characteristics. Their models confirmed that the thermal conductivity of the porous solid decreased with porosity and were reasonably predictive of experimental results for each configuration [44]. Barra et. al. in 2003 performed a computational and parametric study on the flame stabilization in a two section porous burner by varying the properties of each porous section. Their model showed that there was a much larger preheat zone for the porous matrix combustion versus a free flame. The peak flame temperature for the methane and air mixture was 50 K higher in the porous matrix, which was expected. As they varied the porous medium properties they concluded that the matrix properties significantly affected the stability range. They determined that the upstream section should have low thermal conductivity, a low volumetric heat transfer, and a high radiative extinction coefficient and that the downstream section should have a high thermal conductivity, high volumetric heat transfer, and an intermediate radiative extinction coefficient [45]. Tierney and Harris in 2009 began a study on a variety of materials and geometries used in a porous burner for ultra-lean combustion with a particular interest in minimizing greenhouse gas emissions. The materials to be used include alumina, zirconia, silicon-carbide, among other

ceramics and metals. They identified alumina as a good material for the upstream section due to its limited thermal transport properties and silicon carbide as a good combustion zone material due to its good heat transport and thermal shock performance. Preliminary testing of the base case of the study with a packed bed of alumino-silicate saddles achieved a stable lean limit of 3.8% methane, below the 5% flammability limit [9,10,46]. Khatami et. al. in 2007 numerically investigated the effects of porosity and permeability of the upstream and downstream porous sections on the centerline temperature distribution, peak flame temperature, flame structure, and preheating of the inlet gas mixture. Their model quantified and confirmed previous work indicating that the porosity of the upstream preheating section has a direct impact on the mixture temperature as it enters the combustion zone. A smaller porosity increases heat transfer to the gas and increases temperature. An optimal permeability for the preheat zone of $K = 10^{-10}\ m^2$ or less is identified following the so-called Carman-Cozney permeability model given as Equation 2 where d_m is the porous cavity diameter or pore size and ε is porosity [47].

$$K = \frac{d_m^2 \cdot \varepsilon^3}{180(1-\varepsilon)} \qquad (2)$$

A number of studies have hence been reviewed concerning the impact of material and geometrical selection on porous burner performance. It was identified that an optimal configuration and material selection should be made on a case-by-case basis. However, for an overall guideline the preheat section should have a have low thermal conductivity, a low volumetric heat transfer, and a high radiative extinction coefficient for which alumina was identified as a good material and that the downstream section should have a high thermal conductivity, high volumetric heat transfer, and an intermediate radiative extinction coefficient for which SiC was identified as a good material. Most of the reviewed experimental work was

15

performed with a two section burner incorporating an upstream monolith or honeycomb structure and a downstream packed bed although ceramic foam was identified as a better alternative.

<u>Previous Notable Works</u>

There have been many previous works done in the field of porous medium combustion to try to fully understand the mechanics, determine fuel flexibility and establish lean limits for different fuels. Echigo et. al. in 1983 built a heat recuperation burner with a porous permeable wall of stacked wire mesh combined with copper tubing surrounding the burner forming an air jacket for increased preheating of the reactants. The burner was operated at a flow rate of 5, 6, 7 and 8 L/min and was able burn a lean limit of equivalence ratio of 0.1 of a mixture of methane and hydrogen, below the mixture's normal lean limit of 0.284 [48]. Min and Shin in 1991 experimentally investigated the burning of premixed propane-air inside a cordierite honeycomb to provide detailed data for a numerical model. The lean flammability limit was extended from 0.52 to 0.49. It was found that a maximum inlet temperature occurred at 0.53 equivalence ratio. The burner produced a higher than adiabatic flame temperature at the flame front due to the heat recirculation from the solid matrix [49]. Babkin in 1993 performed a review of combustion in inert porous media. He defined four different combustion regimes: combustion in a low velocity regime, combustion in a high velocity regime, combustion of gas in the sound velocity regime, and low velocity detonation in porous media which laid the theoretical background for many later models [50]. Hsu et al. in 1993 performed an investigation of premixed methane combustion within a nonhomogeneous porous ceramic. They used a two section burner, consisting of an upstream and downstream porous ceramic cylinder. They tested multiple matrices of partially stabilized zirconia with porosities of 87%, 85%, 84% and 84% at 10, 30, 45

16

and 65 pores per inch (ppi), respectively. They used the 65 ppi matrix as the upstream section and varied the downstream section in multiple cases. They measured a lean limit of 0.41 equivalence ratio using the 10 ppi matrix, 0.44 for the 30 ppi matrix and 0.51 for the 45 ppi matrix with a confidence of ± 0.03, 0.04 and 0.03 respectively. Each of these was below the lean limit of 0.52 for the combustion of methane in air [51].
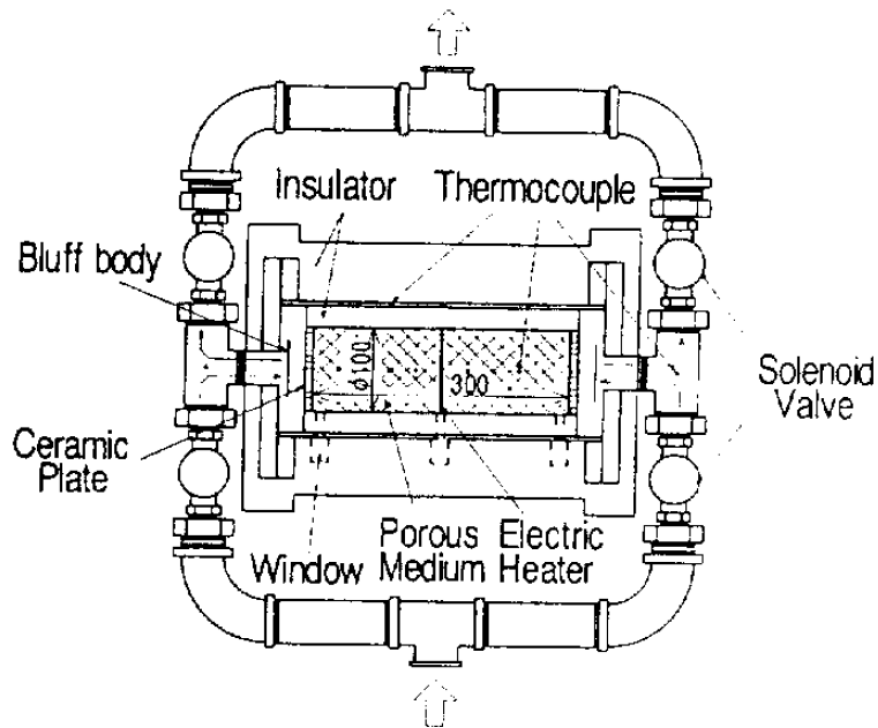
Figure 8. Schematic of a reciprocating flow porous burner used by Hanamura [52]

Hanamura et. al. in 1993 performed a numerical study on combustion within a reciprocating flow system with a porous media. The principle behind it is that with a three section burner, the flow direction could be reversed such that the hot section downstream of the combustion zone would then become the preheat section, more effectively recirculating the stored enthalpy. The burner and valve system are shown in Figure 8. The burner creates a steep trapezoidal temperature gradient within the burner, with the central section being the hottest and cooling

17

towards the ends of the outer sections. Their numerical investigations mostly focused on the optimal time interval to switch the flow direction in order to ensure enough time to heat the downstream section but not so long as to lose the benefit from utilizing that stored enthalpy. Their model predicted a peak temperature 13 times that of the free-flame theoretical and laid the groundwork for experimental investigations [4]. Hanamura and Echigo continued their work on super-adiabatic combustion within a reciprocating flow system with an experimental and numerical investigation of the thermal structure within the burner. The burner consisted of a mesh and a packed bed with porosities of 20% and 87.5%, respectively, in a stainless-steel conduit 300 mm long and 100 mm in diameter. They burned a mixture of 88% methane and 12% other hydrocarbons in air at an equivalence ratio of 0.054, 0.044 and 0.036. As the flow direction was switched the reactant mixture was preheated up to 900 °C for the leanest case, proving the reciprocating flow system a very effective method of heat recirculation [52]. Kennedy et. al. studied the physical phenomena present in the super-adiabatic combustion of methane, hydrogen and acetylene in porous media. They performed a basic experiment with a porous alumina material of 40% porosity, using air to fuel ratios between 20 and 100. They measured a maximum temperature of 1000-1400 °C compared to the predicted adiabatic temperature of 200-600 °C. The experiments performed are detailed in the work of Zhdanok et. al. [53]. To model this they considered a case where the incoming gas was preheated but with no combustion, given as Equation 3, where R = radius of the porous plug, ρ = density, c = heat capacity, g = subscript denoting the gaseous phase, T_c = preheat zone or thermal wave temperature, and T_0 = incoming gas temperature.

$$\Phi = \pi R^2 v_g \left[(\rho c)_g T_c - (\rho c)_g T_0 \right] \tag{3}$$

18

Nothing that $T_c \gg T_0$ and that the heat loss is to the porous solid, denoted with a subscript s. One can equate the loss of heat of the gaseous phase to the gain of heat to the solid phase:

$$\Phi = \pi R^2 v_g (\rho c)_g T_c = \pi R^2 v_t (\rho c)_s T_c \tag{4}$$

Simplifying the equation gives an estimation of the thermal wave velocity as a ratio of the physical properties of the two phases and the velocity of the flow.

$$v_t = \frac{v_g (\rho c)_g}{(\rho c)_s} \tag{5}$$

Repeating this process with a term representing the heat addition by the combustion process yields an equation for the SAC wave where ΔT_a is the adiabatic temperature rise and T_c is the combustion temperature.

$$v = \frac{v_g (\rho c)_g}{(\rho c)_s} \left(1 - \frac{\Delta T_a}{T_c} \right) \tag{6}$$

These numerical predictions were found to correspond fairly well with the experimental results obtained. A better accuracy was obtained by taking into account the increase of specific heat of the incoming gas with temperature, the ignition limit of the mixture and extending the model to included heat flow in the radial direction [5]. Trimis and Durst in 1996 performed developmental work on the design of a combustion heat exchanger based on combustion in porous media. They defined a minimum Peclet number of 65 for flame propagation in porous media defined in Equation 7 where S_L is the laminar flame velocity, d_m is the equivalent porous cavity diameter, c_p is the specific heat capacity, ρ is the density and λ is the heat conductivity of the gaseous mixture.

$$Pe = \frac{S_L d_m c_p \rho}{\lambda} \tag{7}$$

Their experiment involved a two section burner using a packed bed with the entire combustion chamber wrapped in a water jacket to serve as a heat exchanger. They were able to

19

burn at an excess air ratio of 1.9, equivalent to an equivalence ratio of about 0.52. They highlighted the advantages of a combined porous media burner and heat exchanger which was about 10-15 smaller than separate systems with a power dynamic range of 20:1 and showing lower emissions [34]. Hoffmann et. al. performed an experimental study with a reciprocating flow system. They focused on the effect of flow velocity, half cycle for the switching of flow direction and equivalence ratio on performance. They used three different types of ceramic foams in the experiments: cordierite at 6 and 30 ppi and SiC at 13 ppi, all 3 with 87.5% porosity and burned a mixture of 88.0% methane, 5.8% ethane 4.5% propane, and 1.7% butane. They showed that an increasing equivalence ratio created a steeper temperature gradient within the burner, increasing exhaust temperature and therefore heat losses. Exhaust temperature also increases with increasing half cycle, but more notably, there was a strong increase in combustion efficiency with longer half cycles. An equivalence ratio of 0.028 for the 30 ppi matrix was observed, less than half that of the 6 ppi matrix [54].
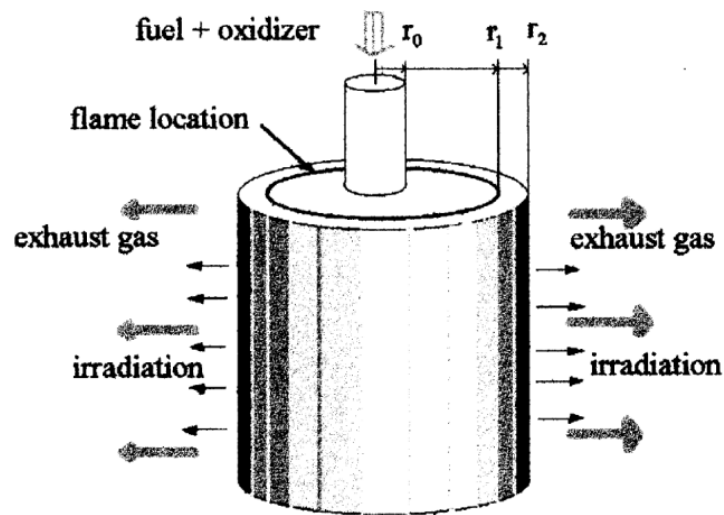
Figure 9. Radial porous medium burner used by Zhdanok [55]

Zhdanok et. al. in 1998 performed a numerical simulation of a radial porous burner, shown in Figure 9, to quantify the effect on operational parameters on flame localization. They concluded that the flame front location was defined not only by fuel flow rate, but also on the ignition coordinate with heat losses at the outer boundary of the porous media being a significant factor in the overall system [55]. Dillon, under the advice of Dr. Joe Shepard, studied flame propagation and quenching in a porous media burner. He used a cylindrical combustion vessel, burning a mixture of hydrogen and air in a packed bed of 6 mm diameter glass spheres. The burner was run to a lean limit of 0.338 with flame propagation apparent between 0.389 and 1 equivalence ratio. One notable result of this experiment was a reported critical Peclet number of 37, lower than the aforementioned value of 65 from Trimis and Durst. This was attributed by the author to the use of hydrogen as a fuel with a higher mass diffusivity than the hydrocarbons used to obtain the value of 65 [56]. Henneke and Ellzey in 1999 numerically modeled the low-velocity regime of combustion of methane in air within a packed bed. They included a complete methane and air kinetics mechanism in their model and it was found to be in good agreeance with Zhdanok and Kennedy's experiments for a mixture at an equivalence ratio of 0.15. They confirmed that the wave speed is dependent on the heat capacity of the solid medium and gaseous phase but was relatively unaffected by the dispersion properties of the porous medium at lower equivalence ratios [57]. Mare et. al. performed a study of the flammability limits for propane and methane combustion in air within porous media and their dependence on the material and geometrical properties of the porous matrix. The burner was tested with a packed bed of glass, stainless steel or brass spheres with a varied diameter between 9.5 and 12.5 mm. Overall, the flammability limits for each experimental case was found to weakly depend on the material being used with a much stronger dependence on the geometrical properties of the

matrix. They reported a lean limit for the combustion of methane between 6.30 and 6.52% for 12.5 mm spheres and between 7.38 and 7.93% for 9.5mm spheres compared to a 5.35% limit with no porous media [58].

Huang et. al. investigated the effects of critical energy content, firing rate, and equivalence ratio on the ignition and extinction of a flame in an inert porous medium. The firing rate is defined by the fuel mass flow, calorific value and the cross sectional area of the empty tube and signifies the rate at which chemical energy is being put into the burner. The device burned a mixture of propane and air in a stack of stainless steel screens. They observed a super-adiabatic temperature at an equivalence ratio of 0.4 of 1000 °C, above the normal limit of 870 °C. They were able to maintain a stable flame down to 0.22 equivalence ratio, below the normal value of 0.57 for propane in air. They observed a dramatic decrease in the critical preheating value necessary for with increasing preheating equivalence ratios at lower values but no effect at equivalence ratios above 0.7 [59].   Mathis and Ellzey experimentally investigated flame stabilization, operating range, and emissions of a two section porous media burner. Three different burner configurations were tested. The first burner configuration used sections composed of an yttria-stabilized zirconia/alumina composite. The second burner configuration used sections composed of zirconia-toughened mullite. The third burner was the same material as the first except the upstream section was 2.5 cm in length instead of 5.1 cm for the first two cases. Each burner had an upstream section at 23.6 ppcm followed by a section at 3.9 ppcm. Results showed a more stable flame using the yttria-stabilized zirconia/alumina composite sections over zirconia-toughened mullite. Flame speed was tested with the third configuration at 0.65 equivalence ratio and was found to have an upper blowout limit of 190 cm/s compared to the normal laminar flame speed of about 14 cm/s without a porous medium. The emission of

UHC was highest at lower firing rates, CO was low at lower firing rates and NO_x emissions were low for all measured cases. [60]. Smucker and Ellzey continued this work in 2004 with an experimental and computational study of the two section porous media burner. Only the yttria-stabilized zirconia foam was considered and the data was used for a mathematical model. They took radial temperature, pressure drop and emission level measurements for the burner for validation of their model. Experiments were conducted with methane fuel and stable operational limits were determined for equivalence ratios between 0.55 and 0.65. Their model had good agreeance at higher equivalence ratio but poor agreeance at the lower limit. This was attributed to using a material with slightly different properties for the model than the material used in the experiments and to the discontinuity at the interface between the high and low porosity sections. It was found that methane was able to burn at a lower equivalence ratio than propane likely due to propane having a lower laminar flame speed [61]. Vogel and Ellzey investigated the velocity limits of combustion in a similar two stage porous media burner. The porous sections used were FeCrAlY with 23.6 and 3.9 ppcm and 84% and 87% porosity respectively. Four burner configurations were tested; one with two sections at 5.08 cm completely shielded within the casing and three end-mounted sections: one with each section at 1.27 cm in length, the second with the upstream section at 1.27 cm and downstream section at 2.54 cm and the third with both sections at 2.54 cm in length. The shielded and end-mounted configurations are shown in Figure 10. For each configuration, the lower and upper velocity limits all occurred near an equivalence ratio of 1.1, suggesting an indifference to media length and position. One main difference is that flame oscillations were observed in all three end mounted configurations but not in the shielded configuration [62].
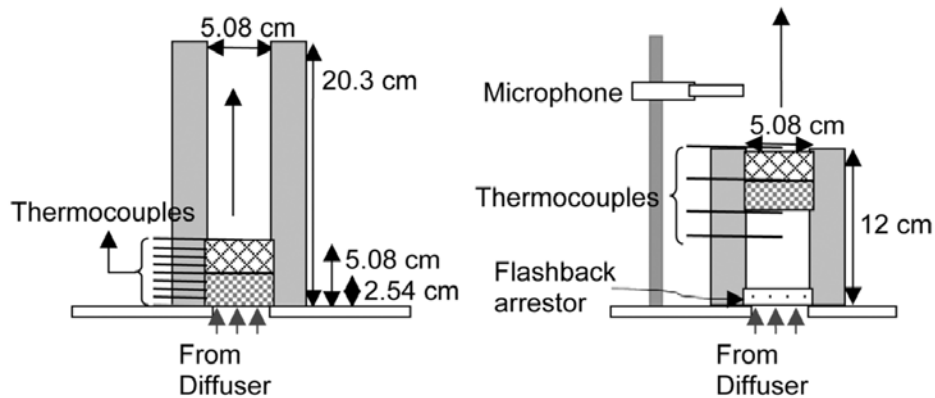
Figure 10. Shielded and end mounted configurations for a two stage porous burner [62]

Al-hamamre et. al. investigated the use of a porous media burner to combust low calorific gases from landfills and pyrolysis processes. The major components of landfill seepage gas were identified as CH_4 and CO_2 and for the pyrolysis processes were H_2, CO, CH_4, N_2 and CO_2. They tested two 10 ppi SiC foams at 10 and 100mm in length and a static Al_2O_3 structure 100mm in length. The SiC foam was found to have a lower blowoff limit due to a higher thermal conductivity where the 100 mm SiC section presented a lower blowoff limit than the 10 mm section. Overall, porous media technology was found to be a very good technology to burn low calorific gases [63]. Kakutkina et. al. in 2006 experimentally studied the combustion of hydrogen, propane, and methane with air within an inert porous media. The medium used was a granular carborundum with grain sizes of 1-2 mm for hydrogen combustion, 2-3 mm for propane combustion and both 2-3mm and 5-6mm for methane combustion. The data was used for validation of numerical models and they identified a minimum stable flow rate for methane combustion of 24 cm/s at around a 1.5 equivalence ratio for their experimental setup [64]. Kamal and Mohamad performed an experimental investigation of a radial flow porous burner. A premixed methane/air mixture was fed axially to a hollow perforated tube surrounded by Al_2O_3-SiO_2 fibers. The concentric tube assembly was mounted on ball bearings, being allowed to rotate

24

with the use of a variable-speed motor. A few different tube designs with varied hole configurations were tested and it was found that the tube with simply the most number of outlet holes performed the best. The burner was tested with a motor spinning the central section of the burner at different rpm, determining the effect of swirl on performance. The swirl was found to increase flame stability in a free flame configuration but cause a pulsation when applied to combustion in a porous media. The burner displayed a practical lean operation of 0.74 equivalence ratio and burning capacities up to 1.7 times those with a free flame [65].
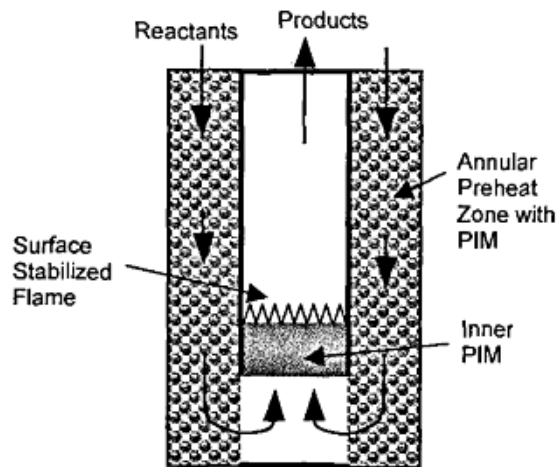
Figure 11. Schematic of the burner used by Marbach [66]

Marbach and Agrawal in 2006 developed a heat-recirculating premixed burner utilizing porous media and preheating annulus shown in Figure 11. They used methane fuel at 0.5 and 1.0 m/s inlet velocity and measured the burner performance with and without the porous media and with and without exterior insulation. They measured reactant and product gas temperatures as well as NO_x and CO emissions. A super-adiabatic peak temperature for the gaseous products was observed and notably, they observed a greater fraction of enthalpy remaining in the product gas for the case of higher inlet velocity. The reactant gas temperature was nearly the same with porous media in the annulus compared to without it; however, the product temperatures were

25

slightly higher showing lower heat loss. The exterior insulation greatly increased the inlet gas temperature from 150 K to about 700 K. An equivalence ratio of 0.39 at the lean blow-out limit was obtained for the lower inlet velocity and emissions increased at the higher flow rate [66].
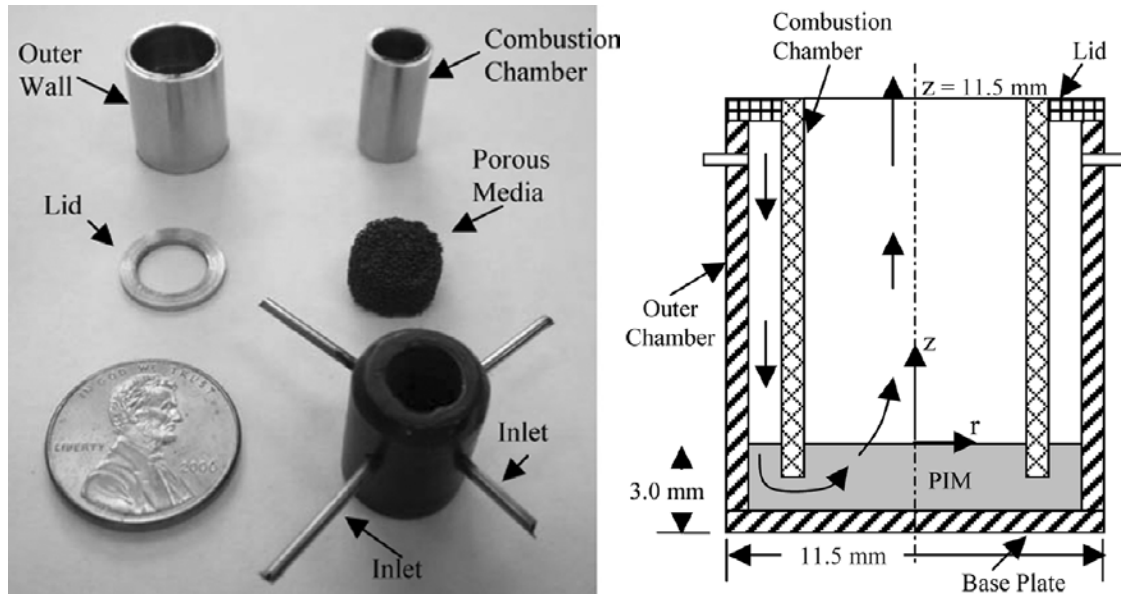
Figure 12. Components and schematic of burner used by Marbach [67]

Marbach et. al. continued work with the miniature combustor and annulus shown in Figure 11. This burner utilized surface stabilized porous media combustion on a SiC coated 40 ppi carbon foam. Figure 12 shows the components of the burner next to a penny for size comparison and an updated schematic of the burner and annulus system. The entire volume of the combustion chamber was 0.364 cm^2. Methane was burned with air at a varied flow rate between 0.25 to 1.0 m/s and an equivalence ratio between 0.5 and 0.8. From the measurements of CO and UHC, combustion efficiency was calculated to exceed 99.5% with emission levels increasing with equivalence ratio. A peak temperature of 1800 K was recorded in the combustion zone with about 1580 K at the exit [67]. Alavandi and Agrawal demonstrated the fuel flexibility of a two-section porous burner by burning lean hydrogen-syngas and methane mixtures. The burner

consisted of upstream SiC coated carbon foams of 26 ppcm and downstream 4 ppcm sections of varying length. A mixture of methane and air mixture was fed into the burner and the methane content in the fuel was decreased from 100% to 0% by volume, with the remaining amount split equally between CO and H_2, the two reactive components of syngas. Adiabatic flame temperature increases for mixtures with increasing amount of H_2/CO however; the burner showed a sustained flame at lower temperatures for fuels with more H_2/CO, likely due to the high reactivity of H_2. The burner was shown to be very effective in burning of fuels with moderate amounts of syngas which resulted in an overall decrease of CO and NO_x emissions and a decreasing lean blowout limit with increasing H_2/CO content [68].
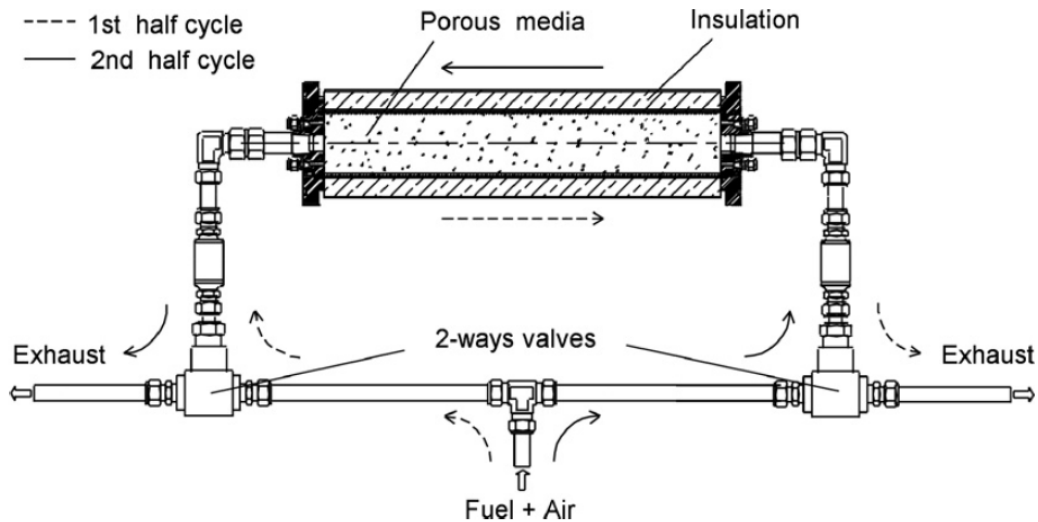
Figure 13. Two valve reciprocating flow burner used by Dobrego [69]

Dobrego et. al. performed a numerical investigation of the effects of heat loss coefficient, reactor length, pressure, particle size and porosity on the lean combustibility limit of a methane and air reciprocal flow combustion reactor, shown in Figure 13. The modeled burner utilizes a two valve system which is simpler in design than previous reciprocating flow reactors which used a 4 valve system. They validated their model with experimental results obtained from

Hoffmann et. al. [54]. Dobrego found that an increasing reactor length generally meant a lower lean combustibility limit. Higher pressure in the system corresponded to a lower limit as well. The porosity of the burner did not have considerable influence on the limit likely because on a small change was possible due to using a packed bed. Foamed ceramics would provide greater room for optimization. The particle size of the packed bed was the most important factor in lowering the lean combustibility limit with the model taking into account dispersion conductivity, photon free path, specific area of porous media and secondary effects. Smaller diameter particles showed a lower lean limit [69].

Shi et. al. numerically investigated the influences of the material properties on the combustion wave speed and maximum temperature of lean combustion in a packed bed porous medium burner. Experimental data from Zhdanok et. al. [53] is compared to the results from the numerical model and shows good qualitative agreement with the exception of maximum temperature. This was attributed by the author to an uncertainty of thermal properties of the packed bed. The wave velocity is found to almost double when the heat capacity of the porous medium is halved. The maximum temperature remained constant with decreasing thermal capacity of the medium. Increasing the conductivity of the solid medium is found to increase the heat feedback mechanism, lowering the maximum temperature and increasing the wave speed [70]. Akbari et. al. in 2009 numerically investigated the effects of turndown ratio and porosity on flame propagation of methane and air combustion in porous medium. Turn-down ratio is defined as the range of admissible firing rates, which correlate with inlet flow rate and are measured in kW/m^2. They varied the porosity between 60 and 90%. An equivalence ratio of 0.43 is found to be the lower limit at which the flame stabilizes in the matrix. Figure 14 is a plot of equivalence

ratio versus porosity, depicting the region of a stabilized flame and where a blowout would occur for higher porosities and lower equivalence ratio [71].
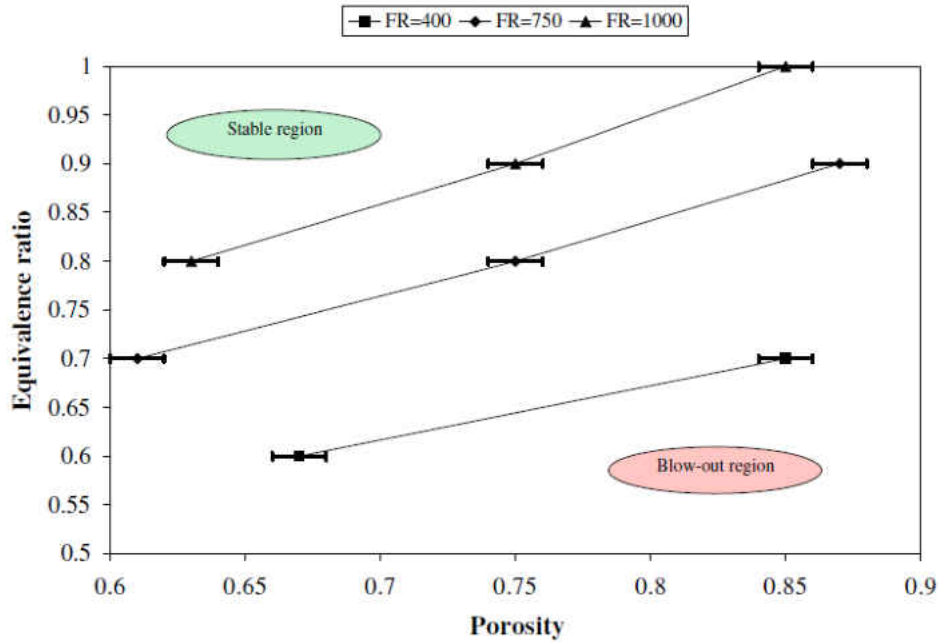
Figure 14. Equivalence ratio vs. porosity for a stable flame [71]

Emissions

Through careful material choice and burner design, porous media combustion can produce lower NO_x and CO emissions when compared to a similar free flame burner. Homogeneity of the temperature field within the burner is very important for low emissions since hot spots can produce large amounts of NO_x and cold spots result in incomplete combustion with high CO and UHC emissions [29]. The amount of NO_x produced depends mainly on the maximum temperatures reached in the center of the combustion region and on the residence time in those hot regions [29]. Durst and Trimis predicted that porous burners would show an overall insensitivity of NO_x emission behavior to firing rates. This was explained by the decreased residence time at higher heat loads and decreased temperatures at lower heat loads [29]. NO_x

emissions are affected very strongly by the excess air ratio since with an increasing excess air ratio, the residence time and maximum temperature both decrease [29]. Porous material with good heat conductivity will help keep a homogeneous temperature field.

Hardesty and Weinberg were of the first to study the emissions of a porous media heat exchanger in 1974. They noted that, unlike conventional systems, the use of leaner mixture ratios will actually have a notable effect on pollutant emission. Increasing the heat recirculation and decreasing equivalence ratio will reduce emissions. NO emissions become negligible altogether if the peak temperature within a burner is restricted to less than 1800 K, which is possible for most porous burner systems [25]. Bouma and Goey performed a numerical and experimental study on the matrix stabilized combustion of methane and air in a ceramic foam burner. They measured CO and NO concentration as a function of power load, given as Equation 8, which is a measure of the calorific content and mass flux of the inlet flow.

$$P = \rho u H \left(1 + s_{CH_4} \frac{n}{X_{O_s}}\right)^{-1} \tag{8}$$

Two plots, given as Figure 15, show the numerical prediction and experimental measurement of CO and NO concentration as a function of power load. The results for NO concentration do not agree with what Durst and Trimis predicted [29]. NO concentration seems to increase with increasing power load. The maximum temperature for the ceramic foam burner at a power load of 100 kW/m^2 was measured at about 1650 K whereas the maximum temperature at 600 kW/m^2 is measured at 2000 K. This is likely the cause of to the large increase in NO concentration [6].

30
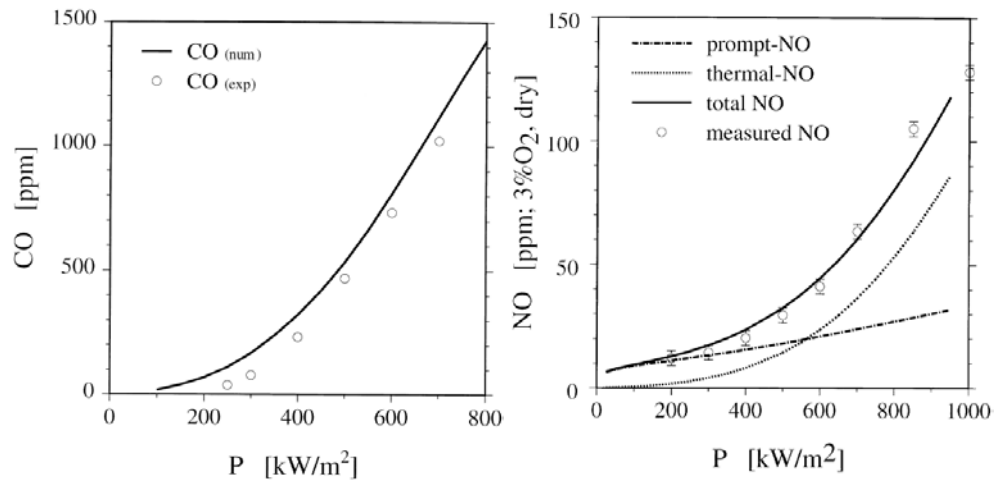
Figure 15. CO and NO concentrations vs. power load [6]

Brenner et. al. developed a numerical code modeling combustion in porous media and used it to perform a numerical parametric study and predict CO and NO_x formation. The model was compared to data from an experimental setup using SiC and Al_2O_3 lamellae. The temperature inside the burner varied from 300 K at the inlet to about 2000K in the flame region. The predicted CO concentration for the SiC matrix was 16 ppm and the predicted concentration for Al_2O_3 was 24 ppm at a firing rate of 1500 kW/m^2. The measured values were 25 ppm and 29 ppm respectively. The difference between the two materials is attributed to the higher heat conductivity of the SiC lamellae. NO_x concentration was difficult to predict for their numerical code due to the discontinuity and imperfect modeling of the flame stabilization at the interface between the preheat and combustion regions [72]. Marbach and Agrawal investigated the performance of surface vs. matrix stabilized porous media combustion. They measured pressure drop, NO_x and CO emissions and lean blow-off limit. They found that for both combustion regimes, NO_x formation was weakly dependent upon the flow velocity and pore size but that the NO_x concentration increased exponentially with equivalence ratio. The CO concentration increased with increasing equivalence ratio for both combustion regimes and decreased with

31

increasing pore size. The NO_x and CO concentrations for different equivalence ratios are shown in Figure 16 at different inlet velocities. The matrix stabilized combustion had a lower lean blow-off limit than surface stabilized for all conditions tested [73].
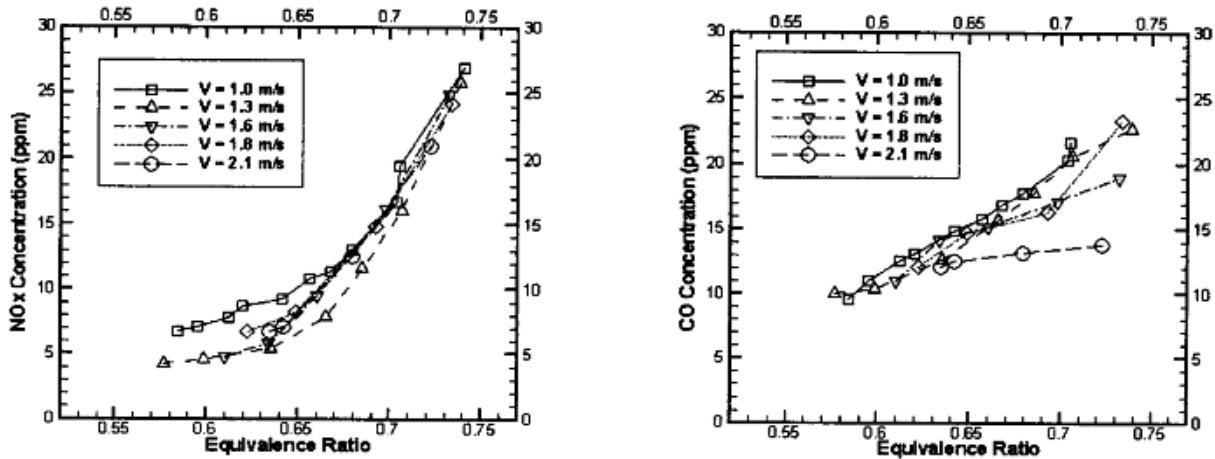
Figure 16. NO_x and CO emissions vs. equivalence ratio for different inlet velocities [73]

Mößbauer et. al. aimed to create a zero emission engine by the use of porous media burners in a steam engine utilizing exhaust gas recirculation. The thermal mechanism for NO_x formation only significantly takes place above 1300 ˚C. The recirculated air consists of mostly inert components such as H_2O, CO_2 and N_2, causing the recirculation to reduce the combustion temperature. Increasing exhaust recirculation also decreases O, N and OH concentrations with only a small change to O_2 concentration. Therefore, the thermal NO mechanism $O + N_2 = NO + N$ is reduced due to its dependence on O concentration. At lower exhaust recirculation rates, the combustion temperature is reduced, causing an increase in incomplete combustion products such as CO and UHC. The end result is that with an optimal exhaust recirculation rate, NO_x formation can be greatly reduced while still maintaining low CO and UHC concentrations [74]. Pickenäcker and Trimis used a multi-staged porous media burner to investigate the potential to decrease NO_x emissions from existing methane/air combustion systems. The burner used a

32

highly porous plate composed of 53% SiO_2 and 45% Al_2O_3 upstream of a lamellae composed of 80% alumina and 20% silica or a SiC foam, each of 90% porosity in the combustion region. The burner had lateral feeds of methane, air or a mixture of both which could be fed into different locations within the porous combustor to create a homogeneous temperature profile. The burner showed a 30-40% decrease in NO_x formation when using at least a 10% lateral feed over each operational firing rate, with a better performance at lower firing rates. The pollutant amount was only slightly affected by the porous structure used but was strongly affected by the homogenization of the temperature field caused by the staging [75].
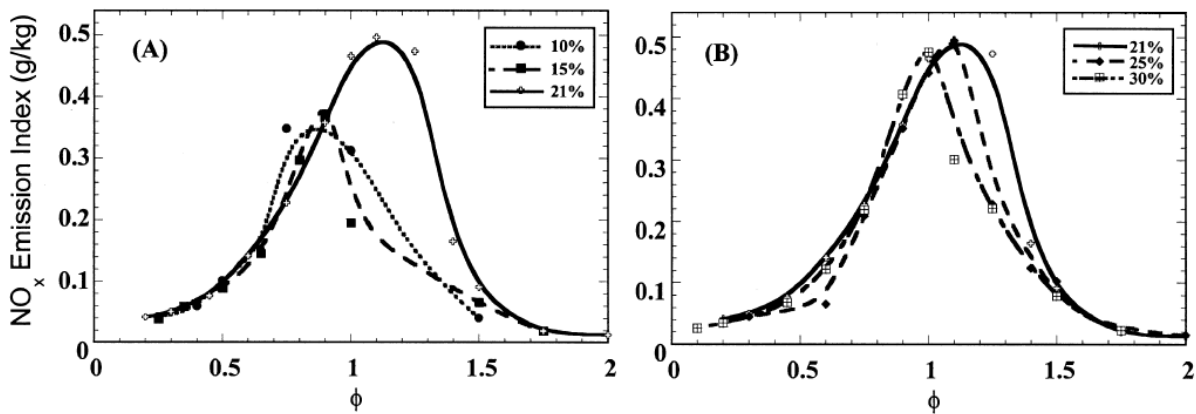
Figure 17. NO_x emission versus equivalence ratio for varying oxidizer concentration [76]

Kennedy et. al. experimentally studied the temperature, combustion waves and emissions of porous media combustion in a packed bed of alumina. Methane was burned with air at equivalence ratios ranging from 0.1 to 2 while the oxygen content of the oxidizer was varied between 10 and 30%. Since the maximum temperature in each case was not over 1650 K, the prompt mechanism was identified as the major pathway for NO_x formation. Figure 17 shows the resulting NO_x measurements for different oxygen contents in the oxidizer versus equivalence

ratio. Even with higher overall temperatures, the mixtures with 10 and 15% oxygen have lower NO$_x$ emission based on fuel inputs [76].
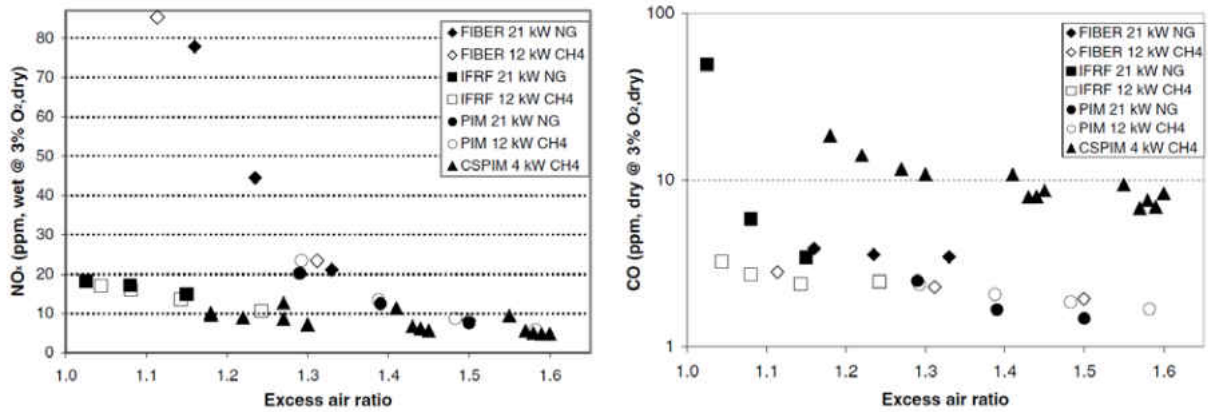
Figure 18. NO$_x$ and CO emissions of different burner types [20]

Rørtveit et. al. compared four different types of burners to determine an optimal configuration for low-NO$_x$ combustion of methane and hydrogen. The four burners are a radiant surface burner from Acotech (fiber), a swirl burner from the International Flame Research Foundation (IFRF), a porous inert material (PIM) and a catalytically supported porous inert material (CSPIM). The porous media burner used corrugated fibers of Al$_2$O$_3$ and SiO$_2$ and the catalytic supported porous media used a SiC monolith with an alumina based washcoat of Pt and Pd. Two plots showing NO$_x$ and CO concentrations vs. excess air ratios (reciprocal of equivalence ratio) for the configurations burning methane and natural gas at different firing rates are shown in Figure 18. They reduced the methane content of the fuel, replacing with hydrogen, and the two porous media burners showed lower emissions with increasing hydrogen content [20].

Porous media burners prove to be able to reduce harmful emissions with special design considerations and material selection. They can maintain a low peak temperature and

homogeneous temperature field, keeping emissions low over a wide range of equivalence ratios and fuel mixtures. The use of catalysts to improve these positive aspects and help facilitate the combustion reaction is a promising technology for the reduction harmful emissions such as NO_x, CO and UHCs.

<center>Catalysts</center>

The use of catalytically active materials to facilitate the combustion process could increase the overall efficiency of the burner and help to reduce emissions [29]. The overall combustion reaction can be described as consisting of two processes: fuel oxidation, or release of the electrons, and oxidant reduction, or acceptance of the electrons. If the proposed fuel is a simple CH_4 molecule then the activation energy to separate CH_4 into hydrogen atoms and hydrocarbon radicals, with further release of the electrons, is not very high. The most problematic aspect is the splitting of O_2, since the covalent bonding in oxygen molecules is very strong. However, if catalysts could be used to promote O_2 molecule splitting, bond energy could be significantly decreased thus facilitating combustion [77]. Therefore, it is fair to expect that significant improvements in the overall efficiency of a porous media combustor coupled with thermoelectric devices can be achieved by exploring advanced ceramics catalysts.

There have been a number of studies on the catalytic effects and benefits of different materials on the combustion of hydrocarbon fuels. Karim and Kibrya in 1986 experimentally investigated the lean blowout limit of the combustion of methane and hydrogen in air. The burner was a cylindrical combustor 150 mm in diameter with a metallic wire mesh as a porous media. They coated the wire mesh with eight different materials by electroplating. The materials listed in decreasing order of effectiveness are Pt, Cu, Ag, Brass, Cr, Cd, Ni, and stainless steel,

<center>35</center>

with the Pt coating supporting lean combustion of methane down to 2.7% by volume, a 0.26 equivalence ratio, and lean combustion of a 50% methane/hydrogen mixture down to a 0.15 equivalence ratio. When comparing the results obtained from the hydrogen combustion, it was found that hydrogen is more sensitive to the catalytic effects of the materials than methane, particularly at lower temperatures [78]. Dupont et. al. investigated the combustion stability, pollutant emissions and radiation efficiency of honeycomb monoliths containing platinum and palladium catalysts for the combustion of mixtures of methane and air. The honeycomb was made of cordierite and had 400 square cells per square inch. They found that the palladium catalyst supported a lower inlet concentration than the platinum one and had a proportional effect over all inlet flow rates tested. The results showed that a minimum stable concentration of 4.4 mol % of CH_4 was seen with Pd at 4.4 grams per piece and 60 L/min flow rate. The burner configuration and resulting lower combustibility limit versus flow rate are shown in Figure 19 for each catalyst [79].
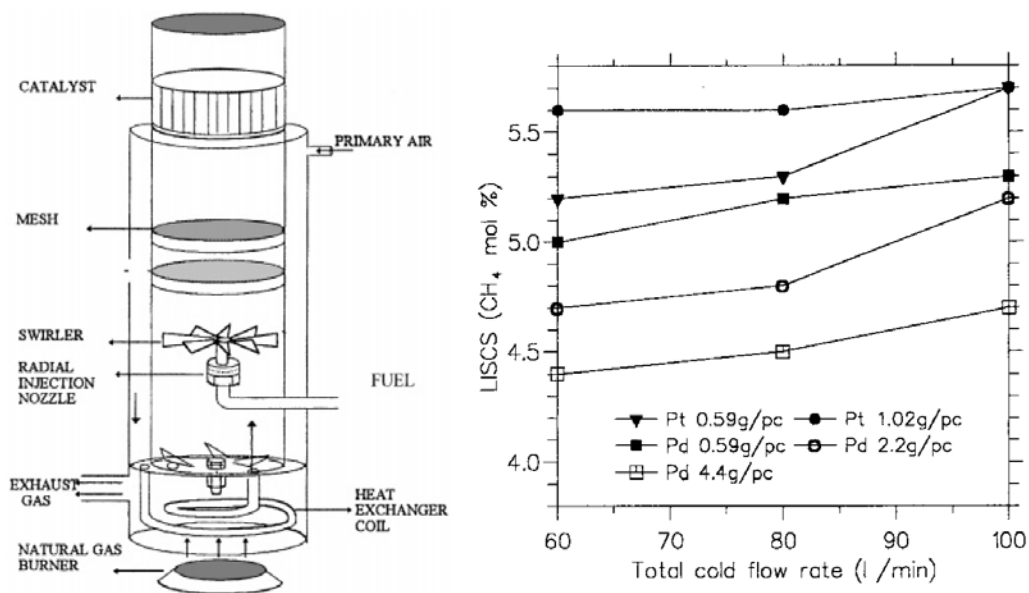
Figure 19. Burner schematic and concentration vs. flows rate plot [79]

Dupont et. al. built on their previous work and developed a numerical model to predict the effect of Pt and Pd catalysts on the lean combustibility limit of methane in air. They tested the catalysts in a stagnant point burner and with the ceramic monolith burner shown in Figure 19. They confirmed that palladium was a better catalyst for methane combustion than platinum, showing a lower lean combustibility limit. The stagnation point burner showed a combustion efficiency of about 30% whereas the monolith burner with Pd catalytic support reached 90-100%, showing only scarce amounts of NO_x, CO and UHCs [80]. Anh et. al. performed an experimental study on the ability of a bare-metal catalyst to extend extinction limits of propane and hydrogen combustion at different Reynold's number flows. They used a spiral counter-flow burner with thin strips of Pt lining the walls. The results showed that the catalyst greatly affected the extinction limits and in a non-symmetrical manner with respect to the lean and rich limits. The extinction limits without the presence of a catalyst were nearly symmetric. With a catalyst, the lean combustibility limit was actually rich of stoichiometric with a limit >40 equivalence ratio at low Re. At higher Re the catalyst enabled slightly leaner mixtures to be burned and at much lower temperatures [81]. Cimino et. al. aimed to develop a burner which combined low and high temperature catalytic activity to widen its operating range. A combination of Pd and $LaMnO_3$ were applied to ceramic monoliths as washcoats. A table depicting the compositions and amounts of the wash coatings along with a plot of conversion efficiency vs. temperature are shown in Figure 20, where PLM-3 was activated at 1000 °C for one hour in the final case. The author notes that the combination of two types of catalytic sites requires good overlapping of the operational windows to be effective in steady state combustion. It can also be seen that only a small amount of Pd makes a large improvement in low temperature combustion efficiency [82].
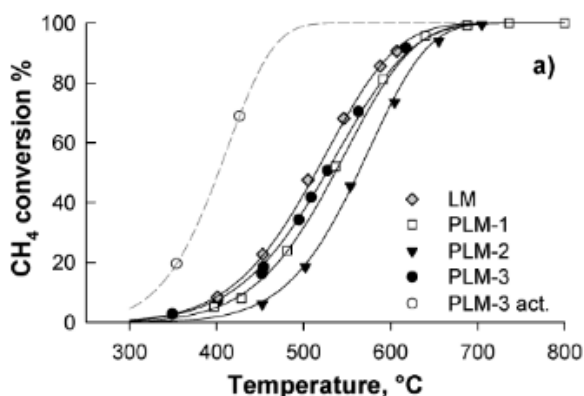
Figure 20. Combustion efficiency and associated washcoat compositions [82]

Arendt et. al. investigated the catalytic activity of $LaMnO_3$ perovskite catalysts in the combustion of methane. The catalyst was deposited on both ceramic and metallic monoliths by dip coating and an orbital stirring procedure. A comparison between structured and powdered catalyst showed a higher catalytic activity of the structured catalysts. It was observed that the catalyst performed better on metallic monoliths at lower temperatures and better on ceramic monoliths at a higher temperature. It was found that the monolith prepared by orbital stirring were more active than those prepared by dip coating for similar deposited weights and that monoliths with a lower deposited weight showed better catalytic behavior [83]. Bijjula and Vlachos studied the catalytic combustion of JP-8 with the aim of utilizing it as a fuel for portable power generation systems. They used a packed bed reactor to study surface ignition, extinction and autothermal combustion with a $Pt/\gamma-Al_2O_3$ catalyst of 1.17 wt.% Pt. They studied JP-8, a six component surrogate fuel mixture, and the individual components of the mixture to try to accurately understand the combustion mechanics of JP-8. The full autothermal temperature plot of JP-8 and some of the other fuels is shown in Figure 21. Notably, the ignition temperature decreases with increasing equivalence ratio for 2,2,4-trimethyl-pentane and methylcyclohexane until reaching a minimum. This is attributed to the surface stoichiometric point of those fuels.

The ignition of JP-8 seems to most closely resemble that of dodecane and tetradecane. Catalytic ignition of JP-8 was shown to occur at very low temperatures of about 270 °C at equivalence ratios of about 0.2 [84].
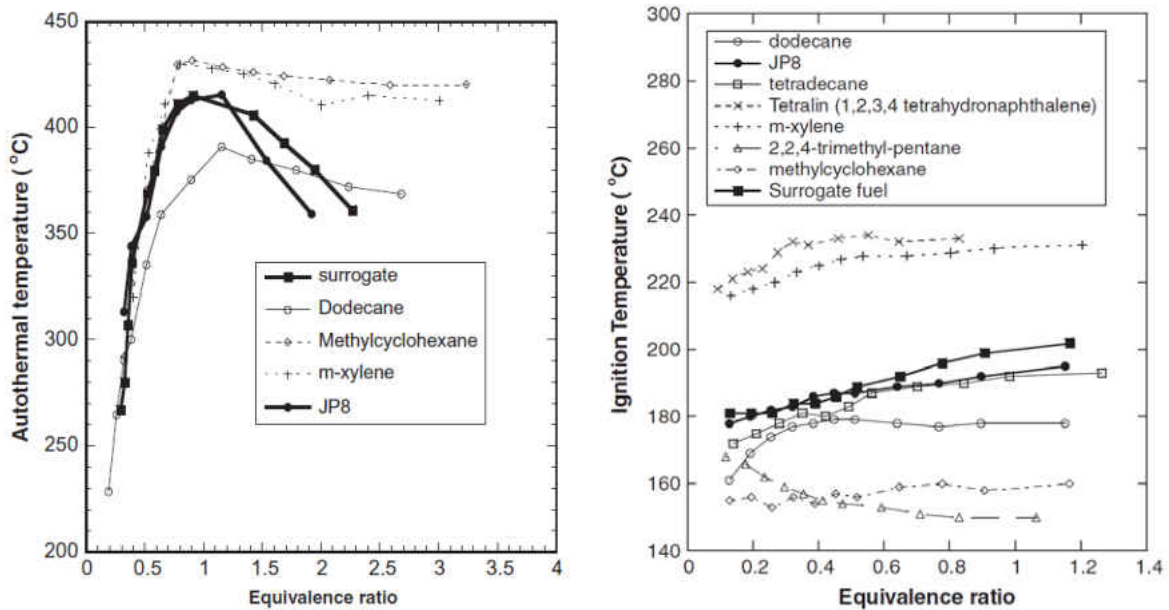
Figure 21. Autothermal and ignition temperatures for JP-8 and surrogate components [84]

Tacchino et. al. experimentally investigated new types of catalysts for the combustion of methane and hydrogen in monoliths. The micro-monoliths were made of SiC with 6mm x 6mm channels. Catalysts were deposited on the monoliths by in situ solution combustion synthesis, dipping them in solution and then placed in an oven at 600 °C bringing the solution to boil, producing the desired catalyst. The monoliths were tested in a burner with methane, hydrogen and a mixture of the two all at equivalence ratio of 0.5. The four catalyst investigated were 2% Pd/(5% $NiCrO_4$), 2% Pd/(5% $CeO_2 \cdot ZrO_2$), 2% Pd/(5% $LaMnO_3 \cdot ZrO_2$), and 2% Pt/(5% Al_2O_3). The catalyst 2% Pt/(5% Al_2O_3) was found to have the highest combustion efficiency for the combustion of only CH_4 or H_2 but not for the combined mixture. The Pd catalysts were better for

the CH_4/H_2 mixtures with 2% Pd/(5% $NiCrO_4$) being the best followed by 2% Pd/(5% $LaMnO_3 \cdot ZrO_2$) and 2% Pd/(5% $CeO_2 \cdot ZrO_2$) [85].

The use of catalysts to enhance the combustion of hydrocarbons has been shown in numerous experimental studies to help improve the performance of hydrocarbon burners. A number of different types of catalysts have been used to extend flammability limits, promote the combustion of different mixtures of fuel and to reduce the harmful emission of NO_x, CO and UHCs. With the lowering of lean flammability limits, a catalyst could be used to minimize the fuel consumption of a porous media burner and help increase the overall efficiency of a power generation system.

Power Systems

Hydrocarbon fuels contain about 100 times more energy per unit mass than lithium-ion batteries [81]. Converting this chemical energy to useful power at a better than 1% efficiency would represent an overall improvement in the powering of portable electronic devices and other battery-powered equipment [81,86,87]. Most portable or handheld devices require 10-100 watts of power, with personal laptops ranging from 20-60 watts, and have a target operating duration of 10 hours [24,88]. As a preliminary calculation, to power a 50 watt device for 10 hours, considering the heat of combustion for methane is 55.6 MJ/kg [89] and an overall conversion efficiency of 1%, would take 3.24 kg of fuel. This amount could be further reduced if the overall efficiency of this conversion was increased to even 2% by the use of the heat recirculation mechanism of a porous medium burner, supportive catalytically active material and properly chosen porous structure (optimal porosity, pore size and material). This represents a great potential for the powering of handheld or portable electronics by a porous burner system.

40

Fernandez-Pello performed a general overview of the miniaturization of hydrocarbon combustion systems for power generation. Some of the difficulties with micro-sized combustors are the thermal and chemical management. The dimensions are so small in these systems that the residence time of the fluid within the combustor is very short. The Reynolds and Peclet numbers are very small due to the short characteristic length, which means that the flows will be mostly laminar. Therefore, mixing will be mostly due to diffusion which needs to occur quicker than the residence time to ensure complete combustion. Many of these micro-combustors utilize piezoelectric, thermoelectric or thermophotovoltaic devices to harvest the energy from the combustion process [86]. Mitsos et. al. addressed portable power generation systems, focusing on the difference between maximizing efficiency vs. energy density for any particular application. Overall, they found for large scale operations that conversion efficiency was the best design parameter but small portable power systems, the maximization of energy density was the optimal objective [90].

A number of works have been done on super-adiabatic combustion or the use of porous media for small-scale power generation. Echigo et. al. investigated super-adiabatic combustion in a reciprocating flow in a porous body for power generation. They proposed to utilize the steep trapezoidal thermal gradient present in their reciprocating flow burner with a thermoelectric porous matrix present in the flow field. Their numerical study and preliminary experiments with ten alumel-chromal thermoelectric elements measured 0.15 watts from a 1040 K temperature gradient with a matched load resistance. Expanding this estimate to a full set of thermoelectric elements would yield up to 5-10 kW/m^2 from the design [91]. Echigo et. al. in 1994 and 1995 continued this work on the reciprocating flow system by developing a mathematical model to analyze how major parameters like flow velocity, the heating value of the combustible mixture,

the thermal conductivity of the thermoelectric elements and the electric power extracted affected the conversion efficiency. They created a dimensionless figure of merit based on the thermal conductivity of the gas and initial temperature and detailed how it was affected by each parameter. They found at an optimal dimensionless figure of merit, their overall conversion efficiency could be as much as 4% at an inlet velocity of 20 cm/s [92,93].
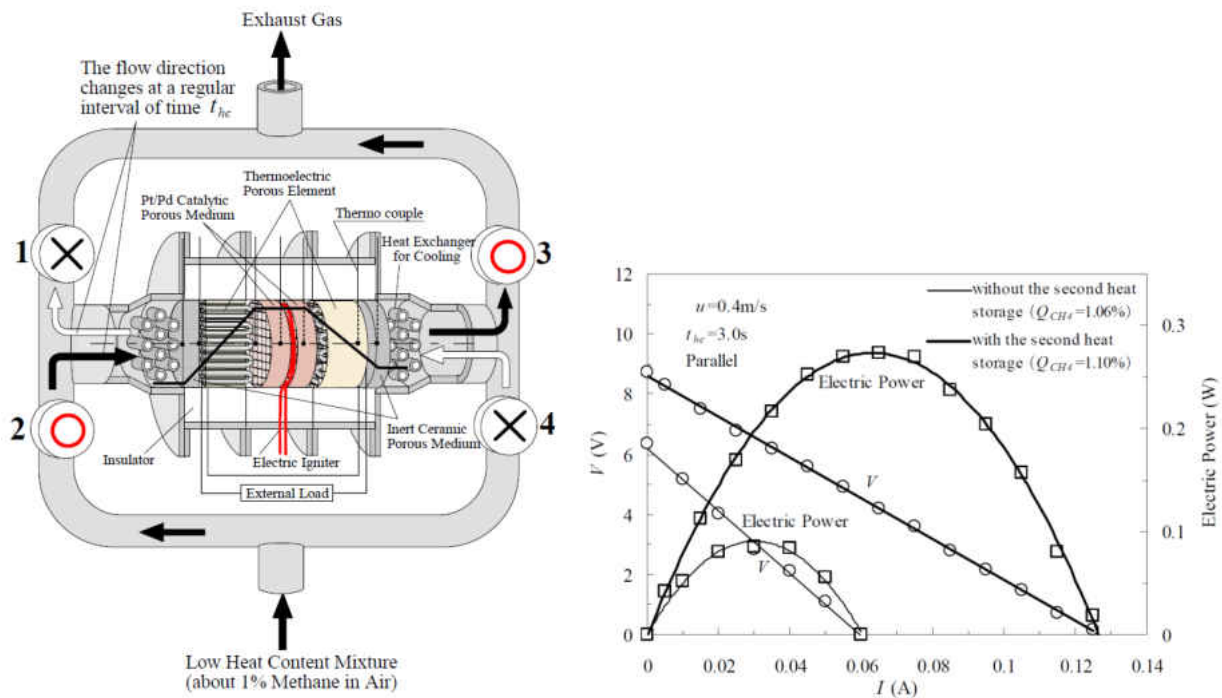
Figure 22. Reciprocating flow burner with power, voltage and current plot [94]

Hanamura and Kumano in 2003 experimentally investigated super-adiabatic combustion in a pair of thermoelectric porous elements. The reciprocating flow burner was based on the proposed system by Echigo et. al., a three section burner with upstream and downstream porous thermoelectric sections to utilize the steep temperature gradient present at those areas. They used a Pt/Pd catalyst layer on an 87% porous honeycomb of $FeSi_2$ thermoelectric elements. A 1% lean mixture of methane and air was introduced to the electrically heated porous media once it reached 600 °C within the burner system shown in Figure 22. The burner reached a maximum

temperature of between 900 and 995 °C and generated a peak power of about 0.3 watts, plotted in Figure 22, with a total thermal efficiency of 0.2%. They suggested that the efficiency could be increased to between 7 and 10% by use of Ge-Si thermoelectric elements [94]. Hanamura and Kumano proposed using thermophotovoltaics instead of thermoelectrics to generate power from a reciprocating-flow porous media super-adiabatic combustor. The porous media would be a thin foam-ceramic sandwiched between parallel quartz glass plates. The thermophotovoltaics could harvest the radiant energy emitted through the quartz glass. Much of the radiant energy would absorbed by the quartz glass but the designed system was expected to reach a 14.4% total thermal efficiency, compared to the predicted 7-10% with thermoelectrics in the previous study [95]. Hunt et. al. designed an auxiliary power unit for a hybrid electric vehicle by using an alkali metal conversion system with a cellular ceramic porous medium, reaching an efficiency of up to 15.5% [96,97]. Katsuki et. al. also developed a power generation system within a reciprocating flow burner with porous thermoelectric elements. The porous elements consisted of two semi-cylindrical Mn- and Co- doped $FeSi_2$ couples with an 80% porous cylindrical Al_2O_3 ceramic foam in the center. The burner was ignited with a stoichiometric mixture and once combustion was stable, the equivalence ratio was turned down to 0.27 with a half cycle of 10 s at a flow rate of 0.84 m/s. The temperature gradient over the thermoelectric elements reached 200 K/cm, with a maximum power for a single element on the order of 100 mW. This equated to an overall energy density of 7 kW/m^3 [14].

Suzuki et. al. developed a micro-scale catalytic combustor of butane with Pt as a catalyst. The focus was on heat release rate, CO and NO_x emissions and reaction rate vs. catalyst temperature. The combustion channel measured 12x12x0.5 mm^3 with an overall size of 34x20x2 mm^3. Porous alumina was used for the micro combustor but generating uniform flow rate with a

simple manifold geometry proved difficult so they used a high-precision tape-casing technology to construct a more complex three dimensional manifold geometry. Under stoichiometric conditions the combustor was able to generate 60 W of heat at 50 sccm with a combustion temperature of 380 °C. This equates to an overall heat release rate of 830 MW/m^3 for the burner [98]. Kamijo et. al. developed a micro-scale combustor with a Pd catalyst for thermophotovoltaic power generation. The system burned a butane and air mixture in a combustion chamber that was 40 mm in diameter and 3.5 mm tall after minor optimization in design from preliminary testing. The burner was operated at equivalence ratio of 0.95 and 10 sccm and showed a 100% fuel conversion to produce a heat generation density of 212 MW/m^3. When the flow rate was increased to 30 sccm, the conversion efficiency decreased but produced a greater heat generation density of 515 MW/m^3 [99]. Okamasa et. al. built a micro-scale burner for the combustion of butane. The burner utilized a Pd catalyst with a combustion chamber measuring 25x25x5.3 mm^3. The burner was run at 2.5 and 5 sccm at an equivalence ratio of 0.95 and 0.5, producing between 5 and 10 watts of heat. The burner achieved complete combustion efficiency at a flow rate of 5.0 sccm with a maximum temperature of 390 °C. The overall heat generation density of the system was calculated as 100 MW/m^3 [100].

The concept of power generation by harvesting the energy released during combustion within a porous medium burner is not novel but is very promising. Many previous experiments suggest an achievable conversion efficiency greater than 1% which would represent an overall higher energy density and power output than current lithium battery systems. The development of a porous burner system to efficiently convert the chemical energy of hydrocarbon fuels to useful power for portable electronics is very feasible.

Other Applications

Porous media combustion has a number of other applications including: blast furnace production of steel, agglomeration of ores, in-situ combustion, smoldering combustion, self-propagating high-temperature synthesis, catalytic combustion, household burners for air and warm water heating systems, premixed industrial burners, air-heating systems for dryers, gas turbine combustion chambers and steam generation [31, 50].

A number of studies have been performed investigated liquid fuel combustion in porous media. Itaya et. al developed a porous ceramic burner in order to investigate the combustion of liquid kerosene with future application aimed towards using porous media in Stirling engines, boilers and gas turbines. The liquid fuel was deposited drop-wise directly onto a 36% porosity mullite plate with a mean pore size of 180 μm. The burner showed a lean flammability limit of between 0.1-0.2 for various inlet flow rates and decreased NO_x emission [101]. Kaplan and Hall built a radiant burner and tested various design configurations using magnesia-stabilized zirconia, silicon carbide, and yttrium-stabilized zirconia porous ceramics. Heptane was impinged on the combustion section using an oil burner spray nozzle at 0.025 L/min. They tested each ceramic type with 4 ppcm and 10 ppcm in the stacked in various configurations along with two different spray nozzles. They concluded that the yttrium-stabilized zirconia matrix supported the most complete combustion but only for prevaporized fuels. The silicon carbide matrix melted at peak temperature. Complete combustion was achieved with the magnesia-stabilized zirconia matrix at a fuel flow rate of 0.025 L/m for equivalence ratios of 0.57-0.67 [102]. Liu and Hsieh experimentally investigated the combustion of liquid petroleum within porous heating burners. The flame temperature ranged from 1050-1250 °C, which is about 200 degrees lower than the adiabatic flame temperature for a corresponding equivalence ratio. The burner showed to have

45

very low NO_x and CO emissions and realized a lean limit lower than the standard flammability limit [103]. Jugjai and Rungsimuntuchart applied the concept of combustion in porous media to increase the efficiency of heat-recirculating domestic gas burners. They constructed a novel semi-confined porous radiant recirculated burner with stacked stainless steel wire meshes with 40 ppi. The new gas burner had an increased thermal efficiency of about 12% higher than that of the conventional one [104]. Agrawal and Gollahalli experimentally investigated the lean combustion of liquid fuels in a porous inert media. They tested different configurations of porous inert media with a 26 ppcm piece as the combustion section and varied the number of 4 ppcm pieces around it. They found that the burner best performed when there was a space between the combustion zone and injector, allowing the fuel to mix. The burner had significant radial heat loss and caused them to develop a prototype with an annular heat recirculation zone which proved to be more efficient, decreasing the formation of CO and NO_x [105]. Vijaykant and Agrawal experimentally investigated the combustion of liquid kerosene inside an SiC coated carbon foam. They tested an air-assist injector and a swirling-air injector at three different upstream locations as well as a number of stacked porous media configurations building on Kaplan and Hall's work with the goal of reducing the emissions of NO_x, CO and soot. They found that with a premix section greater than 45 cm, the fuel was fully premixed and had minimum emissions. An equivalence ratio of 0.63 was the lowest tested and showed the lowest CO and NO_x concentrations [106].

A number of people investigated the use of porous media in reciprocating heat or internal combustion engines. Weclas in 2005 wrote a general overview of various engine concepts, describing the porous structures, materials and their properties with respect to use in a porous medium internal combustion engine. The main benefits listed included: the ability to recirculate

46

energy between engine cycles, the material properties of the porous medium aided a very fast vaporization of the liquid fuel and the engine would exhibit more homogeneous combustion conditions [107]. Hanamura et. al. performed a numerical investigation on the use of porous media in a reciprocating heat engine similar to a Stirling engine. They noted that using a porous medium with a high absorption coefficient, the realized a maximum temperature was lower than the theoretical open flame temperature. The use of the porous medium extended the flammability limits for the combustion engine and proved a promising concept [108]. Durst and Weclas demonstrated the use of porous media in an internal combustion engines for the reduction of harmful emissions. They modified a single cylinder piston by placing a SiC porous media in the engine head between the intake and exhaust valve. Their experiments demonstrated a reduction of NO_x, CO, UHC and soot formation [27]. Macek and Polášek also predicted an improvement of emissions from reciprocating internal combustion engines with a homogeneous temperature field, an attribute of combustion in porous media. Their work mostly focused on the development of a numerical and CFD model to estimate the effects of the porous media within an internal combustion engine and used the code to evaluate possible future improvements [19,109].

A few studies were performed on the use of porous media for syngas and hydrogen production. Drayton et. al. experimentally investigated the production of syngas in porous media combustion by the partial oxidation of ultra-rich methane–air mixtures. They showed that a packed bed of Al_2O_3 spheres of diameters 2-5 mm could support combustion up to an equivalence ratio of 8. They conducted parametric studies on the effect of the equivalence ratio, filtration velocity, reactor pressure, and porous body diameter on combustion temperature. The burner achieved a maximum conversion rate of methane into 65% H_2, 75% CO_2, 10% C_2H_2, and 8% C_2H_4, each at separate conditions [110]. Bingue et. al. designed a burner for hydrogen

production. The burner used a packed bed of alumina pellets and a flow velocity of 12 cm/s. Six oxidizer compositions were investigated between 10 and 35% O_2 while varying equivalence ratio between 1 and 3.5. It was found that maximum hydrogen was produced for the 35% oxidizer mixture at around 2.9 equivalence ratio. Maximum CO was produced for the same oxidizer level at 2.5 equivalence ratio with higher percentages of oxidizer having a maximum product at higher equivalence ratios [111].

Dobrego et. al. numerically investigated the use of a porous media combustor for water purification of organic inclusions or solutes. The burner essentially evaporates the liquid water while simultaneously combusting the organic inclusions and proved to be a promising technology [112]. Avdic et. al. aimed to investigate and develop a household heating system utilizing porous media technology. The final result was a system with lower emissions of CO and NO_x, which could burn a mixture at 0.65-0.78 equivalence ratio at an increased thermal power modulation [16].

CHAPTER THREE: PRELIMINARY DESIGN AND ASSEMBLY

The purpose of the porous medium burner is to burn a lean mixture of fuel and oxidizer to convert the stored chemical energy into thermal energy within the combustion chamber. A thermoelectric device will be used to harvest that thermal energy and convert it into useful electrical energy. The porous burner prototype being used in the current study was designed and built by an undergraduate senior design group at the University of Central Florida, in the Department of Mechanical, Materials and Aerospace Engineering. The following sections were extracted from their final design report and updated for the current work [113]. Preliminary calculations and design were done to ensure the prototype will function as intended and are outlined in the following chapter, including an outline of the design guidelines and goals, computer modeling, heat transfer calculations, thermal expansion predictions and thermoelectric module cooling assembly design.

The CAD drawings were used to give a visual representation of the burner. The 2D drawings were made to aid in the construction and to machine the burner casing to specific dimensions and determination of an optimal material to be used while considering all tolerance. Preliminary heat transfer analyses predicted the thermal gradient within the burner to not only try to predict the heat output, and therefore power generation, but to be used to ensure that thermal expansion would be taken into account in the design. An assembly to house and cool the thermoelectric module was designed, including a thermal resistance element to ensure that the hot-side of the thermoelectric module would not exceed its maximum operating temperature. The cooling manifold ensures the best possible temperature gradient across the thermoelectric element for maximum power generation.

Preliminary Design Guidelines and Goals

A number of requirements were considered during the design and manufacturing of the burner and are listed below:

- The primary goal is to create a burner which will burn a lean mixture of fuel and air within a porous matrix, coupled with a thermoelectric device to harvest the thermal energy and generate power.

- The thermoelectric module should be cooled to meet its design specifications to generate the maximum amount of electrical power.

- The aim is to maximize the overall conversion efficiency, generate the most power with as lean a mixture as possible, to power portable electronic devices such as cellular/satellite phones, GPS devices or a laptop computer.

- Temperature measurements should be included in multiple locations within the burner to obtain an accurate temperature profile and should not interfere with the combustion reaction.

- Stabilization of the reaction at a fixed location within the central porous medium inside the porous reactor is required.

- Analysis of the thermoelectric module's output should be performed to determine the wattage, voltage and amperage of the system.

- The porous media and casing assembly must be designed so that the thermal expansion of the different materials does not damage the components.

- Flow controllers will provide inlet gases and must be able to adjust the concentration and flow rate of the reactant mixture to determine a lean operation limit.

- The porous media should be easily replaceable within the reactor in order to facilitate the testing of catalytic enhancement to the reaction.

- The burner is expected to be portable. Dimensions should be within 1m x 0.1m x 0.1m.

- The combustion zone should be a minimum of 400 K and should not be so high that the heat diffusion between the burner and thermoelectric module exceeds its maximum operating temperature or cause harm to any of the burner components.

- The burner should ignite the flame 95% of the time when turned on and used properly.

- The device should be robust enough to avoid damage from transportation or general use.

- The burner should have no risk of explosion, have no open flame, be capable of a quick shutdown, be well insulated and the exhaust must leave the device at a low velocity and safe temperature.

<u>Computer Aided Design</u>

The purpose of the CAD work was to provide detailed drawings of each part in two and three dimensions in order to visualize how the parts would be configured and to provide all dimensions necessary for the fabrication of any parts which needed to be manufactured. Shown in Figure 23 are the drawings used to manufacture and visualize the burner casing. The center of the casing is cylindrical in order to easily house the cylindrical porous alumina sections. The outside of the casing is rectangular in order for the thermoelectric module to lay flat against it for maximum contact surface. The burner is constructed of two separable halves in order to facilitate the removal and replacement of the porous sections for ease of use. A high temperature gasket material is used at all joining locations to ensure an air-tight fit even considering thermal

expansion of the parts. The material for the case is A36 Low Carbon type steel and was
machined at the University of Central Florida machine shop.
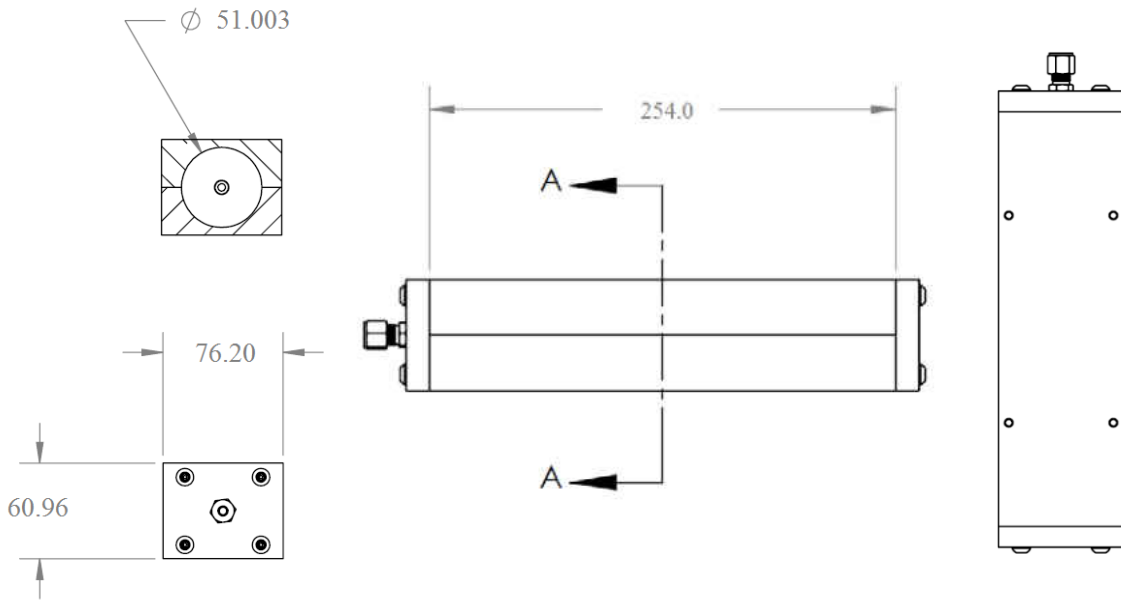
Figure 23. CAD drawings of the burner casing (in mm)
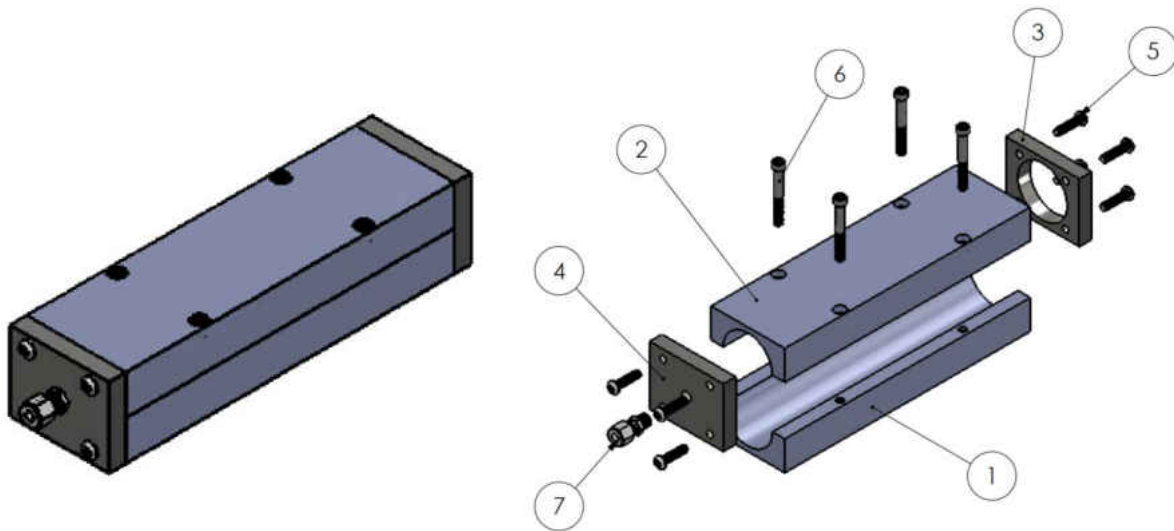
Figure 24. Shaded drawings of the assembled burner casing with exploded view

The casing assembly in Figure 24 consists of: 1) a bottom half to hold the porous alumina
media. 2) A top part which will be separated from the bottom half by a layer of gasket material to

ensure a good fit. 3) An end plate which will have a large enough hole to freely allow the combustion products to exit the burner. 4) An inlet plate which will screw into the top and bottom halves and be separated by a gasket material to ensure a good fit. 5&6) Screws which need special consideration so that they can withstand the high temperatures expected to be reached by the casing while not seizing in the casing. 7) A screw nozzle on the inlet plate to connect the hosing carrying the reactant flow to the burner.

Heat Transfer Analysis

The casing of the burner is made out of A36 steel. It is a good heat conductor and easy to work with when manufacturing. The exterior rectangular shape is a good base to place the thermoelectric devices as they are flat and will allow maximum contact surface between them. The original senior design group a designed the burner to optimize the power output of a thermoelectric module which required a heat flux of $350\ W$. They assumed a maximum internal temperature of 1020 K and calculated the thickness of the casing required to create the desired temperature drop to match the hot side operational temperature of the thermoelectric, 230 °C (~500K). To find the thickness of the casing with a heat transfer rate of $Q_0 = 350\ W$, hot side temperature of $T_{hot} = 1020\ K$, cold side temperature of $T_{cold} = 500\ K$, thermal conductivity of the steel casing $k = 51.9\ \frac{W}{m*K}$, and surface area of the thermoelectric module $A = 0.003136\ m^2$, Fourier's Law of heat conduction is used.

$$d = k \cdot A \cdot \frac{T_{hot} - T_{cold}}{Q_0} = 0.242\ m \tag{9}$$

From the calculations it can be seen that the thickness required for the casing is about 9 inches, too large to be practical, so in order to meet the compact design requirement, an element of thermal resistance was added between the casing exterior and hot-side of the thermoelectric

53

device. In order to find the best material to use, the temperature drop between the casing and the

thermal resistance was calculated. The depth of the thermal element was fixed to something

appropriate which was: $d = 0.25\ inch = 0.00635\ m$. The contribution from the metallic casing

was calculated to be minimal, 11 K, so the temperature drop needed was about 509 K. To find

the appropriate material for a resistance element between casing and thermal electric, Equation

10 was used with the given information.

$$k = \frac{Q_0 \cdot d_{element}}{(T_{hot} - T_{cold}) \cdot A} = 1.392 \frac{W}{m \cdot K}. \tag{10}$$

The thermal conductivity came out to be $1.392\ \frac{W}{m \cdot K}$. A good material to use with the closest

thermal conductivity is quartz, with a thermal conductivity of about $1.4\ \frac{W}{m \cdot K}$.

Thermal Expansion Analysis

The thermal expansion and stresses due to the temperature gradients within the burner during

normal use, specifically the interaction between the porous medium and the casing, are

evaluated. The casing is constructed of A36 steel and for the porous matrix material alumina is

used. If the casing expands more than the porous matrix, a gap would form around the porous

plugs, allowing flow to bypass the matrix. The alumina matrix is very brittle material, and if it

was to expand more than the casing, the ceramics alumina could easily crack. Thermal expansion

in a one dimensional model in the radial direction is calculated using Equation 11.

$$r_f = r_i \alpha \Delta T_{max} + r_i \tag{11}$$

The thermal expansion for the casing is calculated with the coefficient of A36 Steel as

$\alpha_c = 11.7 * 10^{-6}\ K^{-1}$, a maximum temperature change of $\Delta T_{max} = 11\ K$ coming from the

54

preliminary heat transfer analysis in the previous section, and the initial radius, one can find the final radius that casing will have after the change.

$$r_f = 0.025502\alpha_c\Delta T_{max} + 0.025502 = 2.540229 * 10^{-2}m \qquad (12)$$

It can be seen that the final radius for the casing will be 0.02540 m which is very minimal since it is only ten thousandths (0.000102 m) from the initial radius.

Calculating now the thermal expansion for the porous alumina, with the coefficient of thermal expansion for the alumina itself, $\alpha_c = 8.2 * 10^{-6} \ K^{-1}$, its initial radius of 0.0254 m,A temperature gradient of 503 K, and the same equation:

$$r_f = 0.0254\alpha_c\Delta T_{max} + 0.0254 = 2.5504882 * 10^{-2}m \qquad (13)$$

The temperature changes insides of the alumina will not be a large factor concerning the dimensional changes of the porous alumina. Total radius change between the initial and final is approximately only ten thousandths (0.000105 m) as well. The total difference between the final radius of the porous alumina and the final radius of the casing is$1.03 * 10^{-5}m$. The temperature gradient within the casing and porous alumina is not be expected to cause any damages or significant gaps to form in the system.

Thermoelectric Assembly and Cooling

The thermoelectric module assembly is the assembly of parts attached to the steel case which harvest the heat and generate electricity. These parts include the thermal resistance quartz plate, the thermoelectric module, and the impinging jet manifold to cool the thermoelectric module. The quartz plate serves the purpose reducing the heat passing through the steel so that the thermoelectric module does not overheat. The power generated by the thermoelectric module is

a function of the temperature gradient across it. In order to maximize the power output of the module, the cold side needs to be cooled. An aluminum heat sink was originally chosen in the preliminary design, which allowed natural convection to dissipate heat from the cold side of the thermoelectric device. This did not provide enough cooling and was replaced by the impinging jet manifold to reach the desired cool-side temperature of 50-75°C. The manifold is designed to sit on top of the thermoelectric module and provide a 1.5 mm gap between the jet nozzles and the surface of the module. The cooling air enters the manifold inlet, passes through the nozzles and onto the surface of the thermoelectric and then flows up through the slotted depletion areas and through the manifold outlet. The holes are designed to be 0.25 mm diameter to provide the necessary amount of heat transfer. The depletion slots are meant to reduce the boundary layer accumulation caused by several jets overlapping. The inlet and outlet will be fitted with male hose fittings.

The dimensions for the thermoelectric module are very important characteristics in the design of the cooling manifold. This assembly was originally designed for the commercially available thermoelectric device from Thermal Electronics Corporation, Aurora, ON, Canada. The part number is TEG1-1263-6.0 which is 56mm by 56mm in size. It has match load output current and voltage of 3.5A and 4.2V respectively, which produces an estimated power output of 14.7W.

The surface area of this module is therefore $A = 3.136 * 10^{-3} m^2$. Using the area, one can now find the heat flux for through the module with Equation 14 where q = 350 W from the part specification.

$$q'' = \frac{q}{A} = 1.116 * 10^5 \text{ W/m}^2 \tag{14}$$

Assuming a maximum temperature difference of 100 K between the cooling air and the surface of the module, the minimum average heat transfer coefficient can be calculated. This can be used to determine the diameter of the holes for the impinging jet system. The heat transfer is found to be:

$$h = \frac{q''}{\Delta T} = 1.116 * 10^2 \frac{W}{m^2 \cdot K} \tag{15}$$

Now that the heat transfer has been found, the diameter for the impinging jet holes can be calculated with $k_{air} = 0.025 \frac{W}{m*K}$ as the thermal conductivity of air at 350 K.

$$D = \frac{Nu \cdot k_{air}}{h} = 4.48 * 10^{-4} \, m \tag{16}$$

where D is the diameter of the jets and the average Nusselt number for array of impinging jets , is Nu=20, based on experimental findings of Dr. Mark Ricklick and Near Wall Cooling experiments. Dr. Ricklick, a professor at UCF, was consulted by the senior design team for this calculation. Since it is better to have a smaller change in temperature, it is important to have a larger heat transfer, and a smaller jet diameter; however, the smaller the hole, the larger the difficulty to machine them. A compromise must be made between the cost of the machining the manifold and the efficiency of the heat transfer. The manifold assembly is shown in Figure 25.

The size of the original thermoelectric module is 56 mm square, and has a maximum powered output of 14.5 W. The maximum temperature that the TEG modules can withstand is 500 K. It was calculated that with the steel case, the temperature of the case would be 1009 K at the outer surface. To create a safe temperature for the TEG module, it was devised that a quartz plate with low thermal conductivity could be placed between the steel case and TEG. The thickness required was found to be 6.35 mm; a plate 63.5 mm square and 6.35 inch thick was found. The manifold assembly will be clamped to the case using C-clamps for easy attachment.
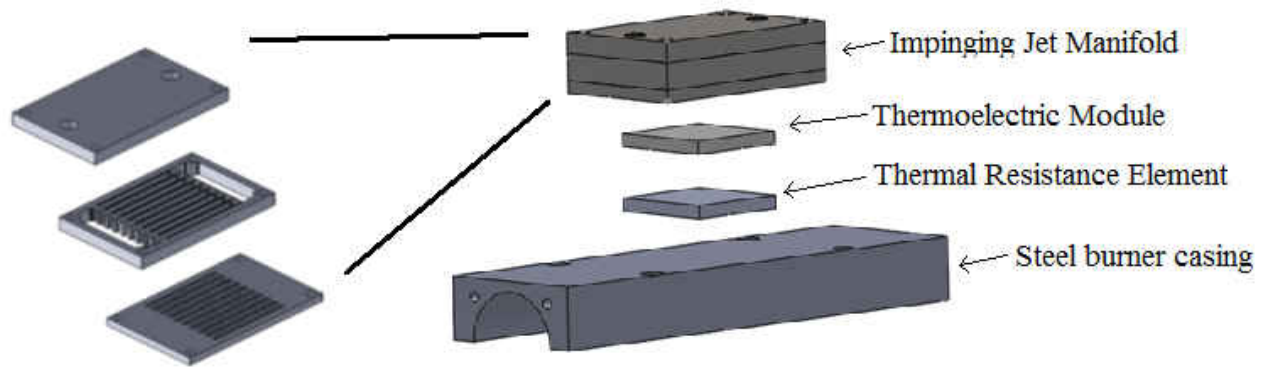
Figure 25. Thermoelectric module cooling assembly

Burner Construction

Construction of the burner was done in Dr. Ruey-Hung Chen's lab at the University of Central Florida. All the casing parts were machined at UCF machine shop. Figure 26 shows the manufactured burning casing, gasket material and porous plug assembly. The gasket material was cut by hand with a rotary tool and drill press to fit in between the two halves of the burner casing and the end caps. The porous alumina was placed inside the casing and finally the two parts of the casing were screwed together with the end caps.

The burner utilizes an intermittent spark igniter which was fed through the upstream honeycomb section as shown in the bottom left photo of Figure 26. The inlet gases are separately controlled by flow controllers during experimental testing. Two flow meters shown in the bottom right photo in Figure 26 were used during the preliminary tests. The methane and air inlet hoses combine at 'T' junction, with the hosing fastened to the front end plate at the other end, of sufficient length to allow mixing. The casing was covered with insulation except the portion where thermoelectric module was placed and the exhaust section. Pictures of the insulated assembly on fire bricks are shown in Figure 27.
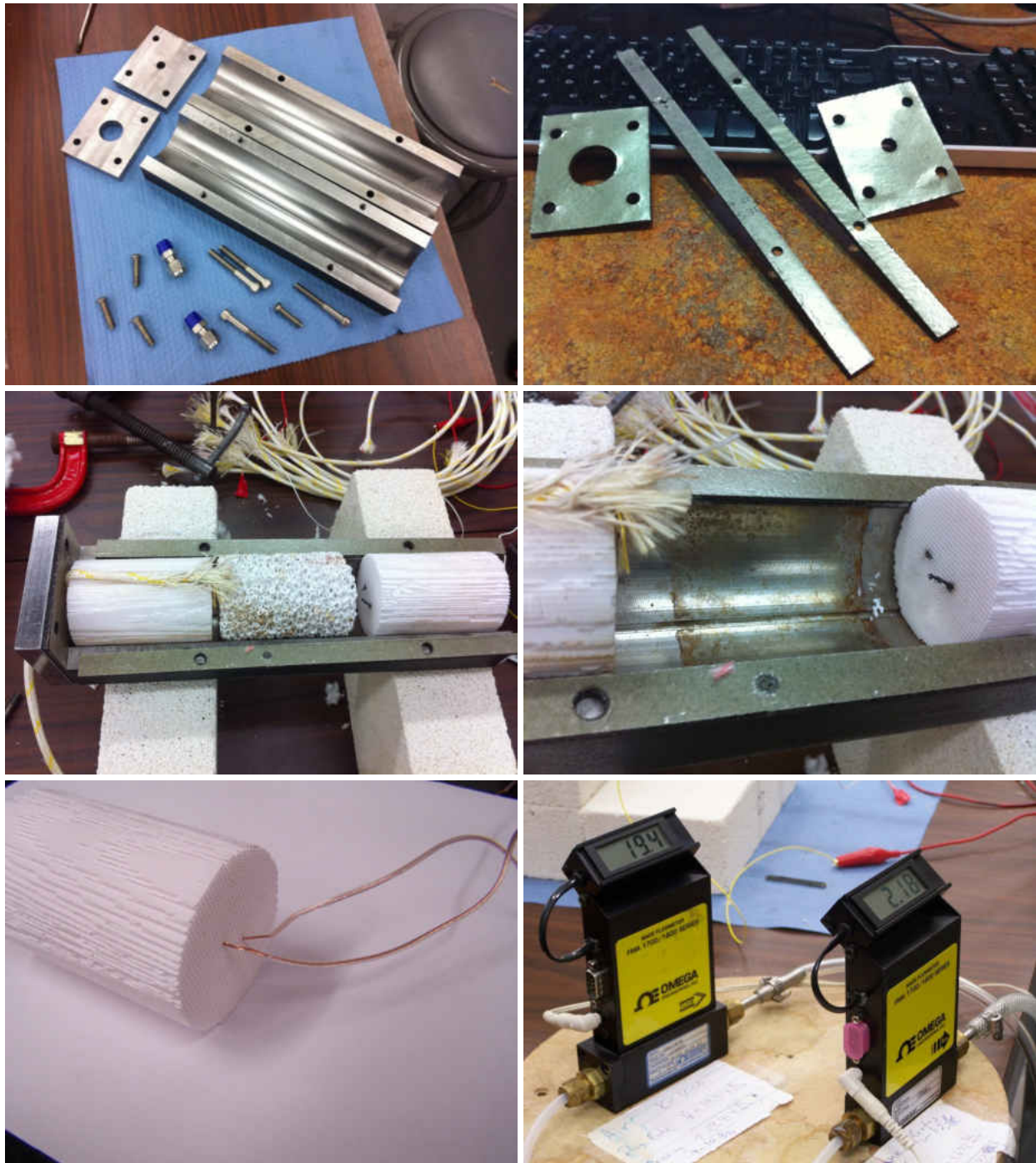
Figure 26. Burner casing, gasket material, burner interior and position of igniter
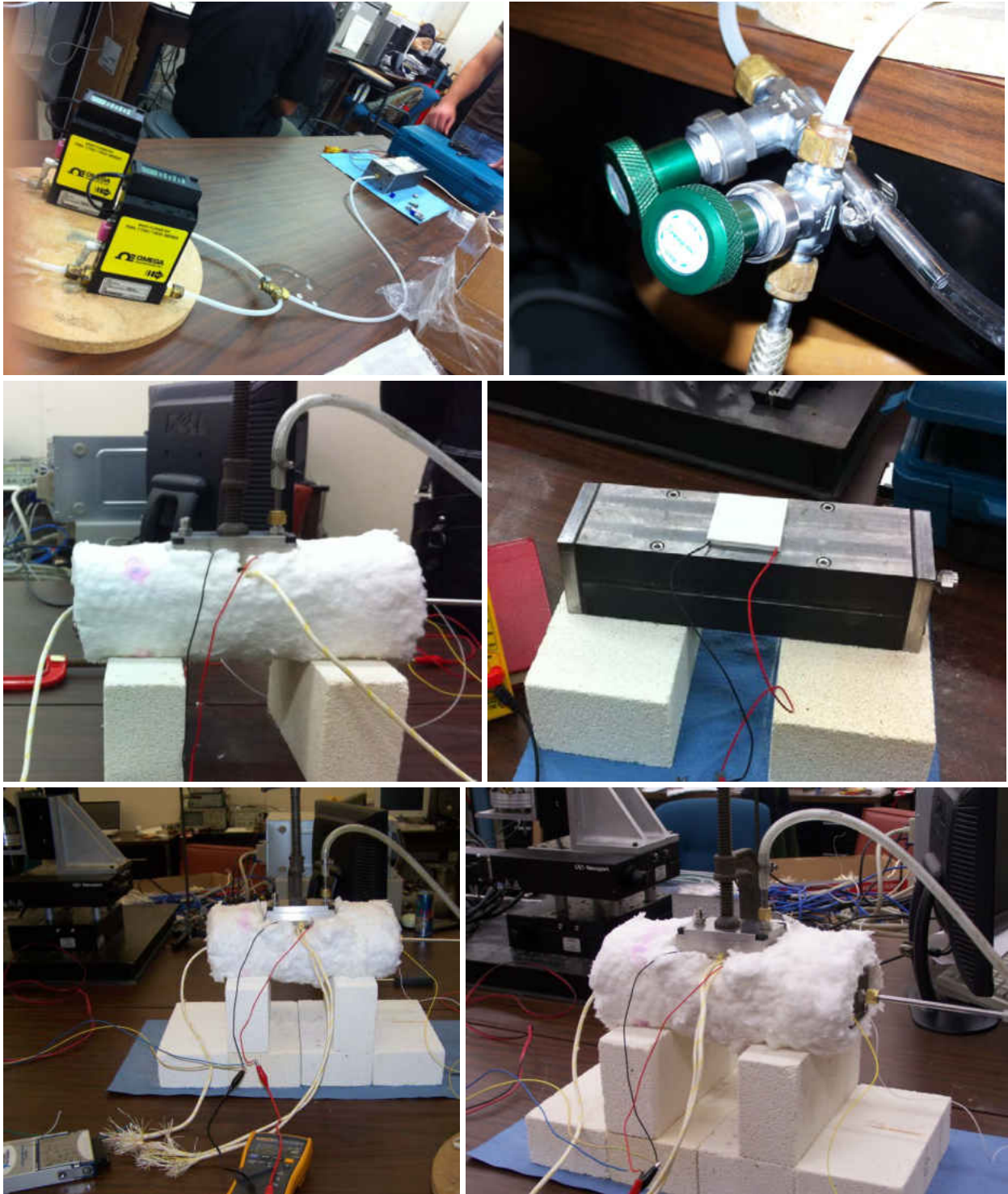
Figure 27. Flow meters, control values and insulated burner assembly

The temperature profile is measured using K-type thermocouples which are connected to a DAQ system and the measurements are viewed using Lab View Signal Express. The burner assembly and thermocouple positions are shown in Figure 28. The parts are labeled as follows: 1) Impinging jet cooling system, 2) Thermoelectric module, 3) Quartz thermal resistance plate, 4) Metallic casing, 5) Low porosity section, 6) Inlet plate, 7) Exhaust side plate, 8) High porosity section for combustion stabilization. The burner was assembled in a fume hood to collect exhaust gases as shown in Figure 29 and 30 with an overall schematic as Figure 31. The testing procedure is detailed in the next chapter.
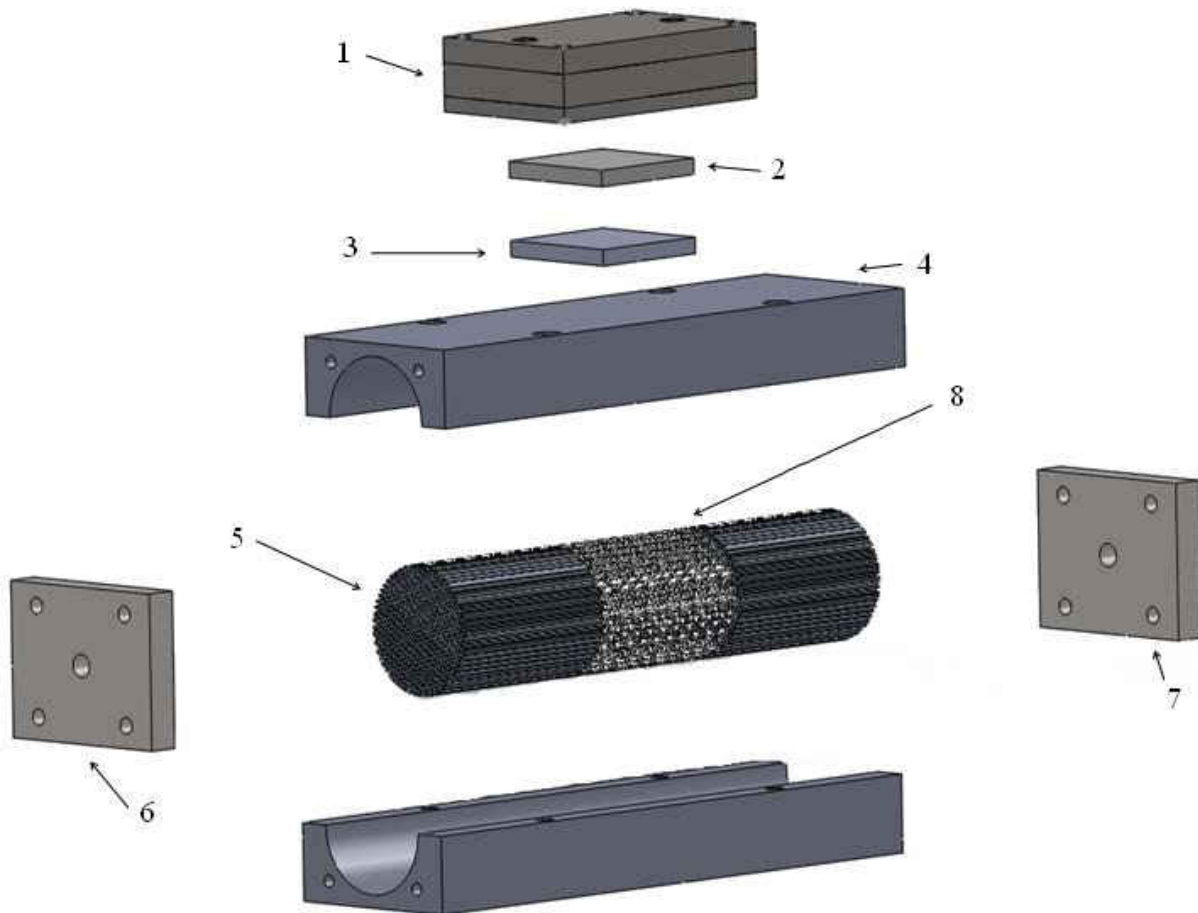
Figure 28. Exploded view of porous burner assembly

Figure 29. Final burner assembly in fume hood
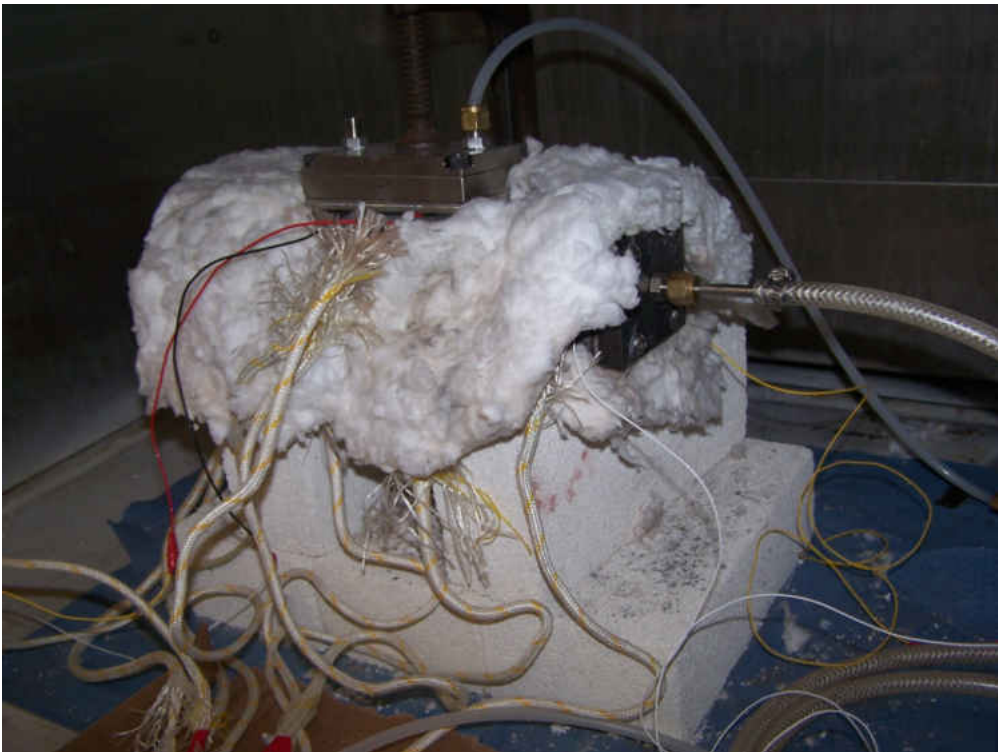
Figure 30. Side view of final assembly
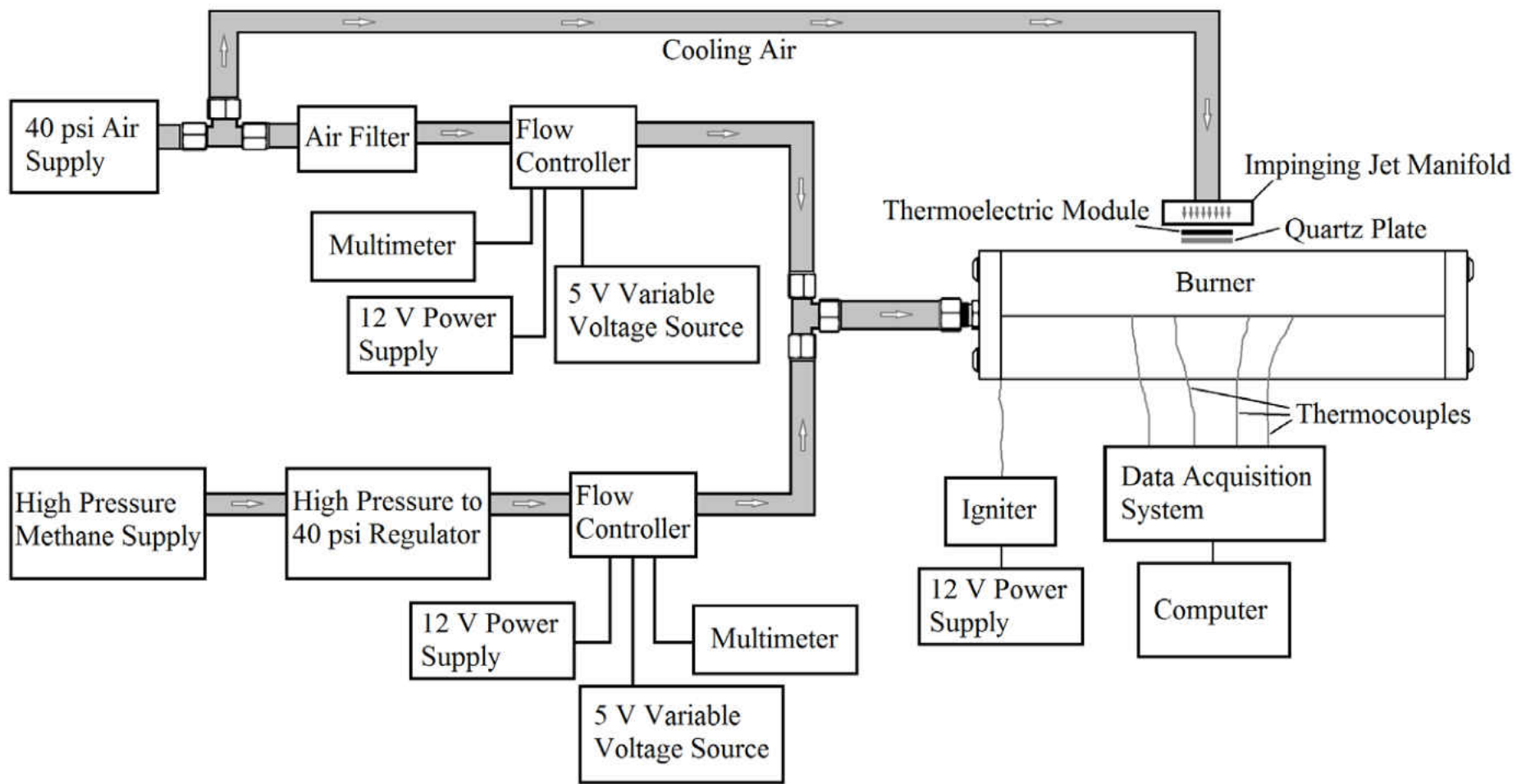
Figure 31. Overall burner system schematic

<u>Design Summary</u>

The final design of the porous media burner for super-adiabatic combustion includes the following parts:

- A rectangular steel casing with a cylindrical interior to house the porous sections.

- A high porosity 99.5% pure alumina reticulated foam (76.2 mm long and 50.8 mm in diameter, porosity of 80%, 20 ppi) that will contain the flame as the central section and transport heat to the casing. Supplied by Süd-Chemie Hi-Tech Ceramics.

- Two lower porosity alumina honeycomb sections (400 cells per square inch) before and after the central section to keep the flame confined. Supplied by Applied Ceramics.

- A thermoelectric device to harvest the heat released by combustion. The current work uses a commercially available Bi_2Te_3 alloy module from Marlow Industries, Inc., model number TG 12-8-01-L. It has a maximum no-load power output of 7.95 W and hot-side temperature limit of 250 °C and 4.97% conversion efficiency.

- A quartz plate to limit the temperature of the hot-side of the thermoelectric.

- An impinging jet manifold to cool the cool-side of the thermoelectric to maximize the temperature gradient, and therefore power output, of the thermoelectric module.

- The flow controllers used to measure the incoming air and fuel flows are OMEGA FMA-3206 models.

- The filter used for the reactant air flow is an Ingersoll Rand 3/8" NPT (F) Air Line Filter.

- The variable voltage sources used as inputs to the flow controllers are GW INSTEK PSS-2005 Programmable Power Supplies.

- The data acquisition system used is a National Instruments USB-6210 16 inputs 16-bit 250 kS/s Multifunction I/O.

- Eight type-K insulated thermocouples to obtain an accurate temperature profile within the burner and to measure the temperature difference across the thermoelectric module. Supplied by OMEGA, #XC-K-24-25, 24awg gauge, rated to 1200 °C.

- KLINGERsil Milam Laminate , Type PSS , high temperature, 1600 °F, gasket material is used between the joining sections of the casing. Supplied by Macroseal, Inc.

- Durablanket S type insulation was used, made from spun ceramic fibers, rated up to 1260 °C. Supplied by Unifrax Corporation.

- The igniter used has a power supply of 117 V and 10 mA firing at a rate of 4Hz.

The metallic burner casing allows for good heat conduction and with a flat exterior is very suitable to mount the thermoelectric module assembly and at the same time provide a stable housing for the porous alumina sections. The casing is split into two separable parts and is sealed with a high temperature gasket to allow of easy replacement of the porous alumina sections. Thermal expansion analyses were conducted to ensure no gaps or untolerable stresses would occur. Preliminary heat transfer calculations were performed and it was found that it is necessary to include a layer of thermal resistance between the casing and the hot-side of the thermoelectric module. A value of $1.392 \frac{W}{m \cdot K}$ for the thermal resistance element was calculated and quartz was chosen with a thermal resistance of about $1.4 \frac{W}{m \cdot K}$. Five of the thermocouples are located inside the metal casing within the flow and 3 are located outside the casing, detailed in the next chapter,

CHAPTER FOUR: TESTING AND EXPERIMENTAL RESULTS

The purpose of these tests is to determine the effectiveness of a catalytic coating on the overall efficiency of a porous media burner. In order to achieve this goal the following well defined and interrelated tasks are performed. Task 1 is the preliminary testing of the designed burner. Initial runs are conducted to determine the functionality of the burner and to determine an optimal flow rate at which to conduct testing. Task 2 includes the selection of a catalytically active coating which is expected to allow a leaner fuel concentration to be burned, improving the overall conversion efficiency of the system. Task 3 outlines the coating procedure for the deposition of a powdered ceramic catalyst onto the central porous alumina section. Task 4 is the characterization of the catalyst coating with Scanning Electron Microscopy (SEM). Images will be taken for both the inert and coated central sections, before use, and after use at both an interior and exterior section of the central porous matrix. These images will be used to determine if the catalyst was active during the combustion process. Task 5 will detail the measurement of the thermoelectric module's output. The experimental procedure to be followed for the testing will be discussed and the experimental results will be presented.

Task 1 – Preliminary Testing

The prototype porous burner was assembled and tested without a catalytic coating on the central section. A stoichiometric ratio of methane and air was burner for preliminary testing. Temperature measurements were taken in several locations: 1) five locations inside burner, 2) one between the casing of the burner and the protective quartz plate, 3) one between the quartz plate and the hot-side of the thermoelectric device, and 4) one on the cool-side of the thermoelectric device. The quartz plate in the current design was specifically used to protect the

thermoelectric device from overheating by the heat generated in the porous burner. Alumina honeycomb is used as the two outer sections of the burner and a highly porous, 80%, alumina reticulated foam is used as central section to stabilize the flame.

The flow controllers were tested and calibrated before use. The flow controllers were attached to a bubble testing apparatus, a glass tube marked with volumes with a small amount of soapy water at the bottom shown in Figure 32. Injecting gas from the flow controllers through the soapy water caused bubbles to be formed inside the glass tube. Recording the time it took for the bubbles formed to fill a certain volume gave the flow rate in liters per minute and when compared to the readings from the flow controllers, allowed the calculation of a conversion factor for each flow controller. The data is provided in Table 2 for the methane controller and Table 3 for the air controller. A linear curve fit was done on the data and the resulting conversion factor for the air flow controller was 1.0374 and 1.094 for the methane flow controller.
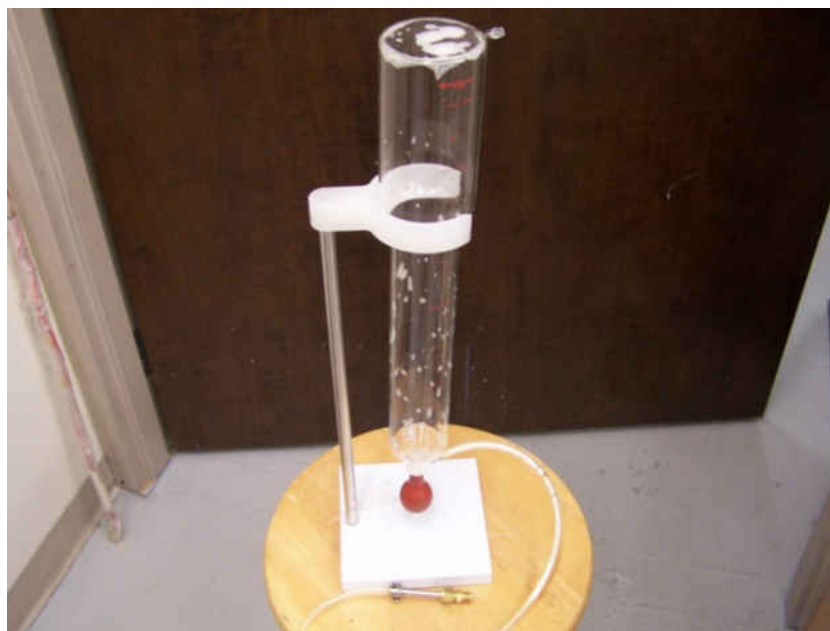
Figure 32. Bubble testing apparatus for calibration

Table 2. Bubble test results for calibration of methane flow controller

Controller output (L/min)	Volume filled (L)	Time (s)	Measured flow (L/min)	Ratio
0.99	0.8	43.87	1.09	1.105
0.99	0.8	43.41	1.11	1.117
0.79	0.8	56.42	0.85	1.077
0.79	0.8	55.11	0.87	1.103
0.59	0.8	74.98	0.64	1.085
0.59	0.8	74.80	0.64	1.088
0.39	0.4	58.35	0.41	1.055
0.39	0.4	57.83	0.42	1.064
0.195	0.2	65.29	0.18	0.943
0.195	0.2	66.45	0.18	0.926

Table 3. Bubble test results for calibration of air flow controller

Controller output (L/min)	Volume (L)	Time (s)	Measured flow (L/min)	Ratio
0.98	0.75	42.24	1.07	1.092
0.98	0.75	41.59	1.08	1.102
0.98	0.75	41.67	1.08	1.102
0.98	0.75	40.49	1.11	1.133
2.00	0.75	20.47	2.20	1.100
2.00	0.75	20.18	2.23	1.115
2.00	0.75	20.28	2.22	1.110
2.00	0.75	20.60	2.18	1.090
4.02	0.75	10.52	4.28	1.065
4.02	0.75	10.46	4.30	1.070
4.02	0.75	10.46	4.30	1.070
4.02	0.75	10.63	4.23	1.052
6.20	0.75	7.37	6.11	0.985
6.16	0.75	7.26	6.20	1.006
6.26	0.75	7.32	6.15	0.982
6.16	0.75	7.22	6.23	1.012
8.32	0.75	5.30	8.49	1.021
8.26	0.75	5.29	8.51	1.030
8.30	0.75	5.27	8.54	1.029
8.32	0.75	5.31	8.47	1.019
10.18	0.75	4.13	10.90	1.070
10.22	0.75	4.21	10.69	1.046
10.18	0.75	4.22	10.66	1.047
10.12	0.75	4.14	10.87	1.074

A trial and error test was done to determine the optimal flow rate for the reactant mixture. Ignition was attempted while varying the flow mixture from 7.5 L/min to 40 L/min and the burner most quickly and stably ignited with an inlet flow rate of 11.5 L/min. This flow rate is kept constant during all the experimental testing.
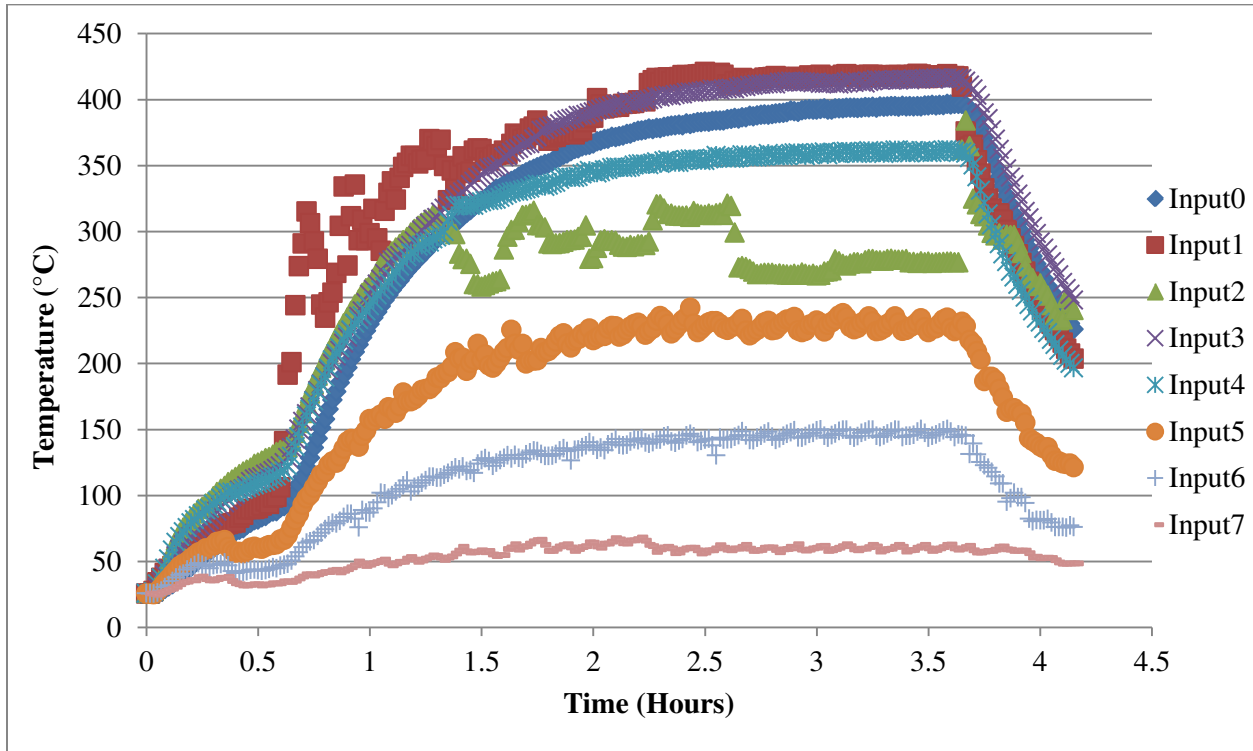
Figure 33. Temperature plot for inert section at stoichiometric mixture with quartz plate

The temperature profile shown in Figure 33 is from a preliminary run. Each dataset corresponds to an individual thermocouple, matched with its corresponding location in Table 4 and Figure 34. From Figure 33 we can see that the outside of the casing of the burner, Input 5, is no hotter than 250 °C. This means that since our thermoelectric can withstand up to a 250 °C temperature on its hot-side, that the presence of the quartz plate to lower the temperature is not necessary. For the experimental tests detailed later on, the quartz plate was removed and only

Inputs 0-5 and Input 7 will be included, since the hot-side of the thermoelectric will be in direct contact with the casing.

Table 4. Detailed thermocouple placement locations

Data set label	Thermocouple location
Input0	Before inlet honeycomb section, 12.7 mm (1/2 the radius) out from the radial center
Input1	Between the inlet honeycomb and the central foam section, 12.7 mm (1/2 the radius) out from the radial center
Input2	Between the central foam section and the exit honeycomb, placed at the radial center
Input3	Below the central foam section, direct bottom middle of the combustion chamber
Input4	Above the central foam section, direct top middle of the combustion chamber
Input5	Outside of the burner casing, middle of the top surface, underneath the quartz plate
Input6	Above quartz plate, bottom (hot) side of the thermoelectric device
Input7	Top (cold) side of the thermoelectric device

Figure 34. Illustration of thermocouple locations

The selection of a catalytically active material to facilitate the combustion reaction is an important task. As a coating, both oxides and non-oxide ceramic compositions were considered. For oxides, two classes of ceramics were considered. One class was mixed ionic electronic cond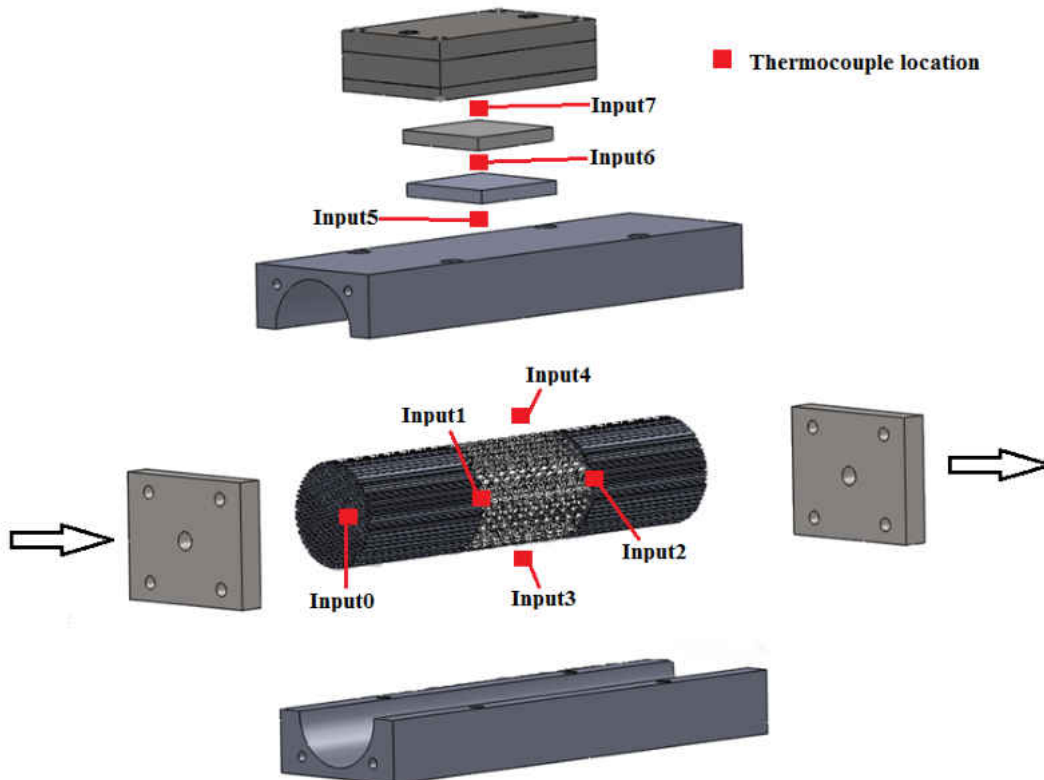ucting perovskites with different ions residing on A and B sites of the ABO_3 perovskite structure. Another class of oxides was the fast ionic conductors with a fluorite structure. From the group of non-oxide ceramics, boron rich compositions, ceramics containing tungsten (W) as one of the elements and SiC are possible catalysts. $LaCoO_3$, $LaMnO_3$, $LaFeO_3$, and $LaCrO_3$ based perovskites were one of the groups of materials of high interest. For example, $La_{0.7}Sr_{0.3}Fe_{0.95}Ru_{0.05}O_3$ perovskite exhibits high ionic and electronic conductivity and is an excellent catalyst that significantly promotes oxygen reduction and, therefore, should actively facilitate a combustion reaction [114,115,116]. Co^{3+}/Co^{4+} were also of extreme interest as cations of very high catalytic activities, so perovskites with Co content on the B site were carefully considered. Another group of ceramics considered is a group of conductors with fluorite structure. CeO_2 doped with Gd_2O_3 and Sm_2O_3 are intensively used as a coating with a fluorite structure. 10-20mol% Gd_2O_3 - 90mol% CeO_2 and 10-20mol% Sm_2O_3 - 90mol% CeO_2 have very high oxygen conductivity, are easily reduced in a reducing environment and become an electronic conductor upon reduction. Gadolinia and samaria doped cerias are well known for their superior properties to facilitate fuel oxidation reactions and, therefore, will also promote combustion [117,118]. What is known of boron rich solids is that the catalicity of pure ZrB_2 is very different than the catalicity of ZrB_2-SiC compounds which are used as leading edges in hypersonic vehicles. ZrB_2 and HfB_2 are candidate materials to use as a catalytic coating. Another candidate of the non-oxide boron rich ceramics that was considered was B_4C. However, the use

of WC powder as a coating is better justified since WC is a good catalytically active anode that is a very promising material to facilitate the hydrogen oxidation reaction in solid oxide fuel cell, if it does not present a problem by oxidizing.

SiC was ultimately decided on as the trial catalyst from advice by Dr. Orlovskaya, project advisor, and being readily available and inexpensive.

<u>Task 3 – Catalyst Coating</u>

The catalytic powder of intrest was coated on the central porous section using a dip coating technique, shown in Figure 35. Dip coating is a very simple slurry coating technique which refers to a) immersing a sample (in this case a porous ceramic foam) into a tank containing a slurry with the coating material; b) keeping the sample in the slurry for a specific amount of time, allowing the coating to bond to the surface; c) removing the sample from the tank and allowing the sample with coating to drain and dry.
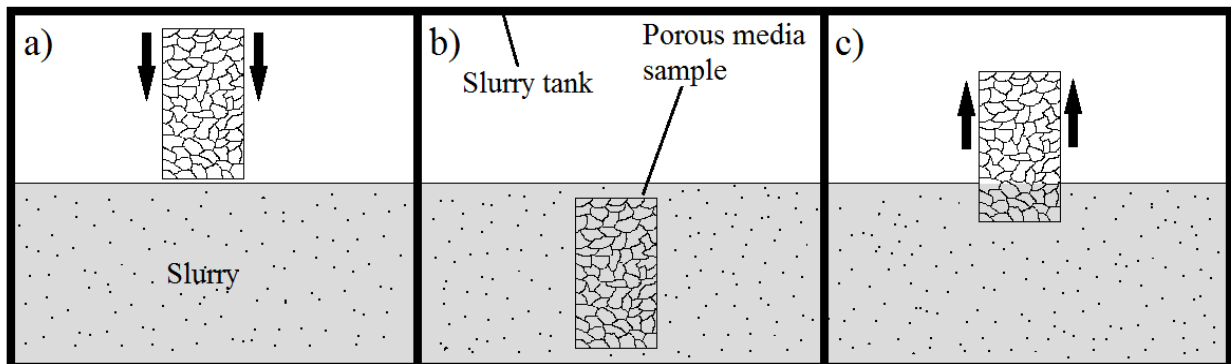
Figure 35. Dip coating procedure of central porous foam section

Dip coating is very straightforward and is the most suitable technique for this purpose since the porous structure and its surface are difficult to coat using other methods, such as spray deposition or sputter coating. Immersing the matrix in the slurry will ensure that all or almost all of the available surface will be covered with coating. The success of dipping depends on the

viscosity of the slurry in the dip tank. The dip coating solution is made by mixing the ceramic powder with propan-2-ol. Efficient mixing of ceramic powder with a solvent will be performed using ultrasound which will allow both an efficient homogenizing and stabilized suspension. In order to determine the loading of the porous burner with ceramic coating, the weight of the central porous part will be measured before deposition and after each deposition. Such measurements will determine how much coating was deposited and is available to promote combustion. If the coating thickness/loading was too little, then repetitive dipping into the slurry will be made, with each dipping followed by slow and consistent drying to ensure that there is no spallation and delamination of the coating layers after deposition. The goal is to develop a homogenous porous coating with high specific surface area strongly attached to the surface of the porous matrix. Three sections were dip coated with SiC as shown in Figure 36. Through trial and error, an optimal mixture ratio of 45 g of SiC powder to 100 mL of propan-2-ol was determined. This produced the desired viscosity necessary to coat the interior surface of the porous media. Three alumina sections were dip coated, covered and allowed to dry for 24 hours. A second dip coating was deemed necessary for an even and complete deposition of the catalyst. The sections were placed back to dry with the reverse side upwards, allowing them to drain in the opposite direction, providing a more even coat. Weight measurements were taken with just the initial alumina sections, after the first dip coating and after the second dip coating to determine how much of the catalyst was deposited and are listed in Table 5.

Table 5. Dip coating weights (in grams)

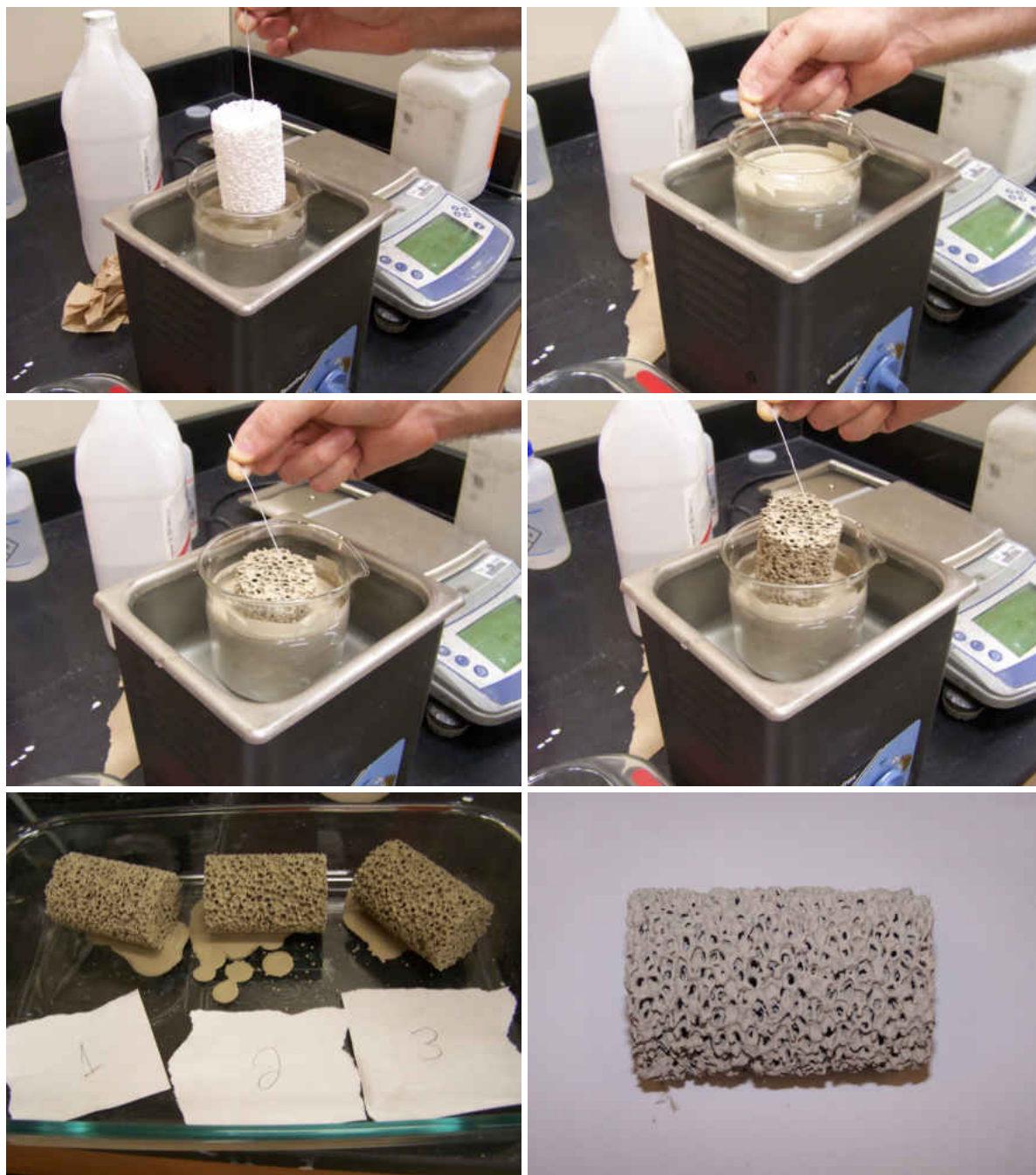| Section #	Before dip coating	After 1st dip	After 2nd dip	Deposited Catalyst
1	108.95	115.01	121.20	12.25
2	117.59	126.68	136.70	19.11
3	120.66	130.29	139.70	19.04

Figure 36. Photos of dip coating procedure and resulting coated central sections

The top four photos in Figure 36 depict the dip coating process. The beaker containing the slurry mixture was placed in a water bath within the ultrasound machine, ensuring homogenization of the slurry. The alumina section was slowly lowered into the slurry by hand, held suspended as to not come in contact with the bottom or sides of the vessel for 60 seconds then slowly removed. The bottom left photo shows all three sections sitting to dry and the bottom right photo is a close up of one of the sections completely dry after the second coating.

<u>Task 4 – Coating Characterization</u>

Both the inert alumina porous media and a section with deposited catalytically active coatings were characterized using Scanning Electron Microscopy (SEM). SEM is an important microscopy technique which is indispensable to characterize the morphology and surface specifics of the coating. The surfaces were characterized at 500x and 5000x both before the combustion reaction to determine the quality of the surface and after combustion in order to detect changes which would help to clarify how the material affected combustion. Grain size and inhomogeneity in the material is studied with particular interest in the microstructural and compositional changes in the catalytic coating as a result of combustion.

The micrographs of uncoated alumina surfaces are shown in Figure 37 with A&B being before testing, C&D from and outer edge of the porous section after testing and E&F from an interior section, closest to the igniter and combustion reaction. The surface of alumina before testing in the lower magnification image, Figure 37A, shows a rather homogeneous grain size and grain size distribution with no excessively large grains present. The surface termination steps can be found at the surface of alumina and more morphological features of the grains can be seen at the higher magnification, shown as Figure 37B. The overall alumina surface is clean from

external impurities and no deposits can be found. After testing with this piece of porous media in the reactor, certain amounts of deposits can be detected, shown in Figures 37C through F. The amount of the deposits is less for alumina on the outer edge of the combustion chamber, Figures 37C and D, with larger quantities of deposits seen at the location near the center of the reactor, where most likely the combustion reaction occurred, Figures 37E and F. Most likely the deposits are products of incomplete combustion and their source and chemical nature has to be studied in further detail.

The surfaces of the porous media after dip coating with the catalytically active SiC ceramic layers are shown in Figure 38. While grain size of alumina without coating is rather large (3-5 micron) the particles of SiC powder are all in the range of less than 1 µm and one can see that the alumina surface is homogeneously coated with SiC before testing (Figure 38A) and the grain size is rather small (Figure 38B). The surface of alumina coated with SiC after use in the combustion chamber in an outer area of the combustion chamber is shown in Figures 38C and D. The surface is still rather homogeneous, Figure 38C, but at high magnification one can see that the surface of alumina is not coated completely with SiC, as a layer of Al_2O_3 grains is still visible, with small SiC particles deposited in different selected locations, shown in Figure 38D. The alumina surface coated with SiC particles nearest to the combustion zone is shown in Figures 38E and F. Some contamination and non-homogeneous areas are visible with no clear deposits (Figure 38E), but at higher magnification one can see that morphology of the SiC fine grains has slightly changed from irregular sharp corner shapes in the unused section (Figure 38B) to a more smooth and rounded morphology after particles were exposed to the combustion (Figure 38F). No visible deposits can be detected on the surface, which might mean that all byproducts of combustion are used by the catalytically enhanced media.

76
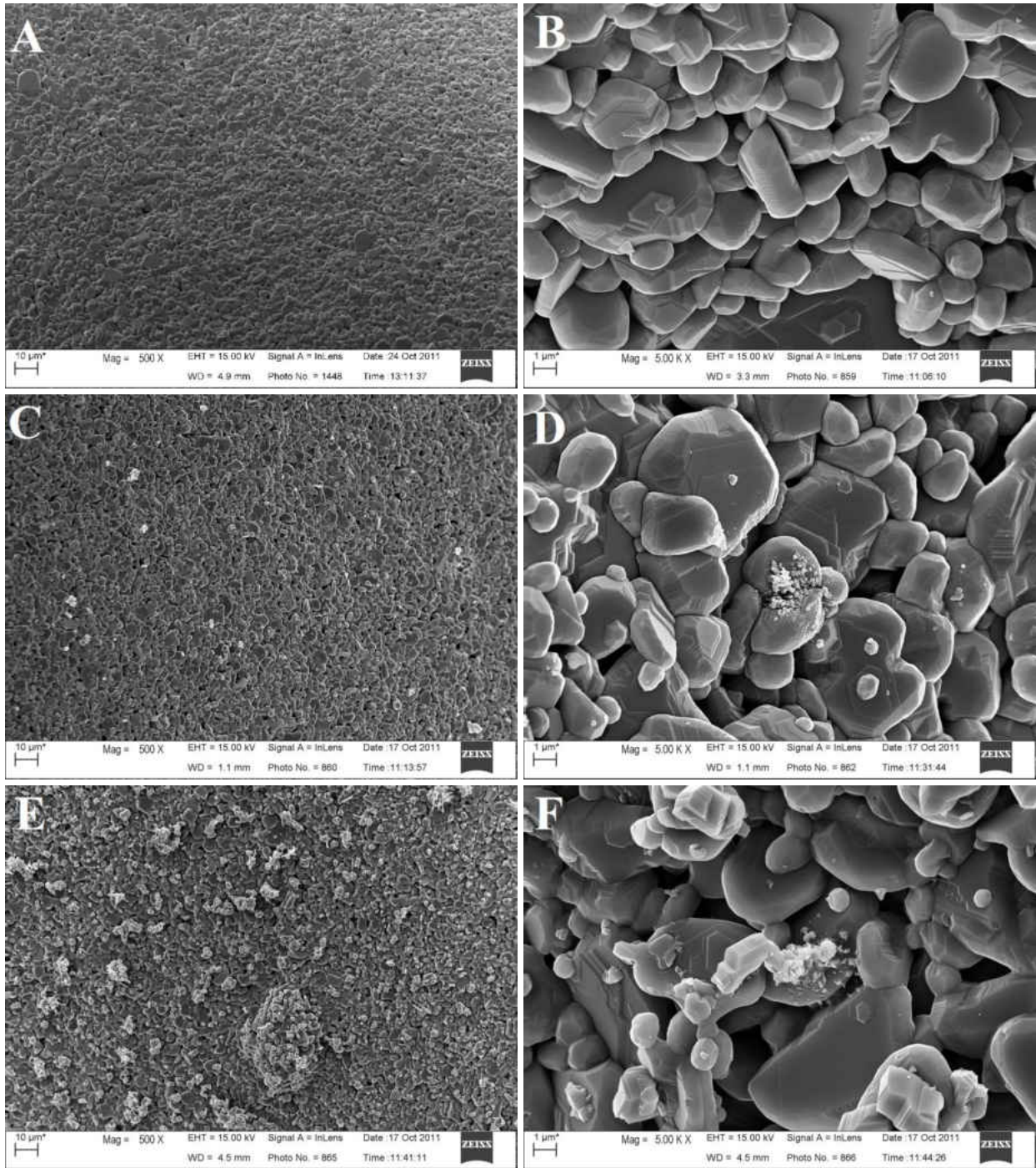
Figure 37. SEM pictures of Al_2O_3: unused (A&B), used at the outer (C&D) and inner (E&F) areas of the combustion chamber at magnifications of 500x (left) and 5000x (right)
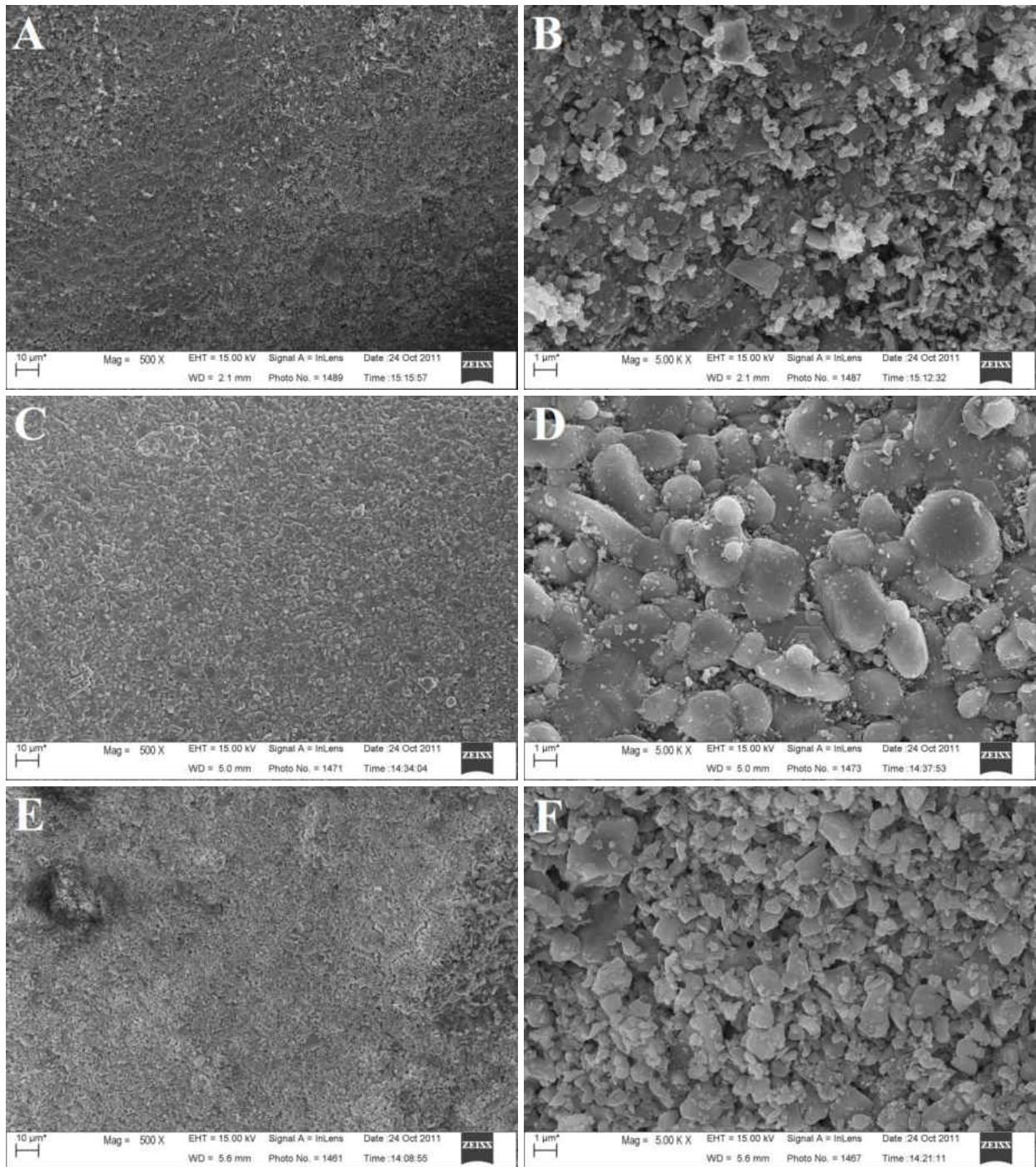
Figure 38. SEM pictures of SiC coated Al_2O_3: unused (A&B), used at the outer (C&D) and inner (E&F) areas of the combustion chamber at magnifications of 500x (left) and 5000x (right)

Thermoelectric modules do not operate the same way regulated power supplies do. As the load resistance of what the device is powering decreases, so does the output voltage of the thermoelectric. Thermoelectric modules have an appreciable internal resistance, meaning that as more current is drawn from the device, more of the available power is dissipated within the module itself [119]. Maximum load power is achieved when the load resistance is matched to the internal resistance of the thermoelectric module. During preliminary runs of the burner, the internal resistance of the thermoelectric was calculated with Equation 17 using a 1.3 Ohm resistor and measuring the load and no-load voltages. The internal resistance was calculated at different times during the preliminary run and the resulting values are listed in Table 6.

$$V_{Load} = V_{No-load} \cdot \frac{R_{Load}}{R_{Internal}+R_{Load}}$$ (17)

The internal resistance was calculated to be between 5 and 6 Ohms over our operating range. A circuit was made with a 5 Ohm resistance to act as the load resistance for all further testing from readily available 10 Ohm resistors for near-optimal load power outputs.

Table 6. Measured internal resistance of thermoelectric module

TE Hot Side (°C)	TE Cold Side (°C)	ΔT(°)	V_{Load} (V)	$V_{No-load}$ (V)	$R_{Internal}$ (Ω)
177.70	45.39	132.31	0.4527	2.433	5.69
192.01	50.66	141.35	0.4477	2.4172	5.72
206.47	54.32	152.15	0.4625	2.5204	5.78
217.77	57.33	160.44	0.4527	2.5296	5.96
223.98	58.28	165.70	0.4576	2.5523	5.95
196.45	51.93	144.52	0.4602	2.5296	5.85
166.37	47.79	118.58	0.4152	2.2466	5.73
148.04	46.83	101.21	0.3537	1.8994	5.68

Thermocouples will take recordings at the hot-side and cold-side of the thermoelectric device during testing. The current, voltage and power will be calculated and plotted for each test run.

The DAQ system used will measure the voltage drop over the load resistor connected to the thermoelectric module and the current and power will be calculated. The results of the measurements with the catalyst will be compared to the measurements performed using the inert Al_2O_3 medium and the effect of the catalyst on overall energy conversion will be determined.

Experimental Procedure

The porous burner will first be run at a stoichiometric mixture of methane and air at the predetermined total flow rate of 11.5 L/min for the inert central section. The burner will be allowed to run until it reaches a steady state temperature and will create base-line results for the operational parameters of the burner. The burner will then be run again with the inert central section except that once that burner has reached a near steady state temperature as determined by the base-line test; the fuel concentration will be slowly reduced. The inlet air flow will be increased alongside a decreasing methane content thereby keeping the total flow rate a constant. The concentration will be reduced every ten minutes, allowing the burner to plateau at the new concentration before further decreasing. This will be repeated until it is seen that the temperatures within the burner are not sustainable at that fuel concentration, thereby establishing the lean operation limit of the burner. If possible, after each temperature fall-off the concentration will be immediately increased and the test repeated, attempting again to determine the lean limit. This procedure will be repeated twice for the inert central section.

The burner will then be tested with the sections with deposited catalytically active material. A base-line run will be performed with a stoichiometric mixture and be allowed to reach a steady state temperature. The burner will then be run at the same lean fuel concentration as found by the testing with the inert central sections. This will allow us to compare the power output and

80

temperature profile at the same concentration. Another test will be performed with the coated section where the concentration will be reduced as low as possible to determine the lean limit of operation of the burner with the coated section. Air at 80 L/min is fed into the cooling system for these tests. In each test the igniter is shut off once ~100 ˚C is measured inside.

Experimental Results

The burner was first run with the inert porous alumina section to obtain a base-line result. A stoichiometric mixture of methane and air was used for this test. The temperature profile is shown as Figure 39. The thermocouple between the inlet and central sections recorded a maximum steady-state temperature of 480 ˚C. The steady state temperature on the hot-side of the thermoelectric device was 225 ˚C and on the cold-side was 61˚C, giving a $\Delta T = 164$ ℃.
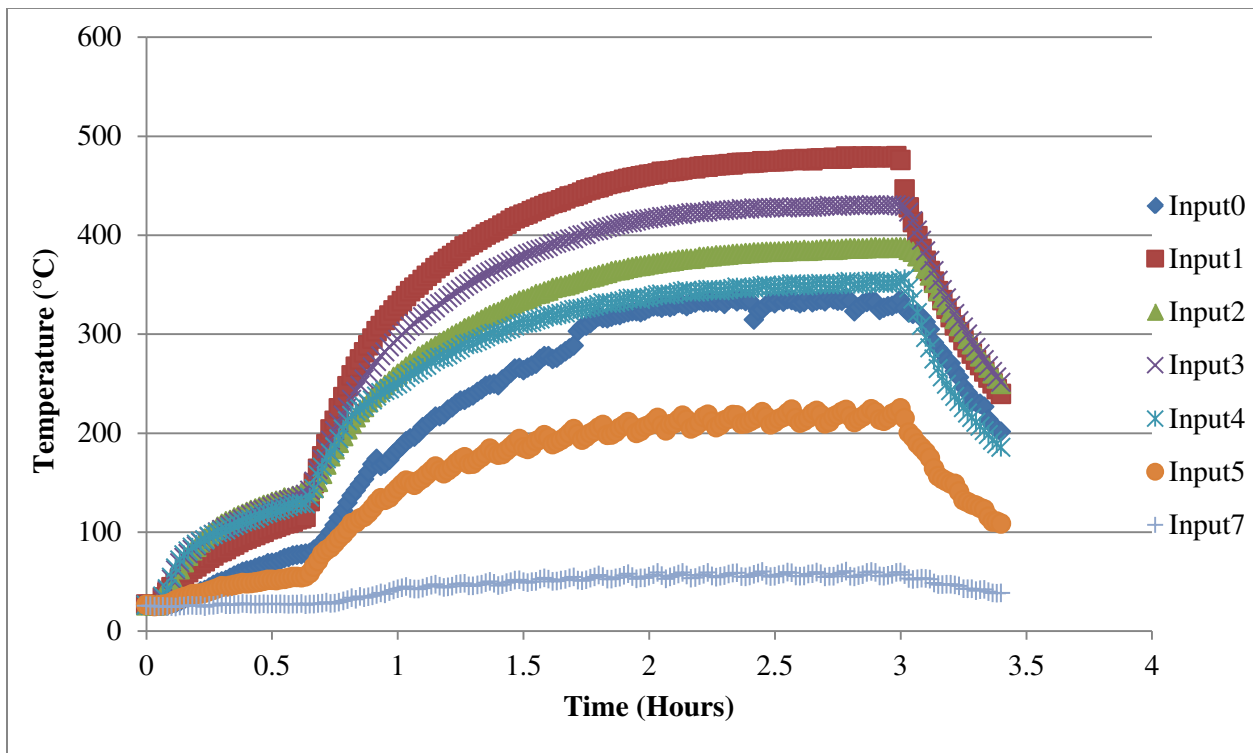

Figure 39. Temperature plot for inert central section, stoichiometric mixture

81

This run confirmed the results from our preliminary testing that the quartz plate is not necessary to reduce the exterior temperature to a value below the maximum operating temperature of the thermoelectric module. The burner took approximately 3 hours to reach its steady state temperature. The associated power plot for the inert section run at stoichiometric conditions is presented in Figure 40. The missing values in the middle of the chart correspond to when the thermoelectric was disconnected from the data acquisition device to measure the no-load voltage with a hand-held multimeter. These measurements were used to calculate the internal resistance of the thermoelectric module in order to have a matched load resistance at the normal operating temperature as discussed in the Power Output section. The measured values were presented in Table 6. The maximum load current for this run was measured as 374 mA. The maximum load voltage was measured as 486 mV. The peak power obtained was 181 mW.
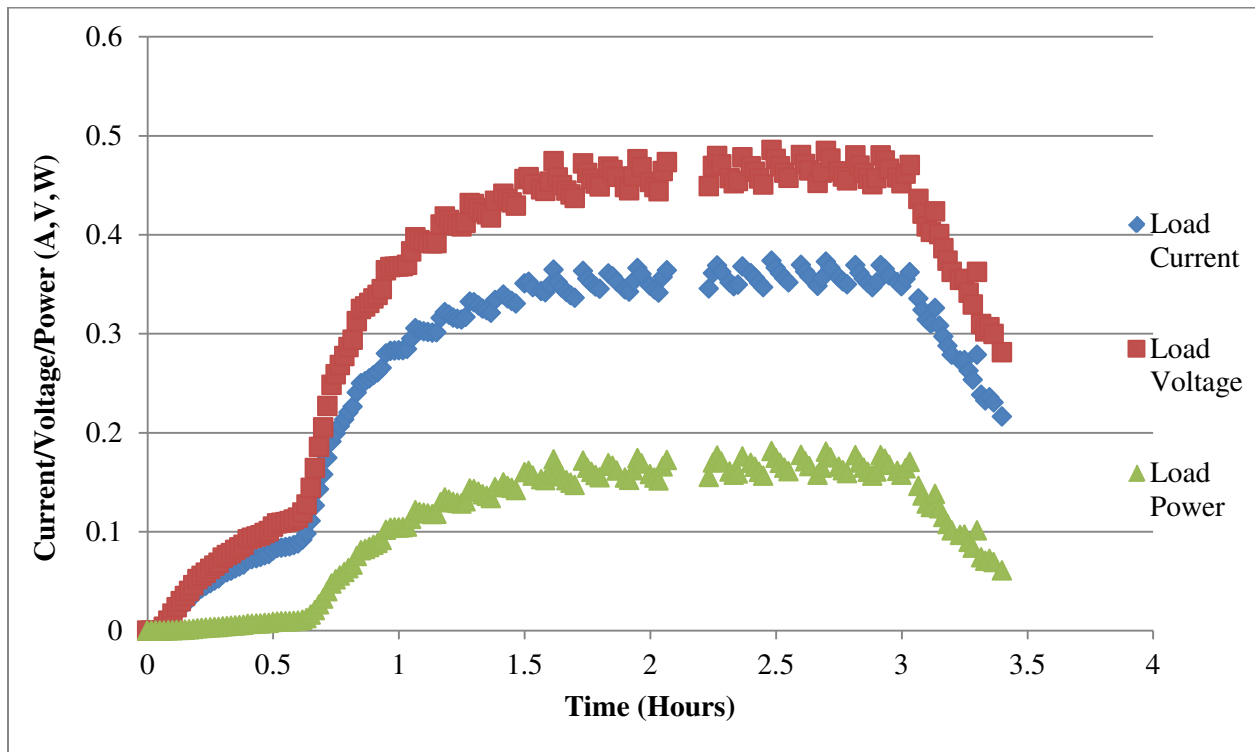

Figure 40. Power plot for inert central section, stoichiometric mixture

The next test of the burner was to determine its lean operational limit with the inert central section. The burner, at a stoichiometric mixture, was allowed to reach a temperature of 470 ˚C, near the measured stoichiometric steady state. The flow rate of the methane was decreased in 0.04 L/min intervals at higher equivalence ratio and at 0.01 L/min near the lean limit to maximize resolution. The air flow rate was correspondingly increased to maintain the 11.5 L/min overall inlet flow rate. The flow rate was decreased approximately every 10 minutes to allow the burner to reach a steady state temperature before further decreasing the concentration. A small temperature plateau is seen in both this and the previous run. The burner heats up to about 180 ˚C before a sudden temperature increase, reaching its higher steady-state value. The small increases in flame temperature seen at the 3.5 hour mark correspond to the flame extinguishing and the concentration being increased to allow a re-ignition before lowering concentration again.
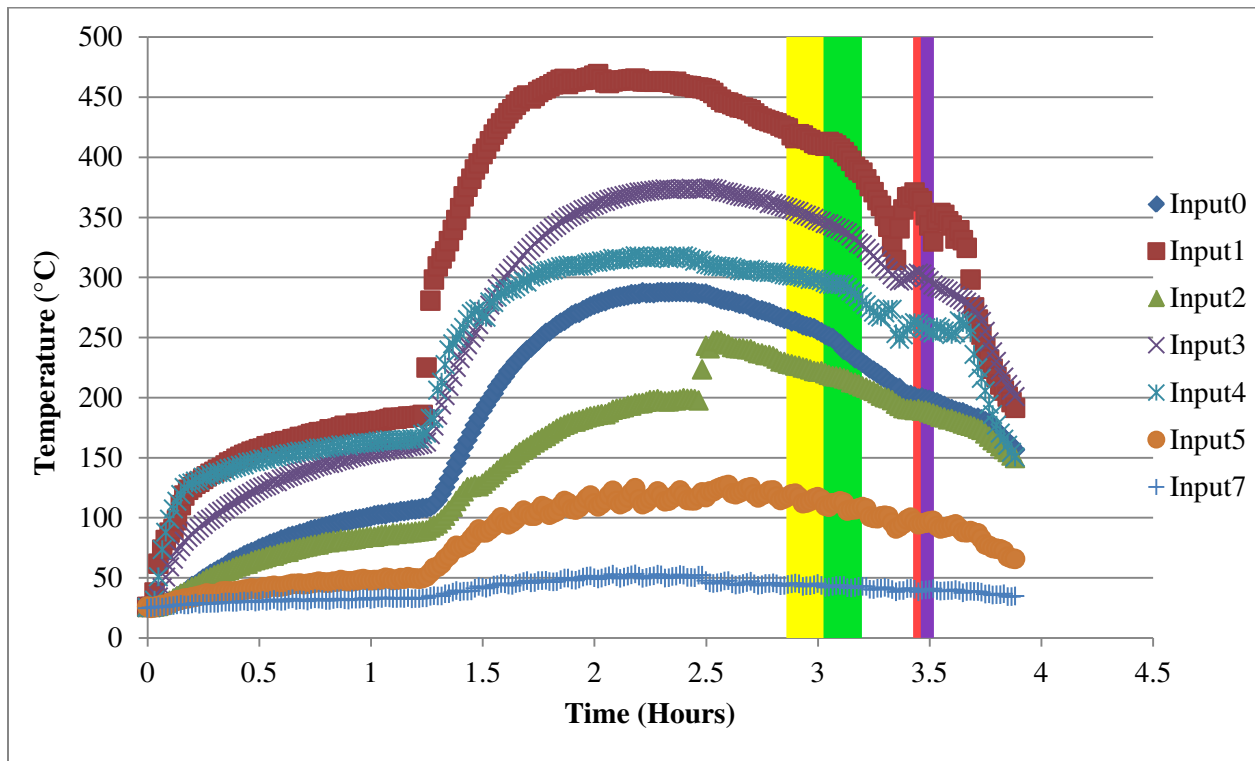

Figure 41. Temperature plot for inert central section at varying equivalence ratio, 1st run

83

The associated power plot for the first lean run with the inert central section is presented in Figure 42. A load resistance of 5 Ohms, as determined from the Power Output section, is used for this and all the remaining tests. The peak measured load current is 239 mA. The maximum measured load voltage is 1.19 V. The peak power is 285 mW.
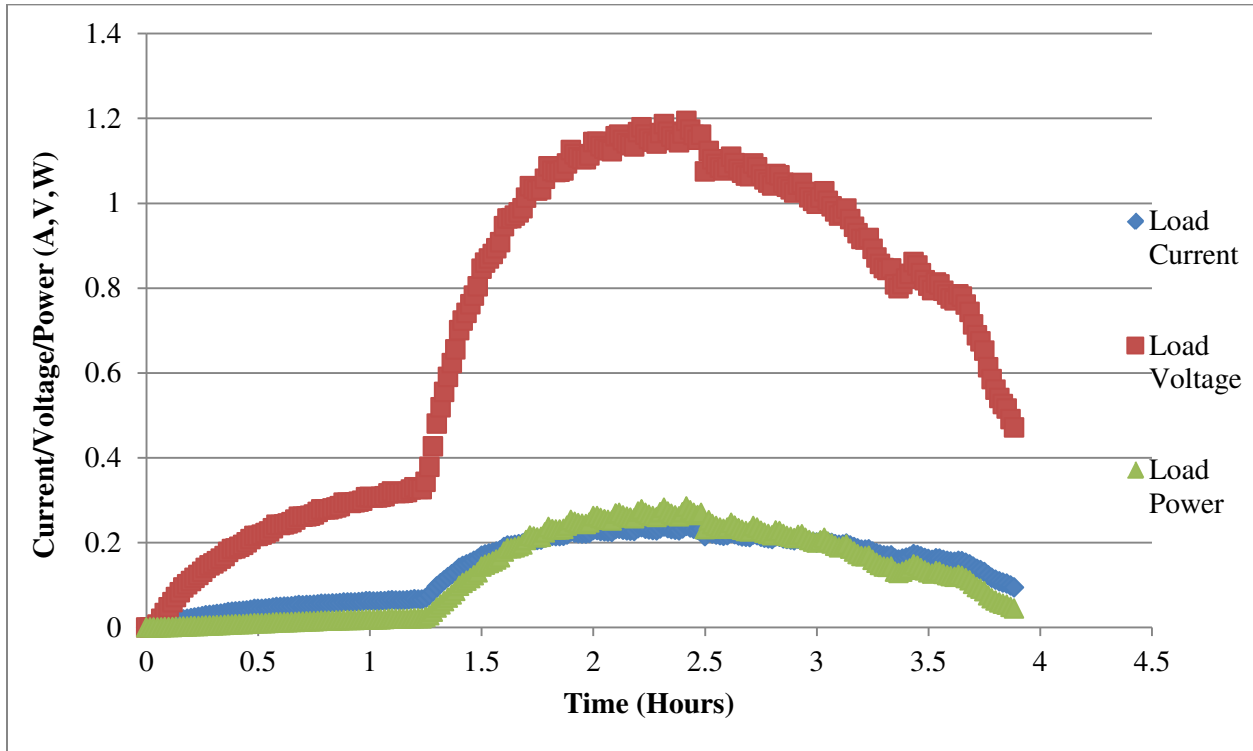
Figure 42. Power plot for inert central section at varying equivalence ratio, 1st run

Figure 43 and 44 are temperature plots, each associated with a specific equivalence ratio. Each plot begins when the inlet mixture is decreased to the corresponding value and records until temperature reaches a steady state and the ratio is further reduced. Figure 43 is the yellow highlight from Figure 41 at an equivalence ratio of 0.609; steady state temperature was achieved at 410 ˚C. As the equivalence ratio was reduced, Figure 44, the green highlight, at equivalence ratio of 0.589 shows the temperature decreasing at a rate of 2.58 ˚C/min. This means that combustion was not sustainable and that the lean limit is between 0.589 and 0.609.

Figure 43. Temperature plot for 1st run of inert section, $\phi = 0.609$, yellow highlight
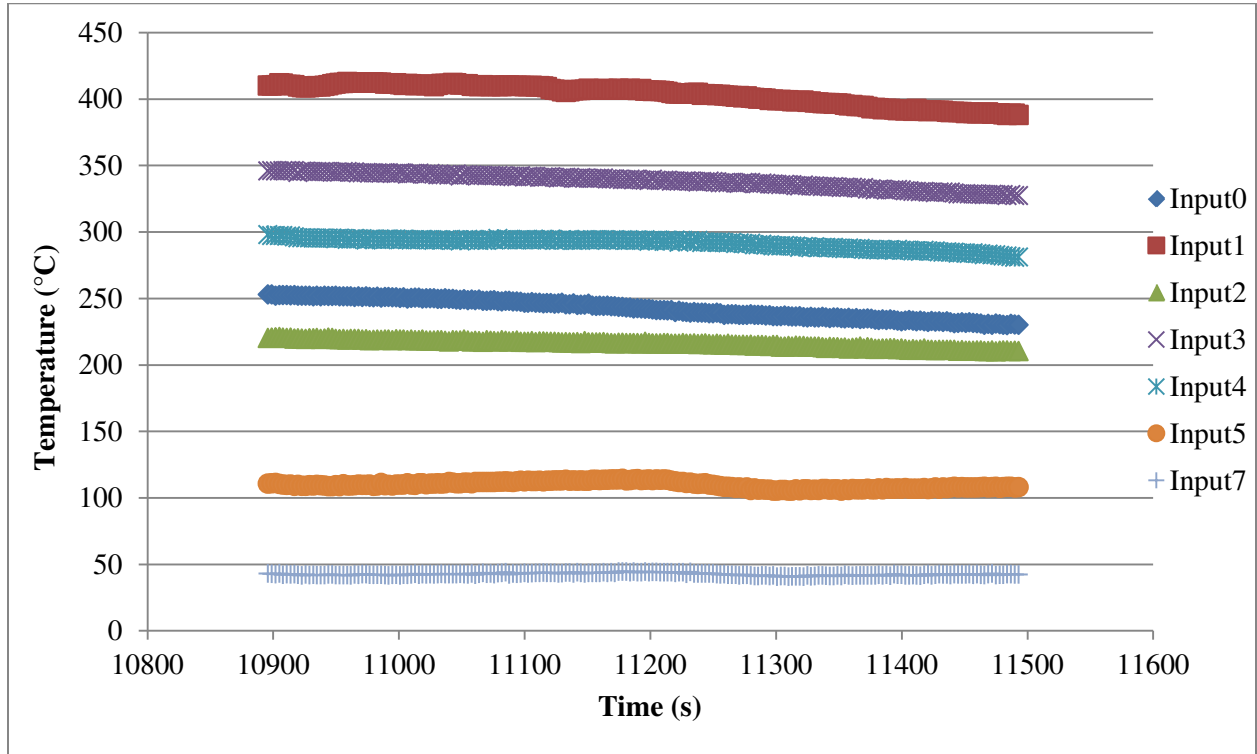
Figure 44. Temperature plot for 1st run of inert section, $\phi = 0.589$, green highlight

85

The concentration was then increased to 0.737 to allow re-ignition and the methane flow rate was again reduced in intervals in order to measure the lean operating limit of the burner. Figure 45 shows the red highlighted segment from Figure 41. At 0.589 equivalence ratio a steady state temperature of 365 ˚C was achieved. Figure 46 shows the purple highlighted section from Figure 41. At an equivalence ratio of 0.572, the temperature continues to drop at a rate of 10.16 ˚C/min and combustion is not sustained. The obtained lean limit for combustion within an inert porous matrix is as low as 0.589.

The smallest resolution obtainable by these tests is determined by the inlet flow rate and the smallest interval input into the flow controllers. With an inlet flow rate of 11.5 L/min and a minimum input of 0.01 L/min of methane, a minimum resolution of overall equivalence ratio of about 0.01 is achievable.
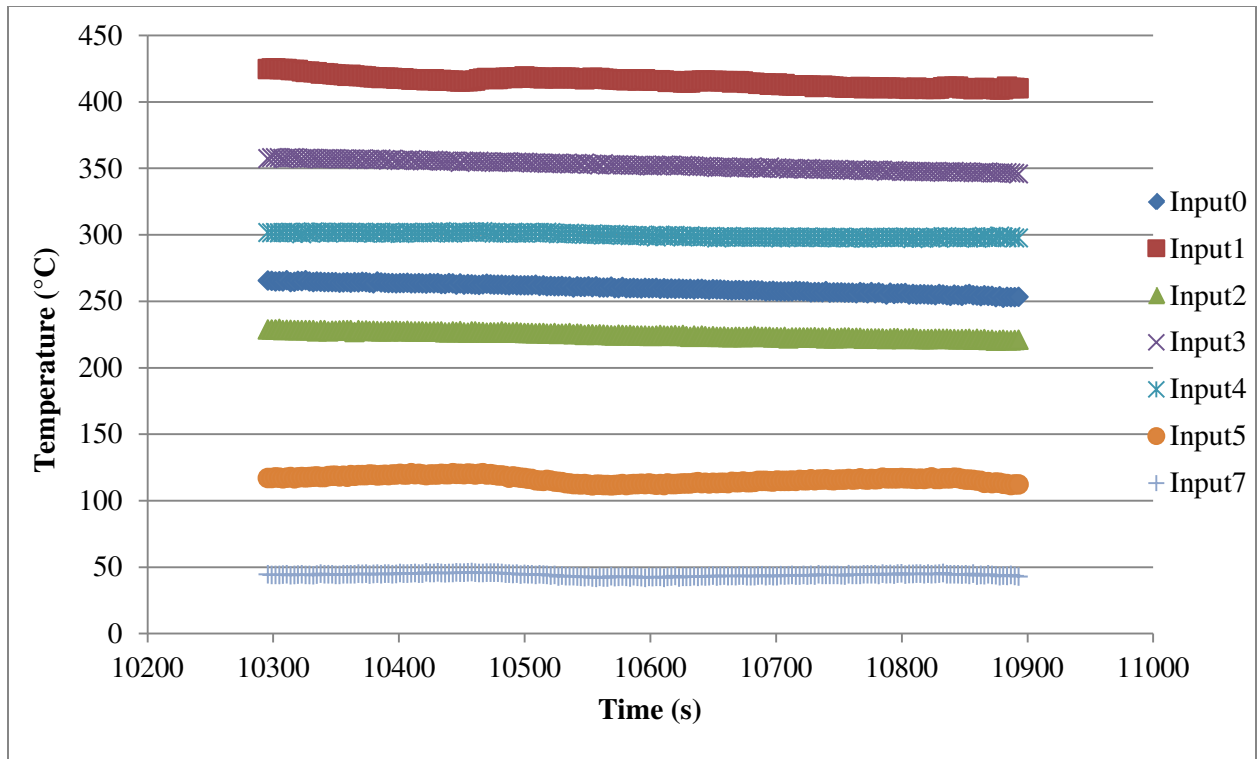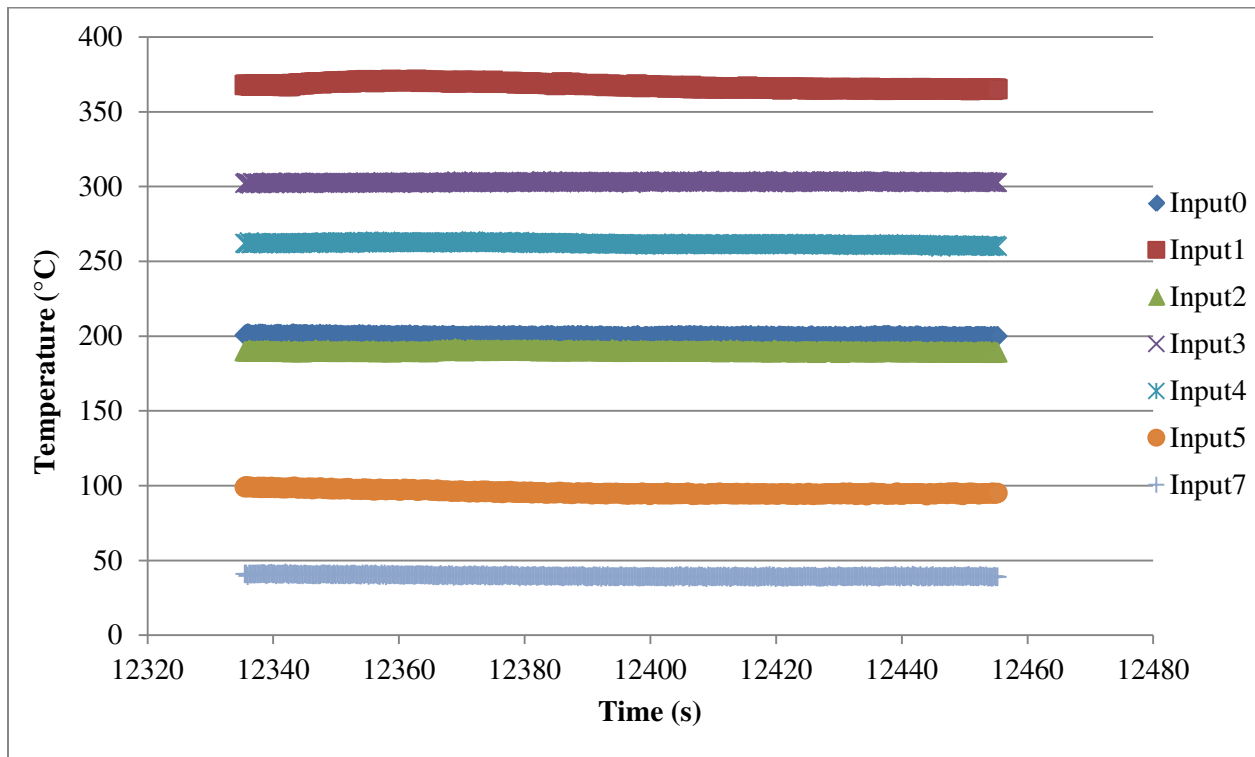

Figure 45. Temperature plot for 1st run of inert section, $\phi = 0.589$, red highlight
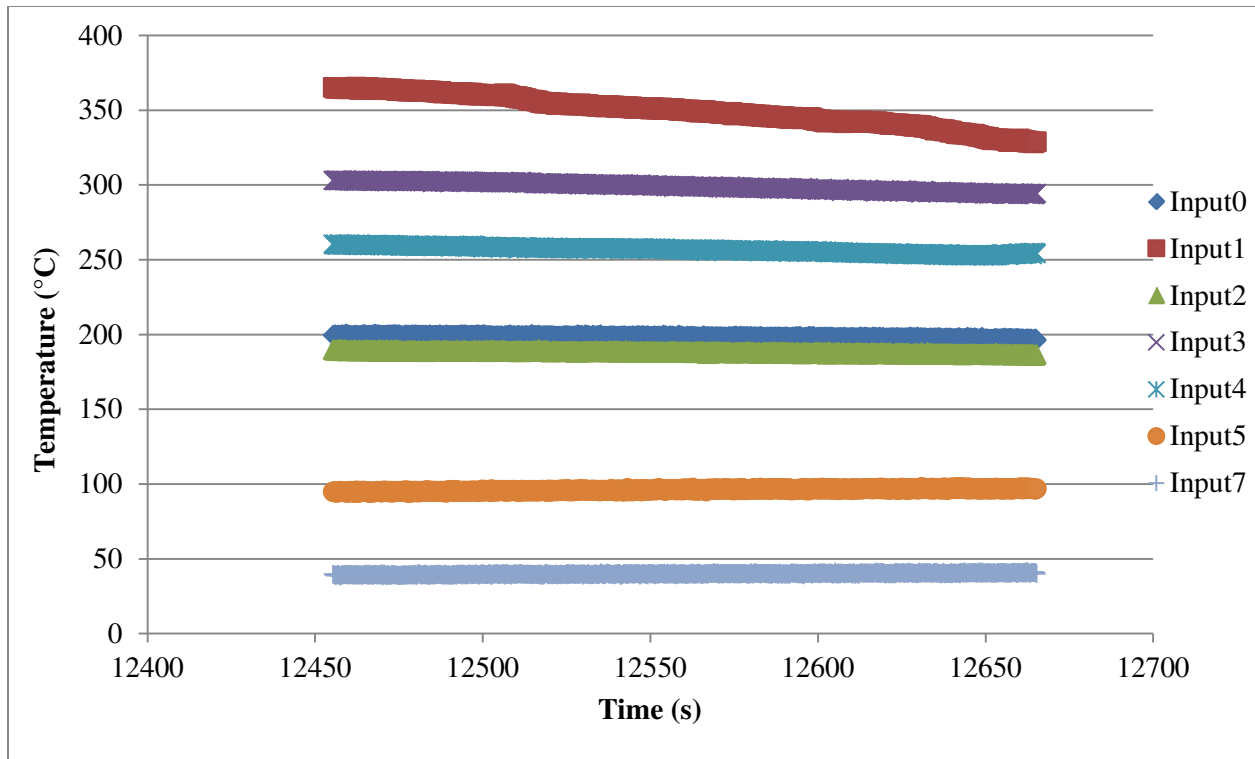
Figure 46. Temperature plot for 1st run of inert section, $\phi = 0.572$, purple highlight

The burner was run again with the inert porous section to try to obtain the lean limit to verify the results obtained in the first test. The temperature profile is shown in Figure 47. The burner was again allowed to reach a near steady state temperature of about 480 ˚C at stoichiometric conditions before the concentration was decreased. The associated power plot is shown as Figure 48. The maximum measured load current is 193 mA. The maximum measured load voltage is 0.964 V. The peak power is 186 mW. Figure 49 shows the yellow highlighted section from Figure 47. At an equivalence ratio of 0.589 a steady state temperature is achieved. Figure 50 shows the green highlighted section and that at an equivalence ratio of 0.579, the temperature continues to drop at a rate of 3.41 ˚C/min and combustion is not sustainable. Both trials of the inert central section determined a lean limit of 0.589 equivalence ratio.

87

Figure 47. Temperature plot for inert central section at varying equivalence ratio, 2nd run

Figure 48. Power plot for inert central section at varying equivalence ratio, 2nd run

Figure 49. Temperature plot for 2nd run of inert section, $\phi = 0.589$, yellow highlight
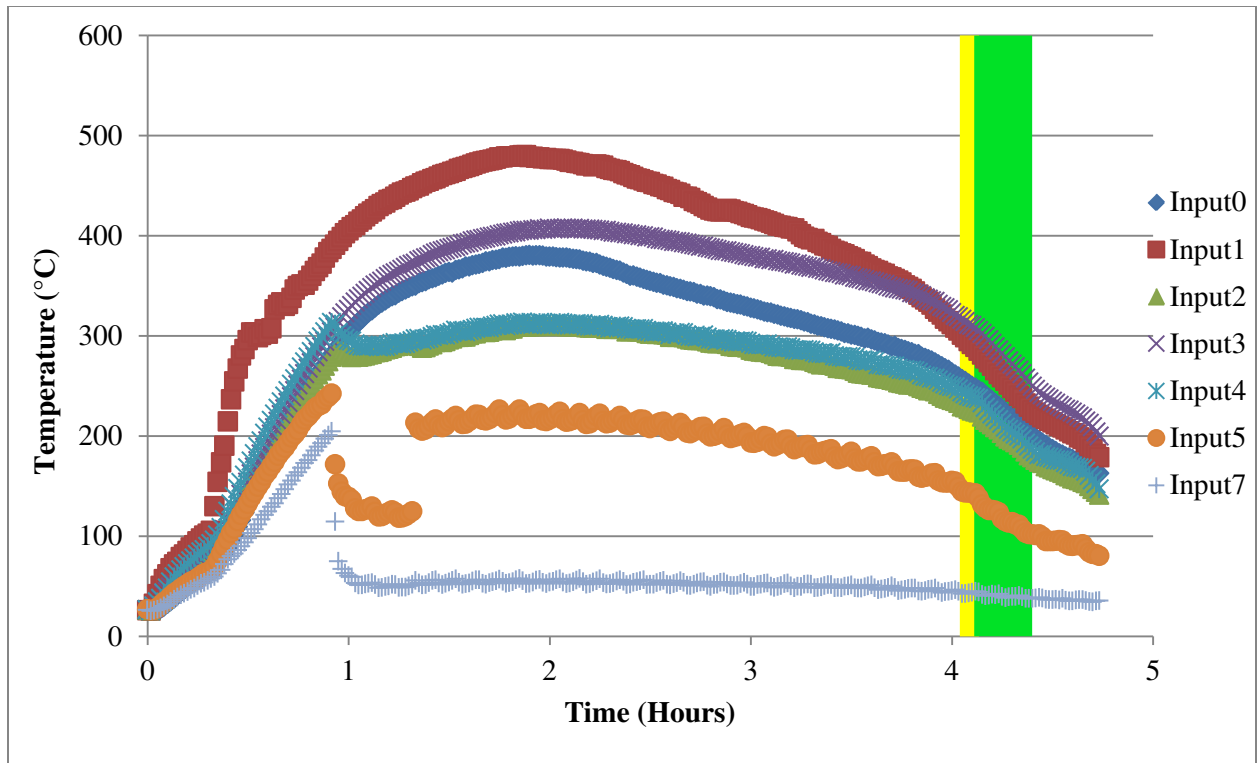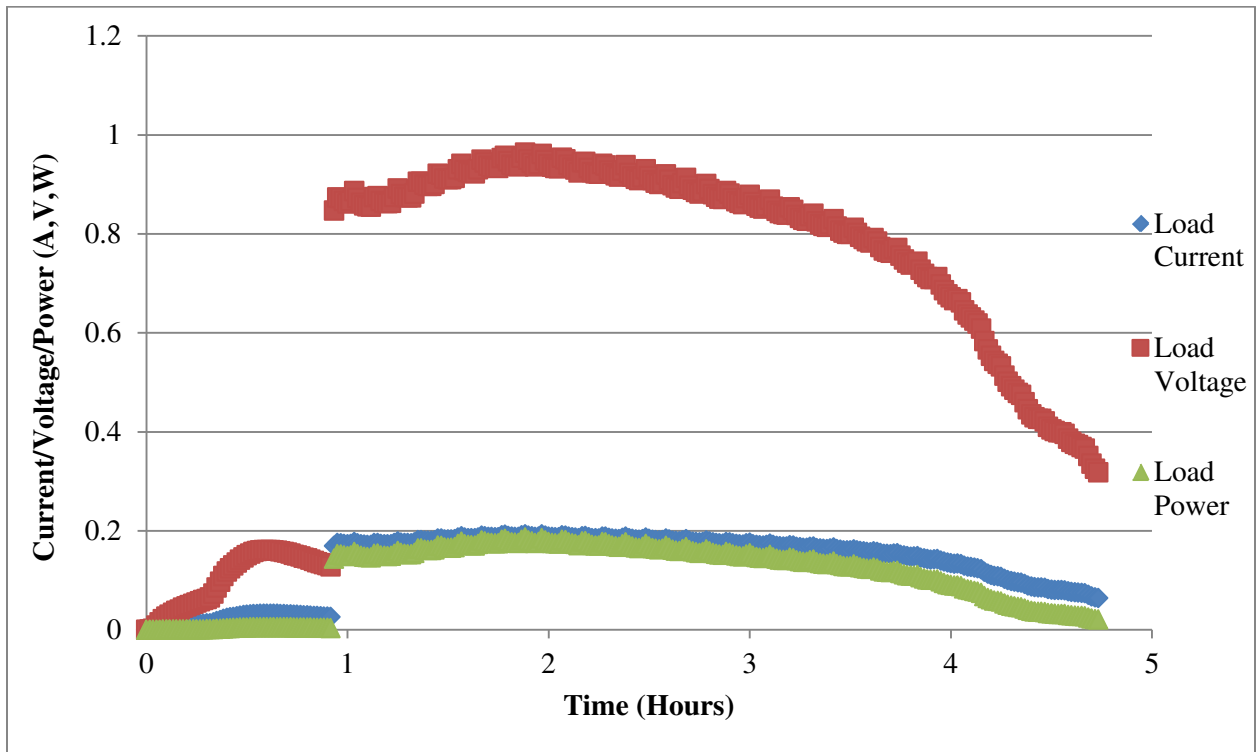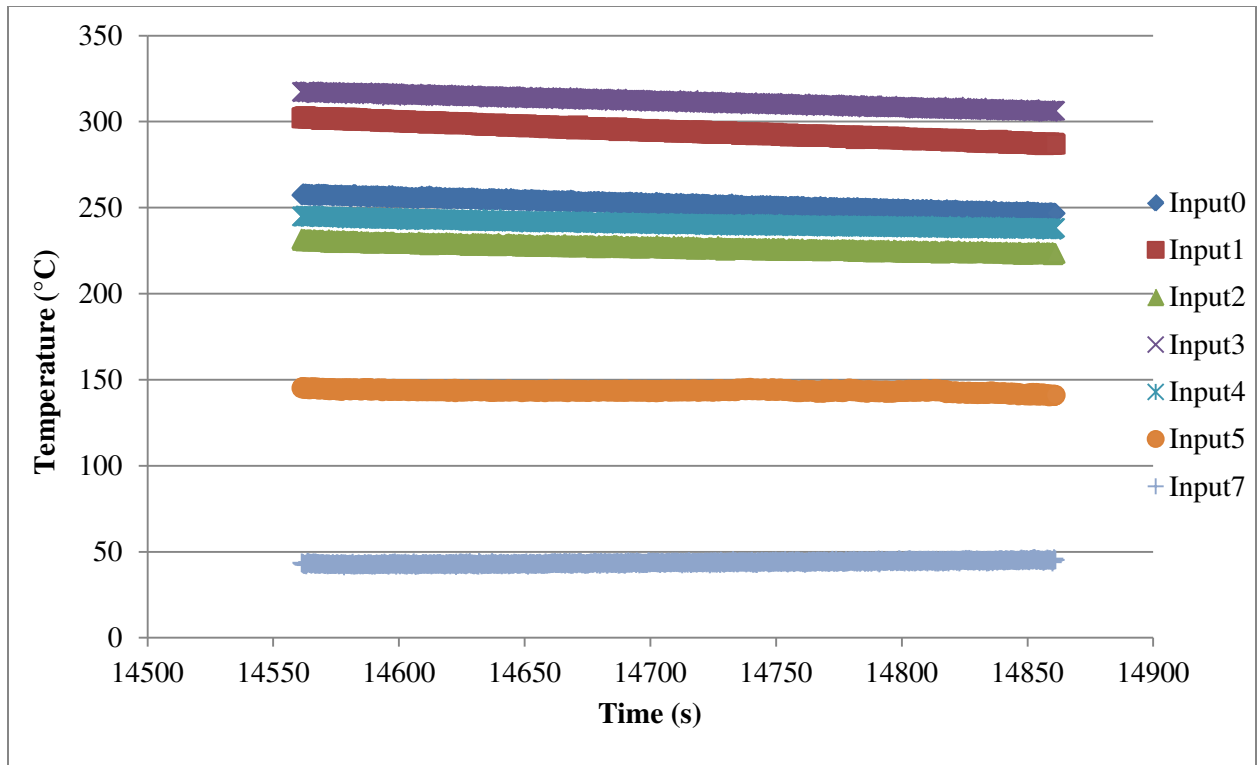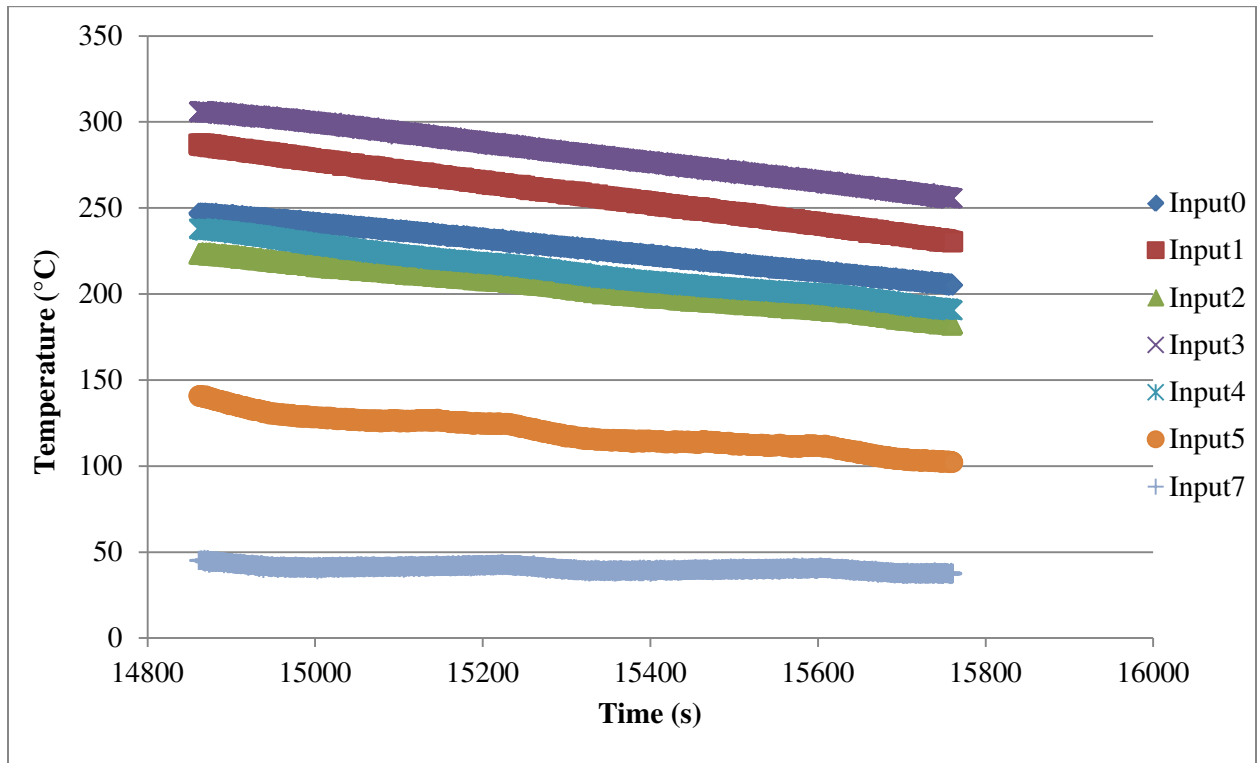

Figure 50. Temperature plot for 2nd run of inert section, $\phi = 0.579$, green highlight

The burner was then run with one of the central sections with deposited catalytically active material at a stoichiometric inlet mixture. For this run, dip coated section #1 from Table 5 with 12.25 grams of deposited material was used. The burner was allowed to reach a steady state temperature which took approximately 5.5 hours. Similar to previous runs, a temperature plateau at a relatively low value for the initial part of the run was seen. After about 2 ½ hours the cooling air flow was turned off as seen by the increase in the temperatures of Input5 and Input7 since it was possible that too much heat was being extracted from the system to achieve stable combustion. After about an hour the temperature suddenly increased, similar to the previous runs, and the cooling was turned back on and the burner achieved a steady state temperature. Shown in Figure 51, the maximum steady state temperature achieved was 544 ˚C. The hot-side of the thermoelectric device only reached 181 ˚C and the cold-side reached 53 ˚C for a $\Delta T = 128\ ℃$. The hot-side of the thermoelectric device is notably lower than in previous runs even though the maximum temperature is larger. The top-side of the central section within the burner, just below the thermoelectric device, shown as Input 4 achieved a maximum temperature 322 ˚C. For the stoichiometric test with an inert central section this location reached a maximum temperature of 355 ˚C which may account for part of the ~ 40 ˚C difference on the hot-side of the thermoelectric. As seen by the temperature profile, the location of Input1 is substantially higher than the others suggesting a more localized combustion region accounting for the temperature difference. Another explanation is that there may have been difference in the amount of contact surface with the metal casing and the central ceramic section in each run. This would mean a decreased amount of heat conduction to the outer casing, causing a lower temperature on the hot-side of the thermoelectric module. Figure 52 is the associated power plot with maximum load current of 249 mA, maximum measured load voltage of 1.246 V and peak power of 311 mW.
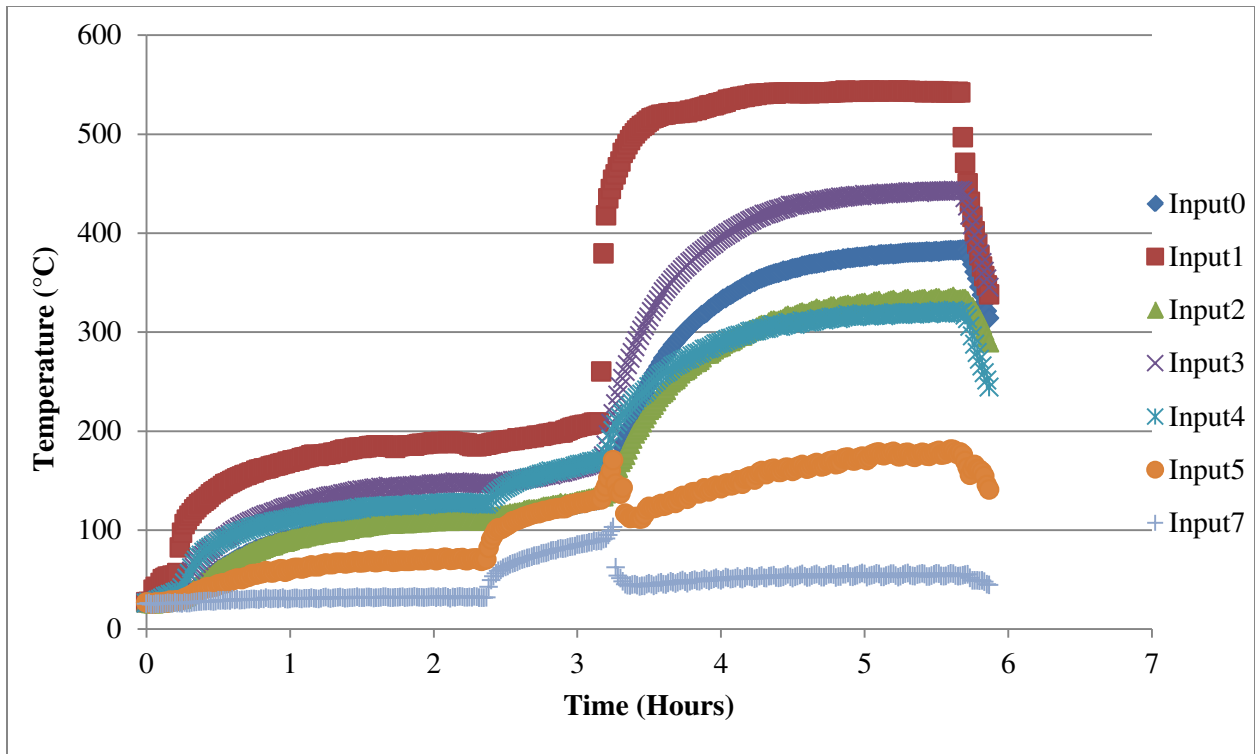
Figure 51. Temperature plot for coated section at a stoichiometric mixture
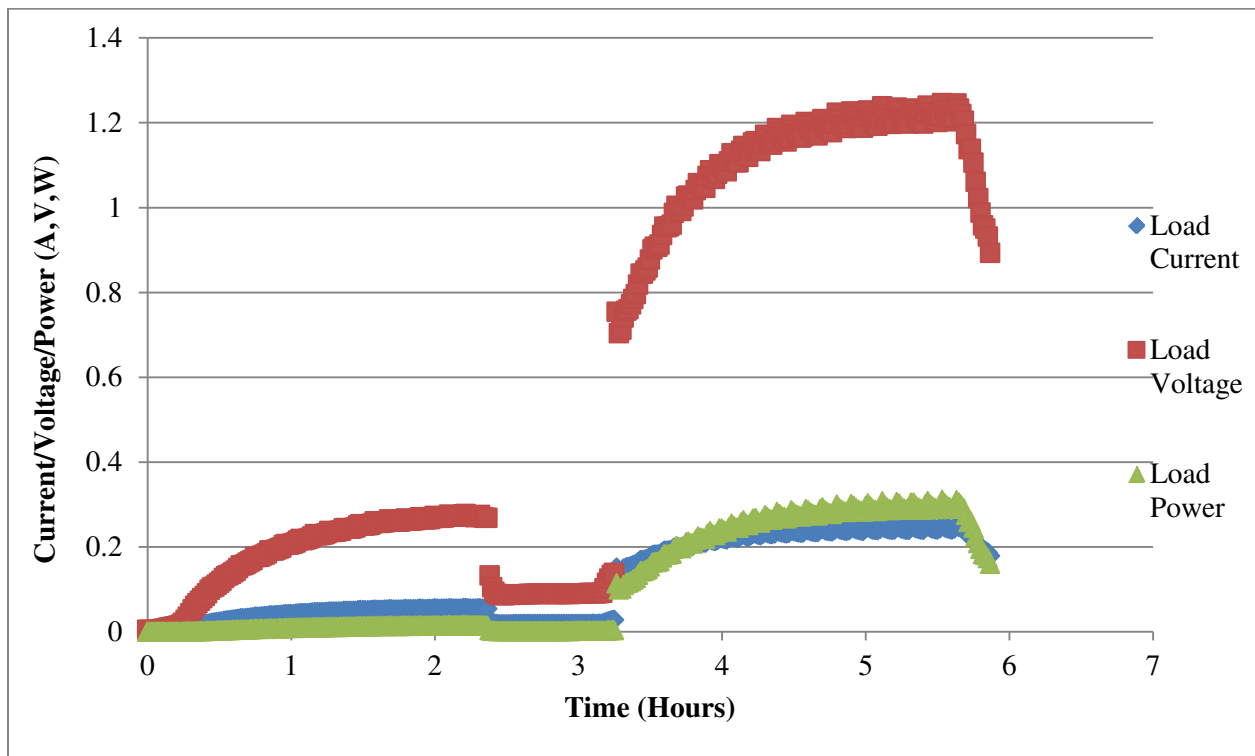
Figure 52. Power plot for coated section at a stoichiometric mixture

91

The burner was run with another dip cpated central ceramic section, allowed to reach a maximum temperature of 573 °C at a stoichiometric ratio and then the inlet ratio was reduced in intervals, allowing a steady state value to be reached in between each decrease to find the lean limit with a coated section. Dip coated section #2 from Table 5 with 19.11 grams of deposited catalyst was used. The burner was Figure 53 shows the overall temperature profile for the burner. The burner was ignited without cooling and was turned on once the first small plateau was passed at around the 2.5 hour mark. Once the peak was reached, a hot-side temperature on the thermoelectric of 128 °C and cold-side temperature of 47 °C is measured. These values are much lower than previously recorded and is likely due to the top central thermocouple within the burner, Input 4, only reading ~280 °C compared to 322 °C and 355 °C from previous runs. This indicates that the temperature peaked right at the front of the central porous section.

Figure 53. Temperature plot for coated section at varying equivalence ratio, 1st run
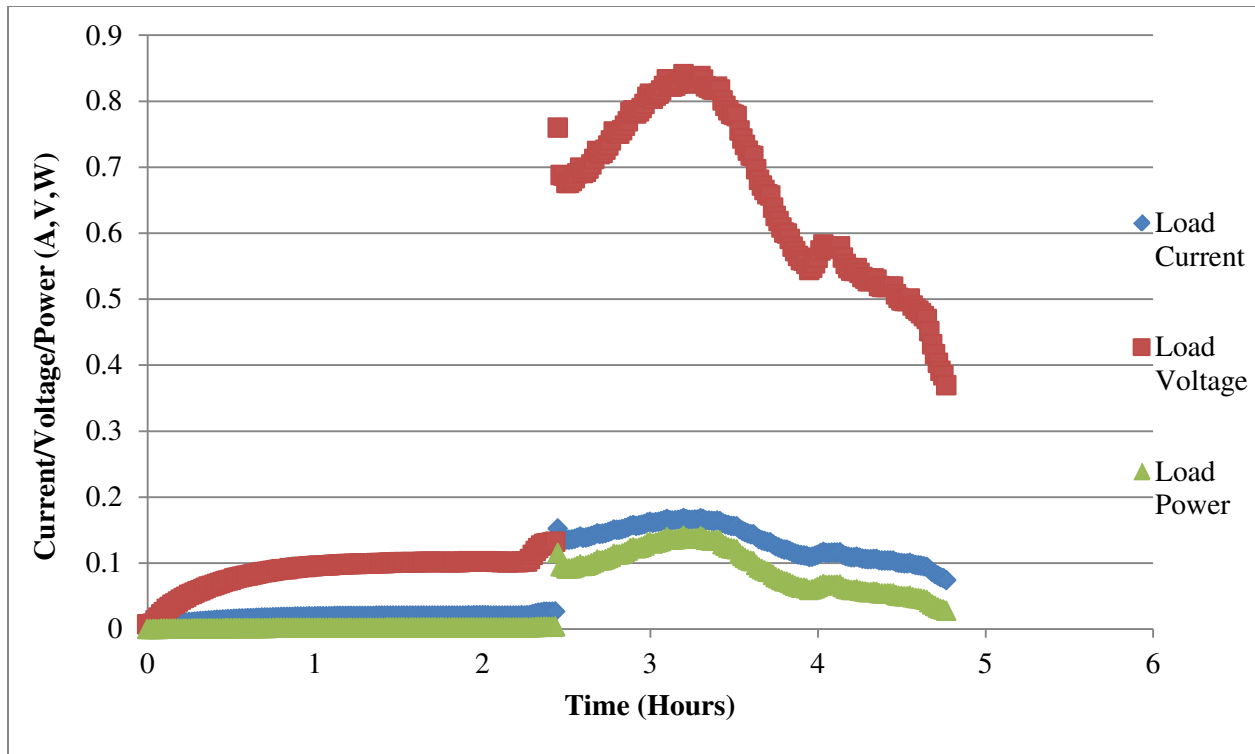
Figure 54. Power plot for coated section at varying equivalence ratio, 1st run

Figure 54 shows the power plot for this lean run with a catalytically coated central section. The large jump at the 2.5 hour mark corresponds to when the cooling was turned on. The peak load current is 168 mA, maximum load voltage is 0.841 V and peak power is 141 mW. The mixture ratio was reduced to determine the lean operation limit with the catalytic section. Figure 55, the yellow highlighted section of Figure 53, shows steady state at an equivalence ratio of 0.698. Figure 56, the green section, shows the temperature decreasing by 7.94 °C/min at an equivalence ratio of 0.649. The concentration was increased to 0.728 to allow the burner to reach a steady temperature and then again reduced. Figure 57, the red section, shows steady state achieved at 0.688 equivalence ratio. Figure 58, the purple highlight, shows the temperature continuously decreasing by 6.50 °C/min at 0.668 equivalence ratio. This means that combustion was not sustainable at this condition and that the lean limit is between 0.688 and 0.668.

93
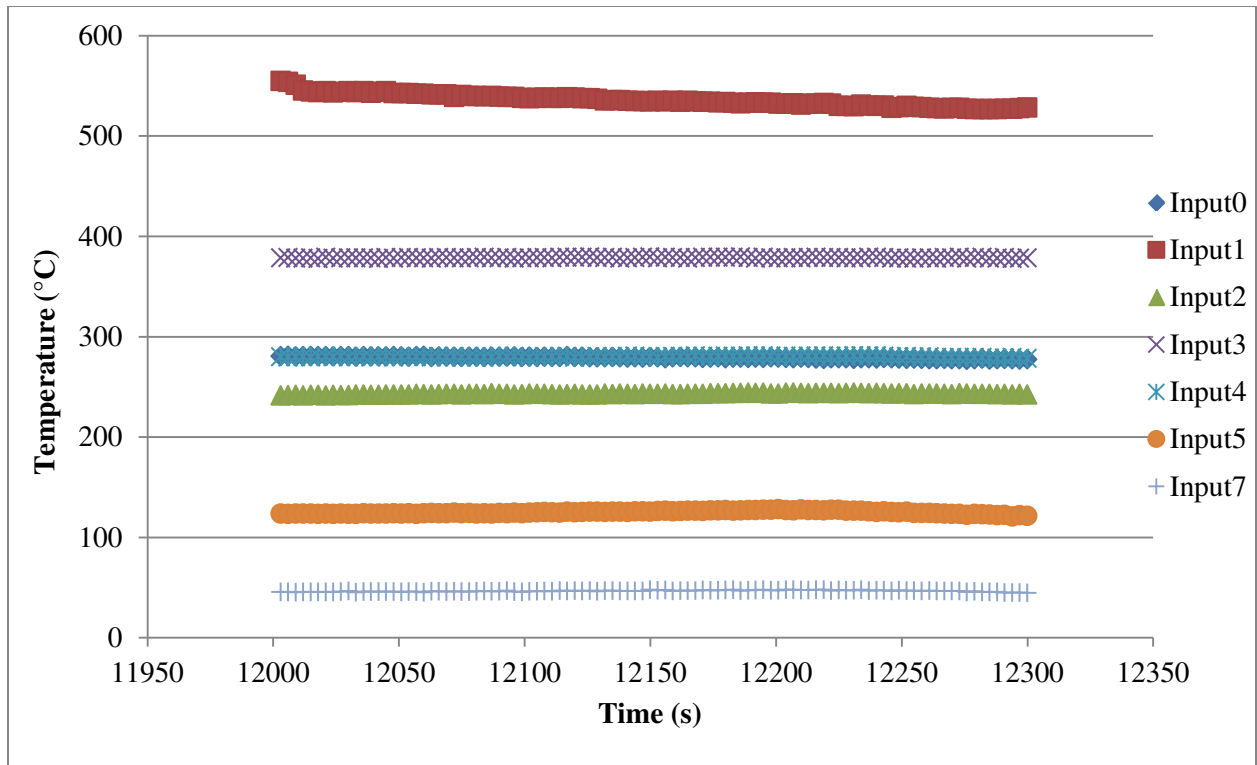
Figure 55. Temperature plot for 1ˢᵗ run of coated section, $\phi = 0.698$, yellow highlight

Figure 56. Temperature plot for 1ˢᵗ run of coated section, $\phi = 0.649$, green highlight

Figure 57. Temperature plot for 1st run of coated section, $\phi = 0.688$, red highlight

Figure 58. Temperature plot for 1st run of coated section, $\phi = 0.668$, purple highlight

The burner is again tested with a central section with a catalytically active deposition to try to determine its lean operation limit. For this run, dip coated section # 3 from Table 5 with 19.04 grams of deposited material was used. The burner was allowed to reach a peak temperature of 508 ˚C at stoichiometric conditions before the cooling was turned and mixture ratio was decreased in intervals. Figure 59 shows the temperature profile for this run. The burner took about one hour to reach its near-peak temperature at stoichiometric conditions. Figure 60 shows the corresponding power plot. The peak measured load current is 165 mA. The maximum measured load voltage is 0.825 V. The peak power is 136 mW. It is noted that the initial plateau for this run was very short and the temperature jump occurred at only 110 ˚C before rising to its peak temperature.
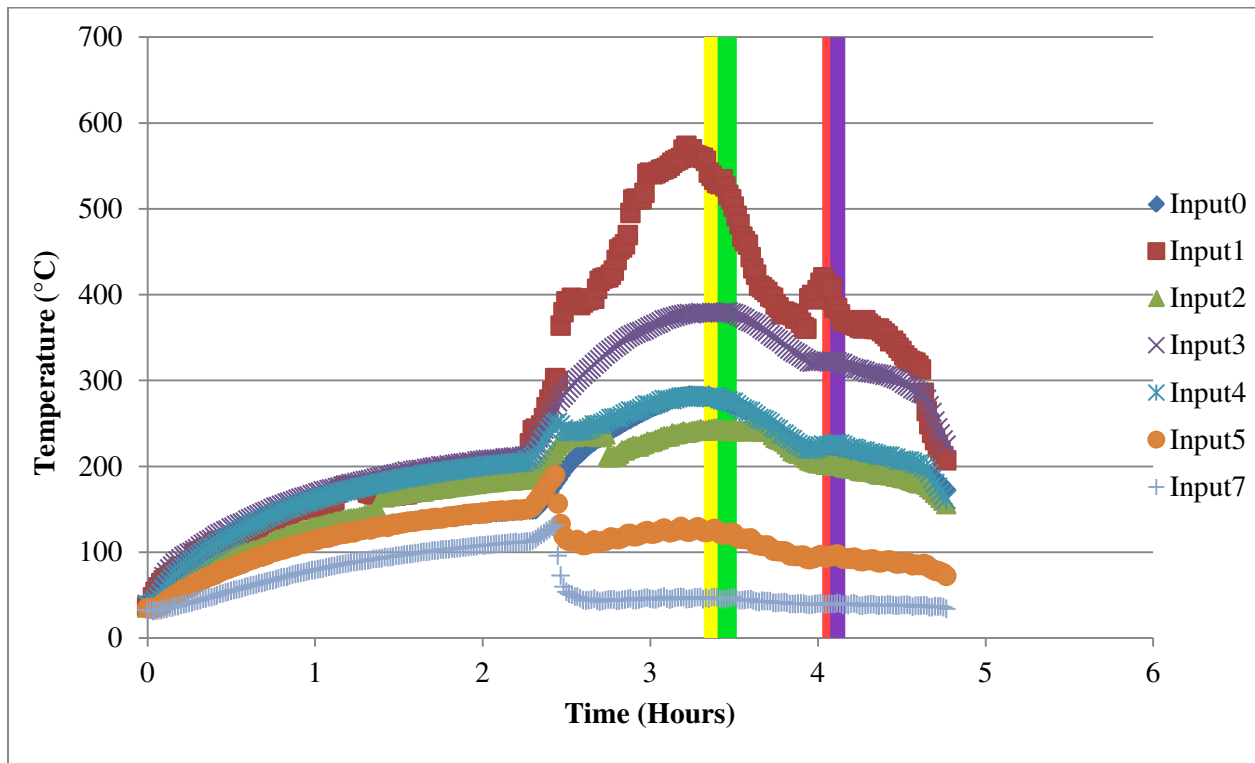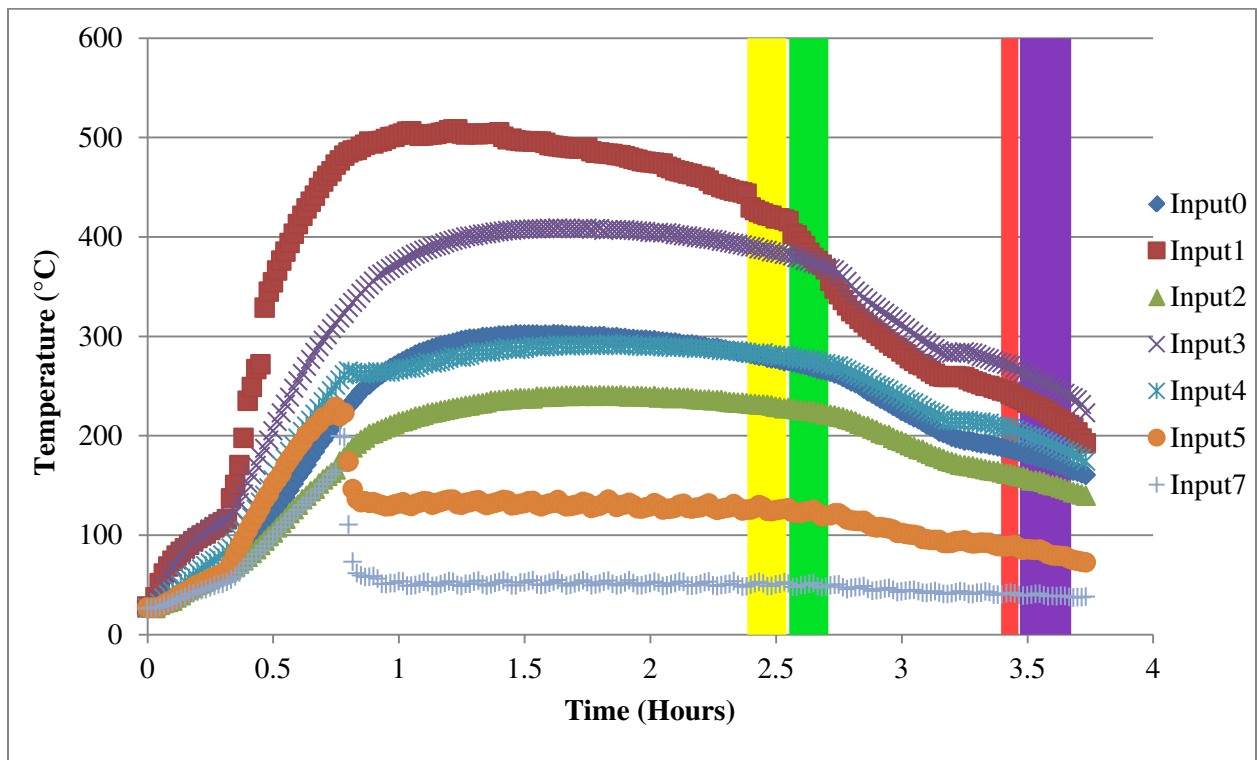

Figure 59. Temperature plot for coated section at varying equivalence ratio, 2nd run
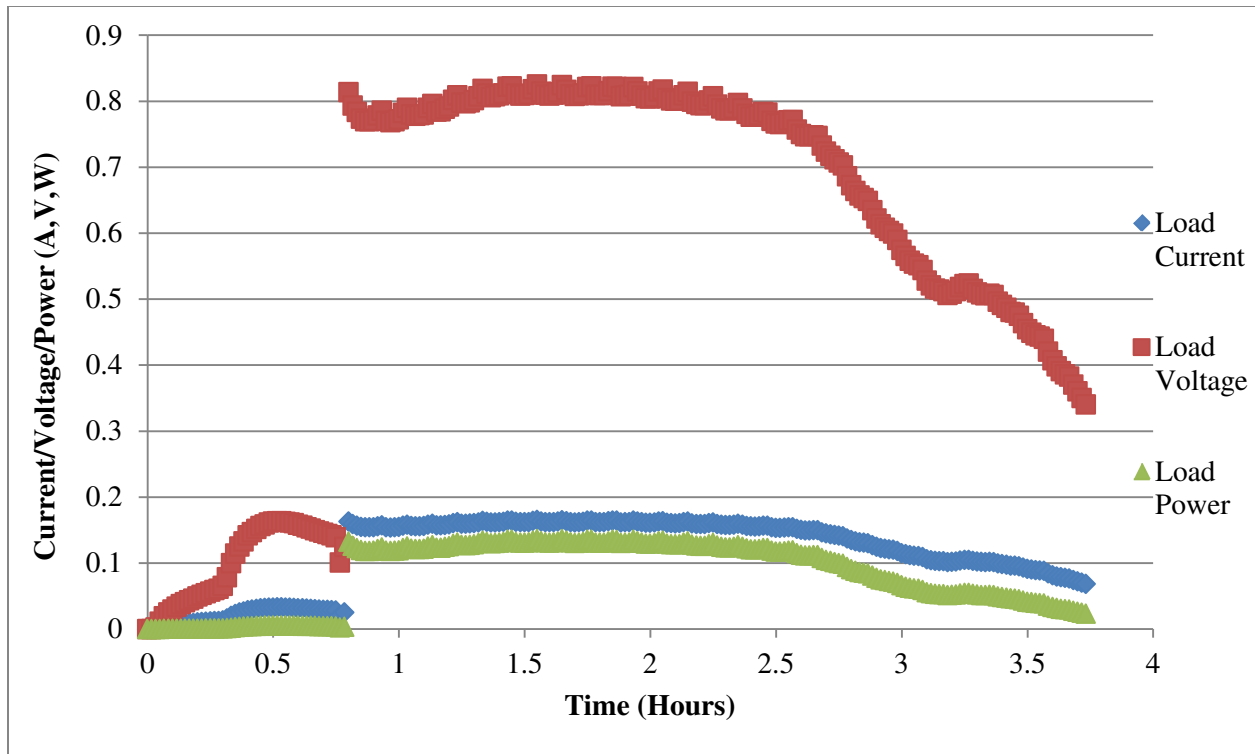
Figure 60. Power plot for coated section at varying equivalence ratio, 2nd run

The equivalence ratio of the inlet mixture is reduced to try to determine a lean operating limit for the burner with a coated center section. Figure 61, the yellow highlighted segment from Figure 59, shows a stable temperature at an equivalence ratio of 0.651. Figure 62, the green highlight, shows the temperature profile declining by 5.14 ˚C/min when the equivalence ratio was reduced to 0.631. The concentration was increased back up to 0.692, allowed to reach a steady level and then further reduced. Figure 63, the red highlight, shows that at an equivalence ratio of 0.634 the temperature remained level. Figure 64, the purple highlight, showed a decreasing temperature profile by 2.03 ˚C/min at an equivalence ratio of 0.631. From this test we can infer that the lean limit for the burner with a catalytically coated central section is between 0.634 and 0.631.

97
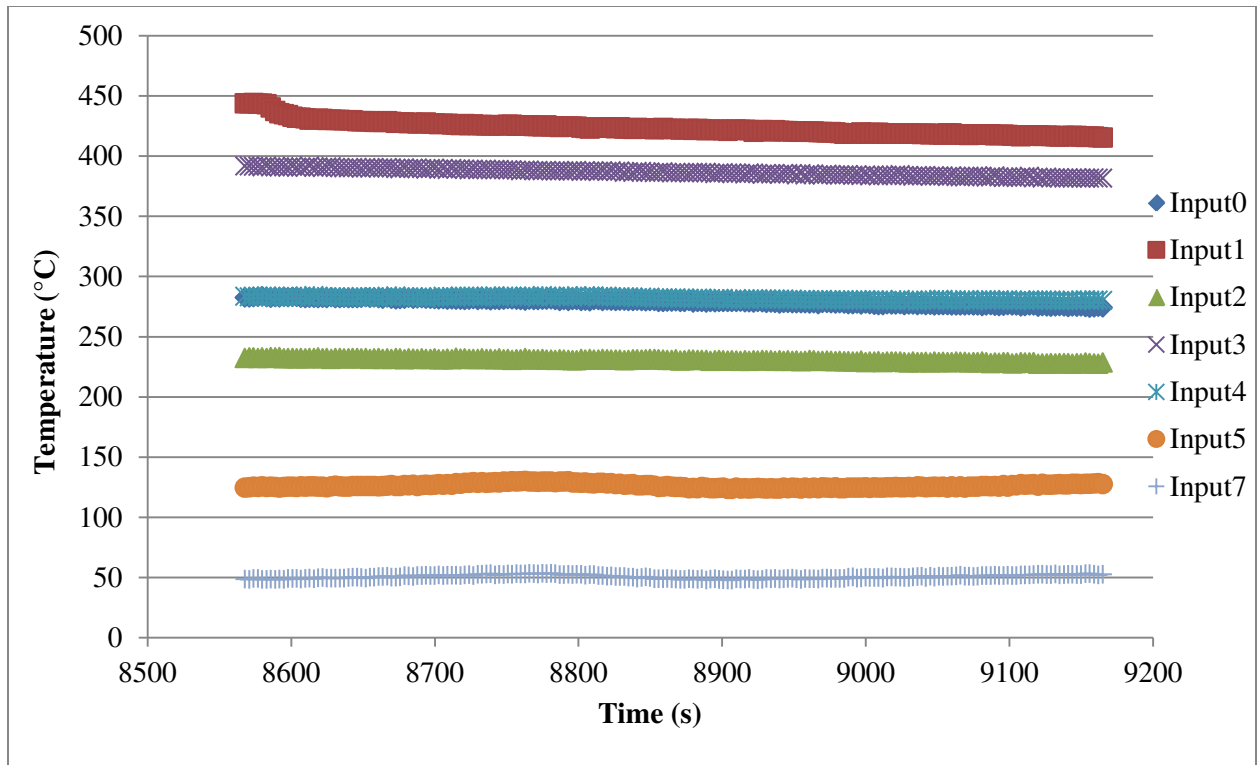
Figure 61. Temperature plot for 2nd run of coated section, $\phi = 0.651$, yellow highlight
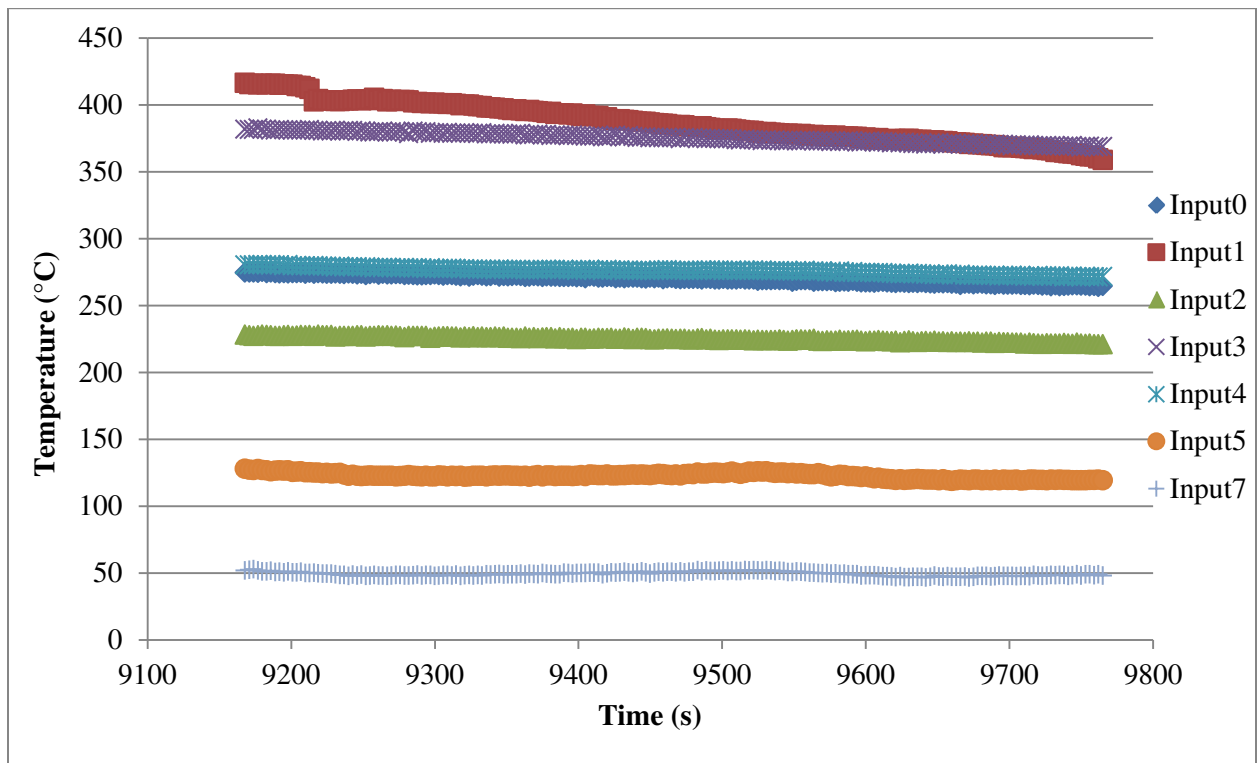
Figure 62. Temperature plot for 2nd run of coated section, $\phi = 0.631$, green highlight
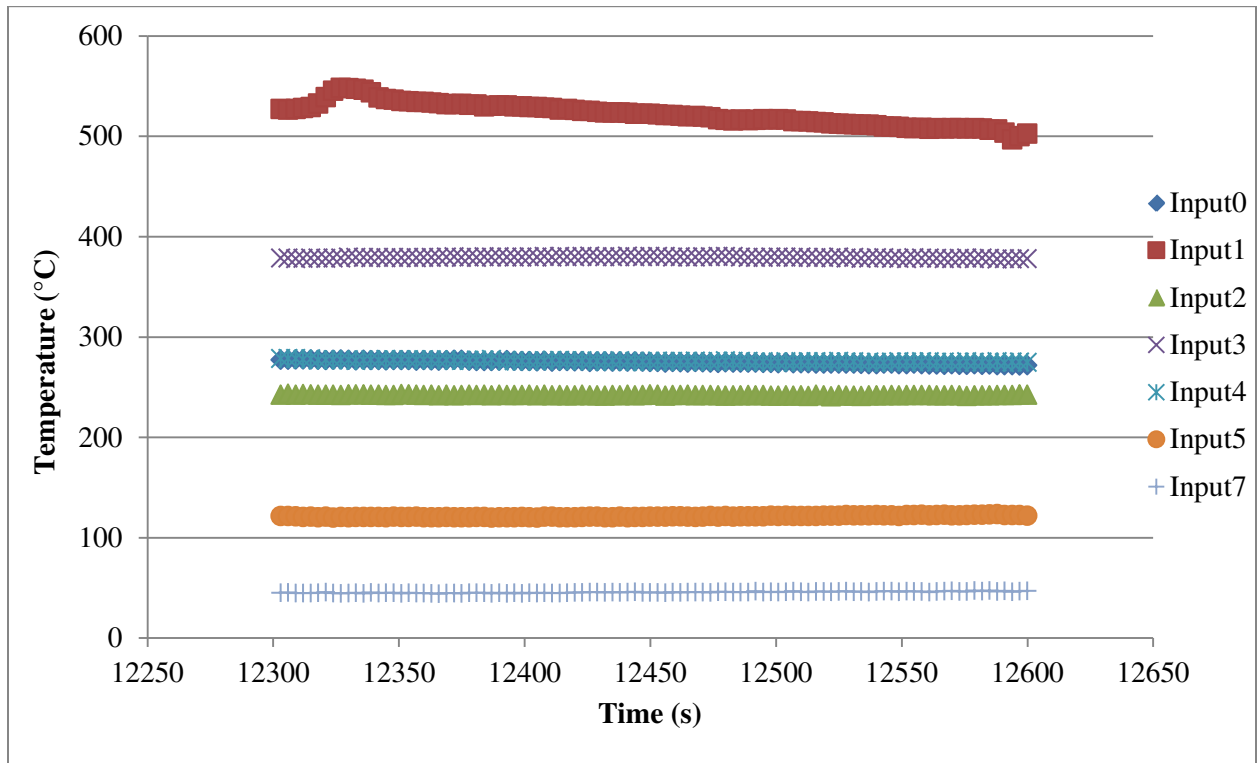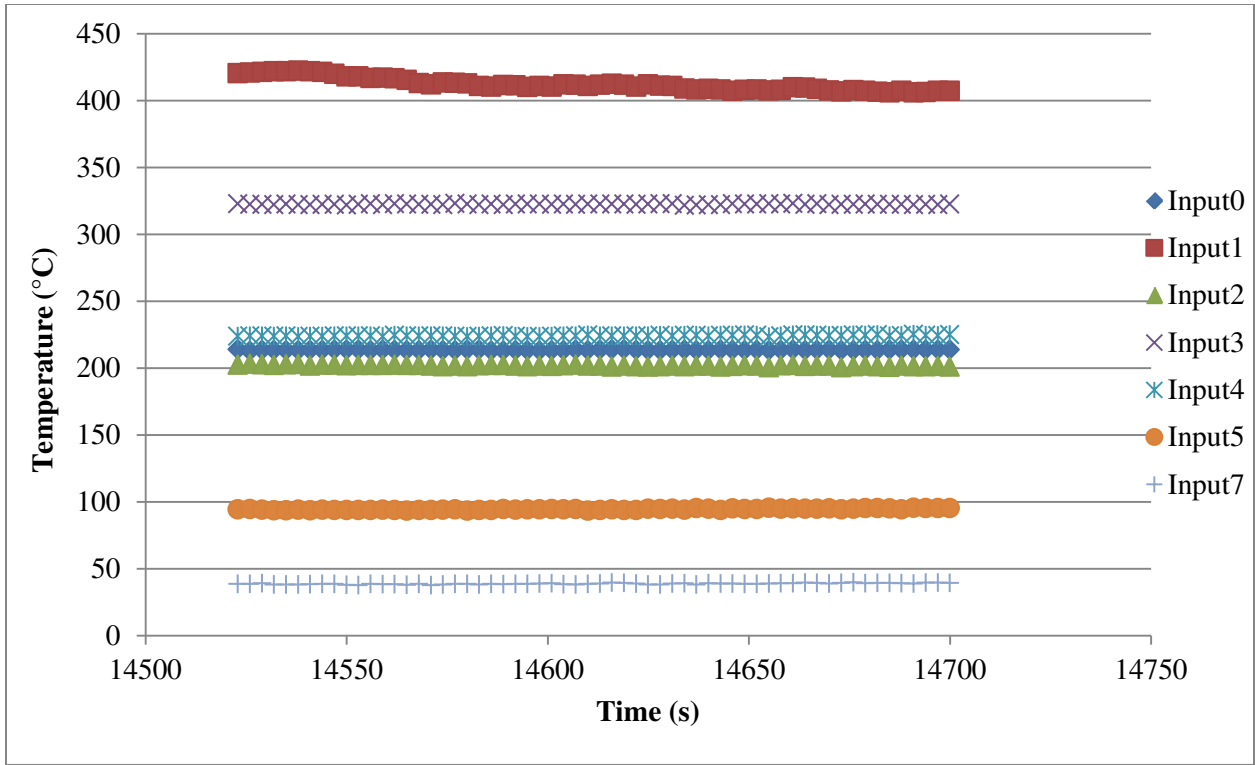
98

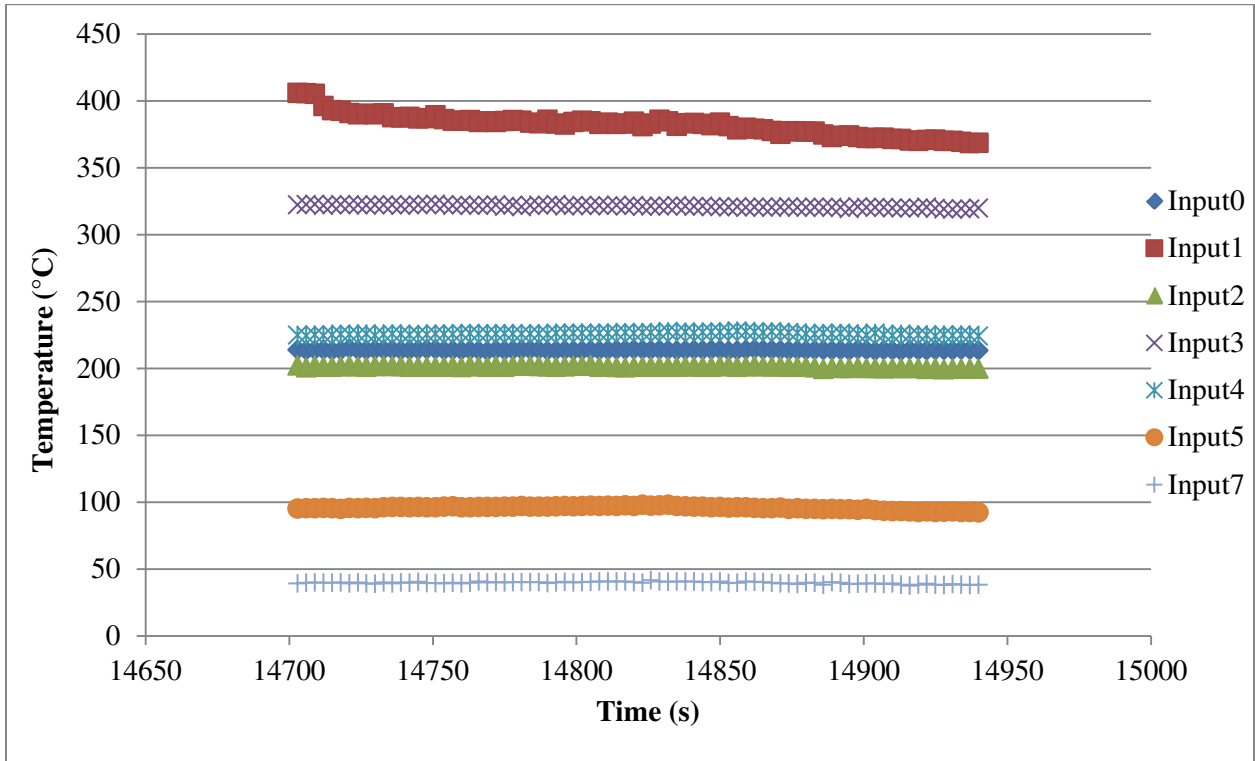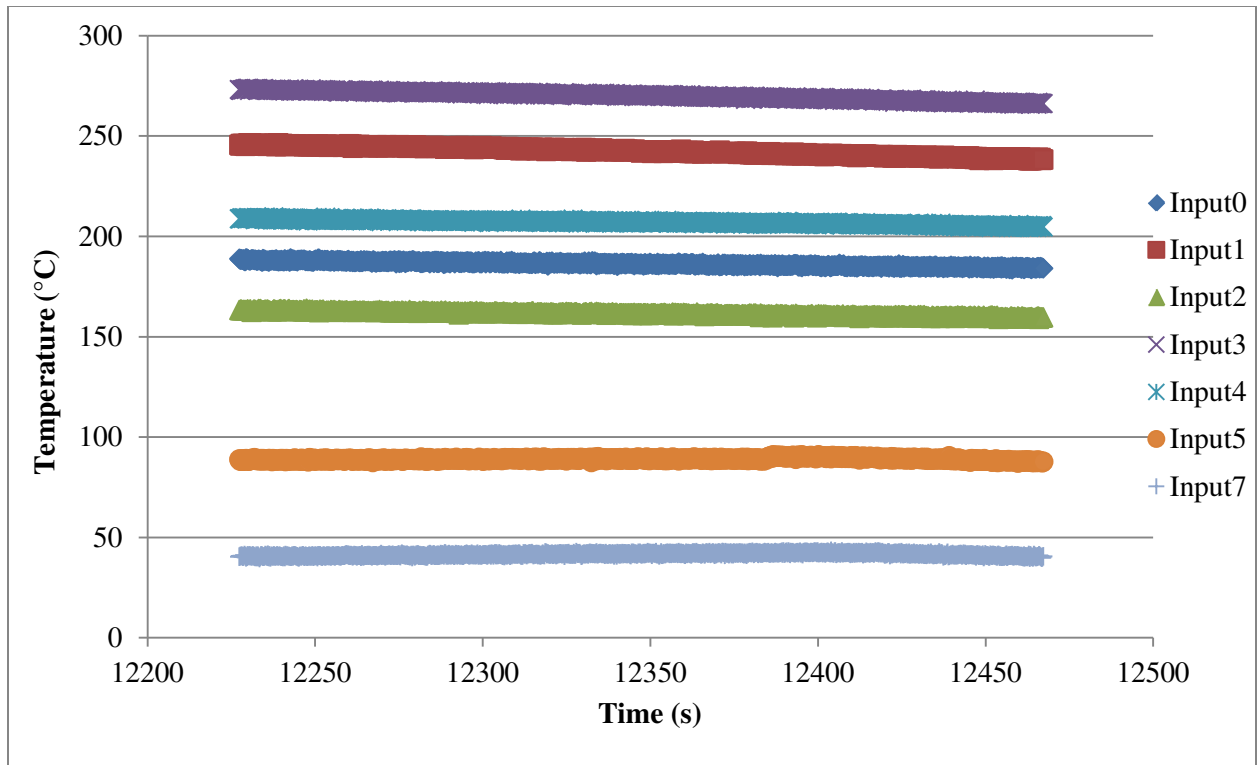Figure 63. Temperature plot for 2nd run of coated section, $\phi = 0.634$, red highlight
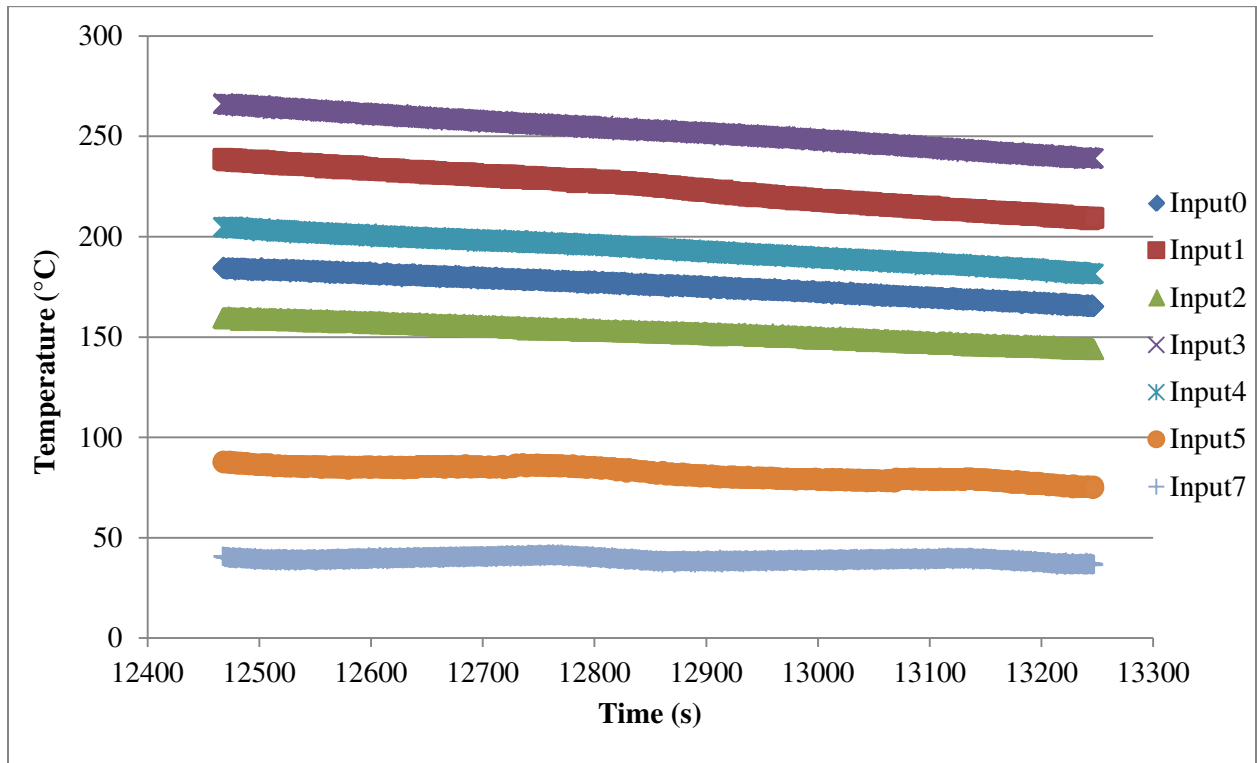
Figure 64. Temperature plot for 2nd run of coated section, $\phi = 0.631$, purple highlight

99

Table 7. Compilation of experimental results

Minimum steady equivalence ratio observed	Inert section stoichiometric mixture	1.000
	Inert section, lean mixture, run 1	0.589
	Inert section, lean mixture, run 2	0.589
	Catalytic section stoichiometric	1.000
	Catalytic section, lean mixture, run 1	0.688
	Catalytic section, lean mixture, run 2	0.634
Peak steady state temperature at lean limit	Inert section stoichiometric mixture	480 ˚C
	Inert section, lean mixture, run 1	365 ˚C
	Inert section, lean mixture, run 2	306 ˚C
	Catalytic section stoichiometric	544 ˚C
	Catalytic section, lean mixture, run 1	407 ˚C
	Catalytic section, lean mixture, run 2	266 ˚C
TEM hot-side temperature at lean limit	Inert section stoichiometric mixture	223 ˚C
	Inert section, lean mixture, run 1	94 ˚C
	Inert section, lean mixture, run 2	141 ˚C
	Catalytic section stoichiometric	181 ˚C
	Catalytic section, lean mixture, run 1	95 ˚C
	Catalytic section, lean mixture, run 2	87 ˚C
TEM cold-side temperature at lean limit	Inert section stoichiometric mixture	60 ˚C
	Inert section, lean mixture, run 1	39 ˚C
	Inert section, lean mixture, run 2	45 ˚C
	Catalytic section stoichiometric	53 ˚C
	Catalytic section, lean mixture, run 1	39 ˚C
	Catalytic section, lean mixture, run 2	40 ˚C
Load current at lean limit	Inert section stoichiometric mixture	374 mA
	Inert section, lean mixture, run 1	171 mA
	Inert section, lean mixture, run 2	125 mA
	Catalytic section stoichiometric	249 mA
	Catalytic section, lean mixture, run 1	116 mA
	Catalytic section, lean mixture, run 2	95 mA
Load voltage at lean limit	Inert section stoichiometric mixture	0.486 V
	Inert section, lean mixture, run 1	0.853 V
	Inert section, lean mixture, run 2	0.625 V
	Catalytic section stoichiometric	1.246 V
	Catalytic section, lean mixture, run 1	0.578 V
	Catalytic section, lean mixture, run 2	0.477 V
Load power at lean limit	Inert section stoichiometric mixture	181 mW
	Inert section, lean mixture, run 1	145 mW
	Inert section, lean mixture, run 2	78 mW
	Catalytic section stoichiometric	311 mW
	Catalytic section, lean mixture, run 1	67 mW
	Catalytic section, lean mixture, run 2	46 mW

A compilation of all the results obtained from testing is listed in Table 7. It includes the minimum achieved lean limit, the peak steady state temperature, the TEM hot- and cold-side temperatures at steady state and the measured load current, voltage and power at the steady state lean limit. The minimum achieved lean limit for the inert porous section was at an equivalence ratio of 0.589. The achieved lean limit for the catalytically coated porous section was 0.634.

The overall conversion efficiency of the burner system is calculated and presented in Table 8 for operation with inert and catalytic central sections at both stoichiometric mixture and the achieved lean limit. The input chemical energy is calculated considering a heat of combustion of methane of 55.6 MJ/kg [89], density of 0.668 kg/m^3 at NTP (20 °C, 1 atm) conditions [89], with an inlet total flow rate of 11.5 L/min, assuming complete combustion and the listed stoichiometric mixture or lean equivalence ratio. The inert porous section at a stoichiometric inlet mixture had the largest hot-side temperature and temperature gradient across the thermoelectric and was closest to the manufacture's specifications but it did not produce the most power. This is likely due to the load resistance not being matched to the internal resistance of the thermoelectric (~5.95 Ohm internal vs. 1.3 Ohm load) which was the case the later runs. The catalytically coated section at stoichiometric had the greatest overall efficiency even though it only had a $\Delta T = 128\,°C$ across the thermoelectric module. Both inert and coated sections, during their lean limit tests, had low peak temperatures and therefore low temperature gradients over the thermoelectric and generated the least amount of power.

Table 8. Overall conversion efficiency

Test conditions	Lean limit	Input chemical energy	Output electrical energy	Conversion Efficiency
Inert, stoichiometric mixture	1.000	676.88 W	181 mW	0.027 %
Inert, lean mixture	0.589	414.86 W	145 mW	0.035 %
Catalytic, stoichiometric	1.000	676.88 W	311 mW	0.046 %
Catalytic, lean mixture	0.634	444.35 W	46 mW	0.010 %

CHAPTER FIVE: CONCLUSION

The porous burner was successful in meeting most of the design guidelines and goals. The notable shortfalls are the low overall conversion efficiency, low power generation and the decreased lean performance with the catalytically coated central sections. The SEM characterization showed notable changes in the microstructure of the catalyst coating, indicating that it was likely active durin combustion. One possible explanation for the poor performance of the catalyst was that the dip coating procedure significantly changed the physical structure of the porous sections as shown in Figure 65. The coating is visibly quite thick, reducing the pore size of the medium which possibly had a significant impact on the medium's heat transfer properties.
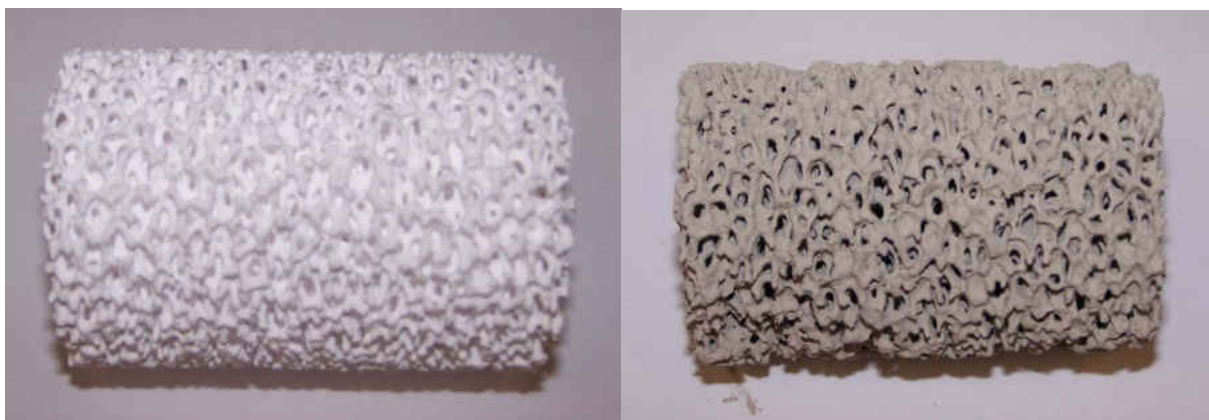
Figure 65. Uncoated and coated alumina foam sections

The change of porosity of the section by the catalyst may have affected the combustion characteristics. During testing, the burner with the catalytically coated section was noticeably more difficult to ignite, requiring disassembly and small changes in the placement of the porous sections and igniter before ignition was achieved. The dip coating process also blocked some of the pores of the porous medium, affecting the gaseous flow. A less viscous solution, drying the sections length-wise to minimize clogged pores or considering other methods of coating the central section with catalytically active material may solve this problem.

The start-up time for each test run was quite long, between 1 and 3 hours in most cases. This is not practical for a portable power source to compete with current batteries. The long start-up time is likely due to the strong influence of thermal and boundary extinction on the combustion process when trying to ignite with a cold porous medium. A method of preheating the central section, which was considered in many of the reviewed experimental cases, would solve this problem. Another option is to use a different material for the central section with higher heat transfer properties. The end goal would be to allow the burner to produce useable power only minutes after ignition.

Power output will be greatly increased by simply attaching more thermoelectric devices although at the current output, 20 watts would take as many as 60 thermoelectric modules to obtain. The power output obtained from the thermoelectric modules was far less than the manufacturer's specifications. Only a small portion of the casing surface was covered with a thermoelectric, particularly for testing purposes, but to become a more efficient power source more thermoelectric devices can be added, utilizing more of the otherwise lost heat. Connecting the thermoelectric modules together and being able to vary their combined internal resistance to match the resistance of the device to be powered would increase power output and overall conversion efficiency.

Surface contact between the interior of the casing and the central porous medium may have been poor, reducing heat flow to the thermoelectric module. The manufacturing tolerances for the steel casing, central porous foam and outer honeycombs sections were all slightly off. The central section was slightly too large to fit inside the burner and had to be filed down prior to use. The honeycomb sections were slightly too small and a piece of gasket material was wrapped around them to ensure the flow would travel through the pores, not around. These imperfections

in manufacturing could have significantly affected the conduction heat transfer characteristics within the burner, effecting overall performance.

Future recommendations include varying the material selection for the central porous section, possibly to SiC or a metal with higher heat transport properties. Different pore sizes and porosities should be considered and their effect on overall performance measured. Numerous catalytic materials were considered in this research and future tests should compare and characterize the performance of these. Many of the experimental set-ups reviewed in literature only had a two-section burner consisting of a pre-heat and combustion section. The lean fuel and air mixtures would not be combustible outside the burner so, with optimization, there is no chance of the flame propagating outside the burner. A two section burner would reduce overall size and increase energy density. The heat losses from the system can be measured in future tests to calculate the overall Carnot cycle efficiency to compare with other power generation systems.

To become a portable and marketable power system the porous burner has to be simplified and self-contained. These experimental tests used two flow controllers, each with their own variable power sources and an electric igniter. This meant that the system took a significant amount of external power to operate; a simpler set-up should be considered. If the cooling assembly were significantly improved, the inlet air flow of ~10 L/min could be used as the impinging flow or to cool a heat-sink also preheating the flow and reducing heat losses. Thermoelectric conversion efficiency is naturally low; other methods of converting the energy released during combustion into useful power should be explored in future work. A porous medium burner will take a significant amount of optimization to be used as a power generation system but is a very promising technology.

LIST OF REFERENCES

1. Mujeebu, M. A., Abdullah, M. Z., Abu Bakar, M. Z., Mohamad, A. A., Muhad, R. M. N., and Abdullah M. K., Combustion in Porous Media and its Applications – A Comprehensive Survey, *Journal of Environmental Management* 2009; 90: pp. 2287-2312.

2. Christo, F., Dally, B.B., Labspeary, P.V., Afsharvahid, S., and Joseph, D., Development of Porous Burner Technology for Ultra-Lean Combustion Systems. Final Technical Report prepared for South Australian State Energy Research Advisory Committee. Galilee Consulting PTY Limited, Australia, 2002.

3. Delalic, N., Mulahasanovic, Dz., and Ganic, E.N., Porous media compact heat exchanger unit - experiment and analysis. Experimental Thermal and Fluid Science 28 (2–3), pp. 185–192, 2004.

4. Hanamura, K., Echigo, R., and Zhdanok, S. A., Superadiabatic combustion in porous medium, Int. *J. Heat Mass Transfer*, vol. 36, no. 13, pp. 3201-3209, 1993.

5. Kennedy, L. A., Fridman, A. A., and Saveliev, A. V., Superadiabatic Combustion in Porous Media: Wave Propagation, Instabilities, New Type of Chemical Reactor, *Fluid Mechanics Research* 1995; 22, No. 2.

6. Bouma, P. H. and De Goey, L. P. H., Premixed combustion on ceramic foam burners. Combustion and Flame 119, pp. 133–143, 1999.

7. Mohamad, A. A., Combustion in Porous Media: Fundamentals and Applications, *Transport Phenomena in Porous Media III* 2005; pp. 287-304.

8. Lloyd, S. A. and Weinberg, F. J., A burner for mixtures of very low heat content, *Nature*, vol. 251, pp. 47-49, 1974.

9. Weinberg, F. J., Combustion temperatures: the future?, *Nature*, vol. 233, pp. 239-241, 1971.

10. Pickenäcker, O., Pickenäcker, K., Wawrzinek, K., Trimis, D., Pritzkow, W. E. C., Müller C, Goedtke, P., Papenburg, U., Adler, J., Standke, G., Heymer, H., Tauscher, W., and Jansen, F., *Innovative Ceramic Materials for Porous-medium Burners,* International Ceramic Review 1999; 48: pp. 326-329 & 424-434.

11. Fend, T., Trimis, D., Pitz-Paal, R., Hoffschmidt, B., and Reutter, O., Thermal Properties, Cellular ceramics; structure, manufacturing, properties and applications, pp. 342-360, 2005.

12. Dobrego, K.V. and Zhdanok, S.A., Physics of Filtration Combustion of Gases. ITMO Publ, Minsk, p. 204 (in Russian), 2003.

13. Hanamura, K., Kumano, T., and Idia, Y., Electric Power Generation by Super-adiabatic Combustion in Thermoelectric Porous Element, *Energy* 2005; 5: pp. 347-357.

14. Katsuki, F., Tomida, T., Nakatani, H., Katoh, M., and Takata, A., Development of a thermoelectric power generation system using reciprocating flow combustion in a porous $FeSi_2$ element, Review of Scientific Instruments, vol. 72, no. 10, pp. 3996-3999, 2001.

15. Hanamura, K. and Echigo, R., Thermal structure of superadiabatic combustion in porous media, Proceedings of the 3rd KSME-JSME Thermal Engineering Conference, Oct. 20-23, Kyongju, Korea, pp. 339-342, 1996.

16. Avdic, F., Adzic, M., and Durst, F., Small Scale Porous Medium Combustion System for Heat Production in Households, *Applied Energy* 2010; 87: 2148-2155.

17. Babkin, V. S. and Laevskii, Y. M., Seepage Gas Combustion, *Combustion, Explosion and Shock Waves* 1987; 23: pp. 531-547.

18. Ellzey, J.L. and Goel, R., 1995. Emissions of CO and NO from a two stage porous media burner. Combustion Science and Technology 107, pp. 81–91.

19. Macek, J. and Polasek, M., 2002. Porous medium combustion in engines may contribute to lower NO_x emissions. In: FISITA 2002 World Automotive Congress, Helsinki. Pap. F02V147.

20. Rørtveit, G.J., Zepter, K., Skreiberg, Ø., Fossum, M., and Hustad, J.E., 2002. A comparison of low-NO_x burners for combustion of methane and hydrogen mixtures. Proceedings of Combustion Institute 29, pp. 1123–1129.

21. Ambrogio, M., Saracco, G., and Specchia, V., Combining Filtration and Catalytic Combustion in Particulate Traps for Diesel Exhaust Treatment, *Chemical Engineering Science* 2001; 56: pp. 1613-1621.

22. Vogt, U.F., Gyorfy, L., Herzog, A., Graule, T., and Plesch, G., 2007. Macroporous silicon carbide foams for porous burner applications and catalyst supports. Journal of Physics and Chemistry of Solids 68, pp. 1234–1238.

23. Tritt, T. M., Thermoelectric Materials: Principles, Structure, Properties and Applications, Encyclopedia of Materials: Science and Technology 2008; pp. 1-11.

24. Dunn-Rankin, D., Leal, E. M., and Walth, D. C., Personal Power Systems, *Progress in Energy and Combustion Science* 2005; 31: pp. 422-465.

25. Hardesty, D. R. and Weinberg, F. J., Burners Producing Large Excess Enthalpies, *Combustion Science and Technology* 1974; 8: pp. 201-214.

26. Wood S. and Harris, A. T., Porous Burners for Lean-burn Applications, *Progress in Energy and Combustion Science* 2008; 34: pp. 667-684.

107

27. Durst, F. and Weclas, M., A New Type of Internal Combustion Engine Based on the Porous-medium Combustion Technique, Proceedings Institution of Mechanical Engineers Part D: *Journal of Automobile Engineering* 2001, vol. 215, pp. 63-81.

28. Trimis, D., Porous Burners in, Cellular Ceramics: Structure, Manufacturing, Properties and Applications 2005, Wiley-VCH 2005, pp. 484-503.

29. Durst, F. and Trimis, D., Combustion by Free Flame Versus Combustion Reactors, *Clean Air* 2002, 3, pp. 1-20.

30. Pantangi, V. K. and Mishra, S. C., Combustion of Gaseous Hydrocarbon Fuels Within Porous Media, *Advances in Energy Research* 2006.

31. Mößbauer, S., Pickenäcker, O., Pickenäcker, K., and Trimis D., Application of the Porous Burner Technology in Energy- and Heat- engineering, *Clean Air* 2002, 3, pp. 185-198.

32. Kamal, M. M. and Mohamad, A. A., Combustion in Porous Media, *Journal of Power and Energy* 2006, 220, part A, pp. 487-508.

33. Viskanta, R., Combustion and Heat Transfer in Inert Porous Media, in. "Handbook of Porous Media", 2nd ed, Vafai, K., CRC Press, 2005, pp. 607-644.

34. Trimis D. and Durst, F., Combustion in a Porous Medium- Advances and Applications, *Combustion Science and Technology* 1996; 121, pp. 153-168.

35. Bowen H. K., Basic research needs on high temperature ceramics for energy applications. *Materials Science and Engineering* 1980, 44, pp. 1–56.

36. Afsharvahid S., Dally B. B., and Christo F.C., On the stabilisation of ultra-lean methane and propane flames in porous media. In: Proceedings of the fourth Asia-Pacific conference on combustion; 2003.

37. Howell, J. R., Hall, M. J., and Ellzey, J. L., Combustion of Hydrocarbon Fuels within Porous Inert Media, *Progress in Energy and Combustion Science* 1996; 22, pp. 121-145.

38. Hunan Taisun Ceramics Co., Ltd., 2007, from http://www.taisun.com.cn/

39. Shanghai Unite Technology co., ltd., 2011, from http://unite863.en.alibaba.com/

40. Wisconsin Stamping, 2008, "Welcome to Wisconsin Stamping & Manufacturing", from http://www.wisconsinstamping.com/

41. Wesclas, M., Potential of Porous Medium Combustion Technology as Applied to Internal Combustion Engines, in. special publication series of the Georg-Simon-Ohm University of Applied Sciences, Nürnberg, Nr. 32, 2005, ISSN 1616-0762.

42. Babkin, V. S., Bunev, V. A., and Korzhavin, A. A., in: Combustion of Gases and Natural Fuels [in Russian] 1980, OIKhF, Chernogolovka.

43. Babkin, V. S., Bunev, V. A., Korzhavin, A. A., Klimenko, A. S., Zubkov, V. I., and Grigor'ev, V. M., Gas Combustion in a Vessel with a Highly Porous Inert Medium, translated from Fizika Goreniya i Vzryva, vol. 21, no. 5, pp. 17-22, 1985, Plenum Publishing Corporation, 1986.

44. Fu, X., Viskanta, R., and Gore, J. P., Prediction of Effective Thermal Conductivity of Cellular Ceramics, International Communications in Heat and Mass Transfer, vol. 25, no. 2, pp. 151-160, 1998.

45. Barra, A. J., Diepvens, G., Ellzey, J. L., and Henneke, M. R., Numerical Study of the Effects of Material Properties on Flame Stabilization in a Porous Burner, *Combustion and Flame* 2003, 135, pp. 369-379.

46. Tierney, C. and Harris, A. T., Materials Design and Selection Issues in Ultra-Lean Porous Burners, *Journal of the Australian Ceramic Society* 2009, vol. 45[2], pp. 20-29.

47. Khatami F., S. R., Safavisohi, B., and Sharbati, E., Porosity and Permeability Effects on Centerline Temperature Distributions, Peak Flame Temperature, Flame Structure, and Preheating Mechanism of Combustion in Porous Media, Journal of Energy Resource Technology 2007, vol. 129, March, pp. 54-65.

48. Echigo, R., Kurusu, M., Ichimiya, K., and Yoshizama, Y., Combustion Augmentation of Extremely Low Calorific Gases (Application of the Effective Energy Conversion Method from Gas Enthalpy to Thermal Radiation), Proceedings of ASME/JSME Thermal Engineering Joint Conference 1983, vol. 4, pp. 99-104.

49. Min, D. K. and Shin, H. D., Laminar Premixed Flame Stabilized Inside a Honeycomb Ceramic, *International Journal of Heat and Mass Transfer* 1991, vol. 34, 2, pp. 341-356.

50. Babkin, V. S., Filtrational Combustion of Gases. Present State of Affairs and Prospects, *Pure and Applied Chemistry* 1993, vol. 65, no. 2, pp. 335-344.

51. Hsu, P.-F., Evans, W. D., and Howell, J. R., Experimental and Numerical Study of Premixed Combustion Within Nonhomogeneous Porous Ceramics, *Combustion Science and Technology* 1993, vol. 90, pp. 149-172.

52. Hanamura, K., Echigo, R., Thermal Structure of Superadiabatic Combustion in Porous Media, Proceedings of the Third KSME-JSME Thermal Engineering Conference; October 20-23, 1996, Kyongju, Korea, vol. 2, pp. 339-342.

53. Zhdanok, S., Kennedy, L. A., and Koester, G., Superadiabatic Combustion of Methane Air Mixtures under Filtration in a Packed Bed, *Combustion and Flame* 1995, 100, pp. 221-231.

54. Hoffmann, J. G., Echigo, R., Yoshida, H., and Tada, S., Experimental Study on Combustion in Porous Media with a Reciprocating Flow System, *Combustion and Flame* 1997, vol. 111, pp. 32-46.

55. Zhdanok, S. A., Dobrego, K. V., and Futko, S. I., Flame Localization Inside Axis-symmetric Cylindrical and Spherical Porous Media Burners, *International Journal of Heat and Mass Transfer* 1998, vol. 41, pp. 3647-3655.

56. Dillion, J., Combustion in Porous Media, Ae104c Final Report, California Institute of Technology, June 8, 1999.

57. Henneke, M. R. and Ellzey, J. L., Modeling of Filtration Combustion in a Packed Bed, *Combustion and Flame* 1999, vol. 117, pp. 832-840.

58. Mare, L. di, Mihalik, T. A., Continillo, G., and Lee, J. H. S., Experimental and Numerical Study of Flammability Limits of Gaseous Mixtures in Porous Media, *Experimental Thermal and Fluid Science* 2000, vol. 21, pp. 117-123.

59. Huang, Y., Chao, C. Y. H., and Cheng, P., Effects of Preheating and Operation Conditions on Combustion in a Porous Medium, *International Journal of Heat and Mass Transfer* 2002, vol. 45, pp. 4315-4324.

60. Mathis, W. M. Jr. and Ellzey, J. L., Flame Stabilization, Operating Range, and Emissions for a Methane/Air Porous Burner, *Combustion Science and Technology* 2003, vol. 175, pp. 825-839.

61. Smucker, M. T. and Ellzey, J. L., Computational and Experimental Study of a Two-section Porous Burner, *Combustion Science and Technology* 2004, vol. 176, pp. 1171-1189.

62. Vogel, B. J. and Ellzey, J. L., Subadiabatic and Superadiabatic Performance of a Two-section Porous Burner, Combustion Science and Technology 2005, vol. 177, pp. 1323-1338.

63. Al-Hamamre, Z., Diezinger, S., Talukdar, P., Issendorff, F. Von, and Trimis, D., Combustion of Low Calorific Gases from Landfills and Waste Pyrolysis Using Medium Burner Techology, Trans IChemE, *Process Safety and Environmental Protection* 2006, vol. 84(B4), pp. 297-308.

64. Kakutkina, N. A., Korzhavin, A. A., and Mbarawa, M., Filtration Combustion of Hydrogen-Air, Propane-Air, and Methane-Air Mixtures in Inert Porous Media, *Combustion, Explosion, and Shock Waves* 2006, vol. 42, no. 4, pp. 372-383.

65. Kamal, M. M. and Mohamad, A. A., Development of a Cylindrical Porous-Medium Burner, *Journal of Porous Media* 2006, vol. 9(5), pp. 469-481.

66. Marbach, T. L. and Agrawal, A. K., Heat-recirculating Combustor Using Porous Inert Media for Mesoscale Applications, *Journal of Propulsion and Power* 2006, vol. 22, no. 1, pp. 145-150.

67. Marbach, T. L., Sadasivuni, V., and Agrawal, A. K., Investigation of a Miniature Combustor Using Porous Media Surface Stabilized Flame, *Combustion Science and Technology* 2007, vol. 179, pp. 1901-1922.

68. Alavandi, S. K. and Agrawal, A. K., Experimental Study of Combustion of Hydrogen-syngas/Methane Fuel Mixtures in a Porous Burner, *International Journal of Hydrogen Energy* 2008, vol. 33, pp. 1407-1415.

69. Dobrego, K. V., Gnesdilvo, N. N., Lee, S. H., and Choi, H. K., Lean Combustibility Limit of Methane in Reciprocal Flow Filtration Combustion Reactor, *International Journal of Heat and Mass Transfer* 2008, vol. 51, pp. 2190-2198.

70. Shi, J.-R., Xie, M.-Z., Liu, H., Li, G., and Zhou, L., Numerical Simulation and Theoretical Analysis of Premixed Low-velocity Filtration Combustion, *International Journal of Heat and Mass Transfer* 2008, vol. 51, pp. 1818-1829.

71. Akbari, M. H., Riahi, P., and Roohi, R., Lean Flammability Limits for Stable Performance with a Porous Burner, *Applied Energy* 2009, vol. 86, pp. 2635-2643.

72. Brenner, G., Pickenäcker, K., Pickenäcker, O., Trimis, D., Wawrzinek, K., and Weber, T., Numerical and Experimental Investigation of Matrix-Stabilized Methane/Air Combustion in Porous Inert Media, *Combustion and Flame* 2000, vol. 123, pp. 201-213.

73. Marbach, T. L. and Agrawal, A. K., Experimental Study of Surface and Interior Combustion Using Composite Porous Inert Media, *Journal of Engineering for Gas Turbines and Power* 2005, vol. 127, pp. 307-313.

74. Mößbauer, S., Grüber, W., and Trimis, D., Exhaust Gas Recirculation in Porous Burners for Target Application Zero Emission Steam Engines, Sixth International Conference on Technologies and Combustion for a Clean Environment, 9-12 July 2001, pp. 709-716.

75. Pickenäcker, O. and Trimis, D., Experimental Study of a Staged Methane/Air Burner Based on Combustion in a Porous Inert Medium, *Journal of Porous Media* 2001, vol. 4(3), pp. 197-213.

76. Kennedy, L. A., Saveliev, A. V., Bingue, J. P., and Fridman, A. A., Filtration Combustion of a Methane Wave in Aie for Oxygen-Enriched and Oxygen-Depleted Envrionments, Proceedings of the Combustion Institute, vol. 29, 2002, pp. 835-841.

77. O'Hayre, R., Cha S.-K., Colella, W., and Prinz F. B., Fuel Cell Fundamentals, John Wiley & Sons, Inc, NY, 2006.

78. Karim, G. A. and Kibrya, M. G., Variations of the Lean Blowout Limits of a Homogeneous Methane-Air Stream in the Presence of a Metallic Wire Mesh, *Journal of Engineering for Gas Turbines and Power* 1986, vol. 108, iss. 3, pp. 446-449.

79. Dupont, V., Moallemi, F., Williams A., and Zhang, S.-H., Combustion of Methane in Catalytic Honeycomb Monolith Burners, *International Journal of Energy Research* 2000, vol. 24, pp. 1181-1201.

80. Dupont, V., Zhang, S.-H., Bentley, R., and Williams, A., Experimental and Modelling Studies of the Catalytic Combustion of Methane, *Fuel* 2002, vol. 81, pp. 799-810.

81. Anh, J., Eastwood, C., Sitzki, L., and Ronney, P. D., Gas-phase and Catalytic Combustion in Heat-recirculating Burners, Proceedings of the Combustion Institute 2004, vol. 30.

82. Cimino, S., Lisi, L., Pirone, R., and Russo, G., Dual-site Pd.Perovskite Monolithic Catalysts for Methane Catalytic Combustion, *Industrial and Engineering Chemistry Research* 2004, vol. 43, pp. 6670-6679.

83. Arendt, E., Maione, A., Klisinska, A., Sanz, O., Montes, M., Suarez, S., Blanco, J., and Ruiz, P., Structuration of $LaMnO_3$ Perovskite Catalysts on Ceramic and Metallic Monoliths: Physico-chemical Characterisation and Catalytic Activity in Methane Combustion, *Applied Catalysis A: General* 339, 2008, pp. 1-14.

84. Bijjula, K. and Vlachos, D. G., Catalytic Ignition and Autothermal Combustion of JP-8 and its surrogates over a Pt/γ-Al$_2$O$_3$ Catalyst, Proceedings of the Combustion Institute (2009), doi:10.1016/j.proci.2010.05.008.

85. Tacchino, S., Vella, L. D., and Specchia, S., Catalytic Combustion of CH$_4$ and H$_2$ into Micro-monoliths, *Catalysis Today* 2010, vol. 157, pp. 440-445.

86. Fernandez-Pello, A. C., Micropower Generation Using Combustion: Issues and Approaches, Proceedings of the Combustion Institute (2002), vol. 29, pp. 883-899.

87. Krumpelt, M., Krause, T. R., Carter, J. D., Kopasz, J. P., and Ahmed, S., Fuel Processing for Fuel Cells in Transportation and Portable Power Applications, *Catalysis Today* 2002, vol. 77, pp. 3-16.

88. Mulhern, J. III, Approximate Desktop, Notebook, & Netbook Power Usage, from http://www.upenn.edu/computing/provider/docs/hardware/powerusage.html, University of Pennsylvania, retrieved 10/21/2010.

89. Glassman, I. and Yetter, R. A., Combustion: Fourth Edition, Elsevier Inc. Burlington, MA, 2008.

90. Mitsos, A., Chachuat, B., and Barton, P. I., What is the Design Objective for Portable Power Generation: Efficiency or Energy Density?, *Journal of Power Sources* 2007, vol. 164, pp. 678-687.

91. Echigo, R., Hanamura, K., Yoshida, H., Koda, M., and Tawata, K., Sophisticated Thermoelectric Conversion Devices of Porous Materials by Super-Adiabatic Combustion of Reciprocating Flow and Advanced Power Generation System, XI International Conference on Thermoelectrics, October 7-9, 1992, Arlington, USA.

92. Echigo, R., Yoshida, H., Tawata, K., Koda, M., and Hanamura, K., An Advanced Thermoelectric Generation Concept Based on Steep Temperature Gradient Yielded by Combustion in Porous Thermoelectric Elements, Proceedings of the Tenth Inernational Heat Transfer Conference, vol. 3, 1994, pp. 173-178, Brighton, UK.

93. Echigo, R., Tawata, K., Yoshida, H., and Tada, S., Effective Heating/Cooling Method for Porous Thermoelectric Device in Reciprocating Flow Combustion System, Proceedings of the ASME-JSME Thermal Engineering Joint Conference 1995: Lahaina, Maui, Hawaii, March 19-24, vol. 4, iss. 4., pp. 389-396.

94. Hanamura, K. and Kumano, T., Electric Power Generation by Super-adiabatic Combustion in Thermoelectric Porous Element, 1st International Energy Conversion Engineering Conference; Portsmouth, Virginia, 17-21 August 2003, pp. 1182-1185.

95. Hanamura, K. and Kumano, T., Thermophotovoltaic Power Generation by Super-Adiabatic Combustion in Porous Quartz Glass, Thermophotovoltaic Generation of Electricity: 5th Conference, 2003, pp. 111-120.

96. Hunt, T. K., Ivanenok J. F. III, and Sievers, R. K., AMTEC Auxiliary Power Unit for Hybrid Electric Vehicles, 29th Intersociety Energy Conversion Engineering Conference 1994, Monterey, CA; pp. 1419-1424.

97. Hunt, T. K., Low Emission AMTEC Automotive Power System, Final report for Department of Energy Contract, 2001.

98. Suzuki, Y., Horii, Y., Kasagi, N., and Matsuda, S., Micro Catalytic Combustor with Tailored Porous Alumina, Micro Electro Mechanical Systems, 2004, 17th IEEE International Conference on. (MEMS), pp. 312-315

99. Kamijo, T., Suzuki, Y., Kasagi, N., and Okamasa, T., High-temperature Micro Catalytic Combustor with Pd/nano-porous Alumina, Proceedings of the Combustion Institute 2009, vol. 32, pp. 3019-3026.

100. Okamasa, T., Lee, G.-G., Suzuki, Y., Kasagi, N., and Matsuda, S., Development of a Micro Catalytic Combustor using High-precision ceramic Tape Casting, *Journal of Micromechanics and Microengineering* 2006, vol. 16, pp. S198-S205.

101. Itaya, Y., Suzuki, T., and Hasatani, M., Combustion Characteristics of a Liquid Fuel in a Porous Burner, Proceedings of the ASME-JSME Thermal Engineering Joint Coneference 1995; Lahaina, Maui, Hawaii, March 19-24, vol. 3, pp. 99-104.

102. Kaplan, M. and Hall, M. J., The Combustion of Liquid Fuels within a Porous Media Radiant Burner, *Experimental Thermal and Fluid Science* 1995, vol. 11, pp. 13-20.

103. Liu, J. F. and Hsieh, W. H., Experimental Investigation of Combustion in Porous Heating Burners, *Combustion and Flame* 2004, vol. 138, pp. 295-303.

104. Jugjai, S. and Rungsimuntuchart, N., High Effciency Heat-recirculating Domestic Gas Burners, *Experimental Thermal and Fluid Science* 2002, vol. 26, pp. 581-592.

105. Agrawal, A. K. and Gollahalli, S. R., Liquid Fuel Combustion using Porous Inert Media, Army Research Office and Air Force Office of Scientific Research Contractors' Meeting in Chemical Propulsion, Arlington, Virginia, June 12-14, 2006, pp. 125-128.

106. Vijaykant, S. and Agrawal, A. K., Liquid Fuel Combustion within Silicon-carbide Coated Carbon Foam, *Experimental Thermal and Fluid Science* 2007, vol. 32, pp. 117-125.

107. Weclas, M., Porous Media in Internal Combustion Engines, "Cellular ceramics; structure, manufacturing, properties and applications", 2005,WILEY-VCH Verlag GmbH & Co., pp. 580-595.

108. Hanamura, K., Bohda, K., and Miyairi, Y., A Study of Super-Adiabatic Combustion Engine, *Energy Conversion and Management* 1997, vol. 38, no. 10-13, pp. 1259-1266.

109. Macek, J. and Polášek, M., Simulation of Porous Medium Combustion in Engines, Colloquium FLUID DYNAMICS 2000, IT AS CR, Prague, 2000, pp. 79-85.

110. Drayton, M. K., Saveliev, A. V., Kennedy, L. A., Fridman, A. A., and Li, Y.-E. (D.), Syngas Production using Superadiabatic Combustion of Ultra-rich Methane-air Mixtures, 27th International Symposium on Combustion, The Combustion Institute, 1998, pp. 1361-1367.

111. Bingue, J. P., Saveliev, A. V., and Kennedy, L. A., Optimization of Hydrogen Production by Filtration Combustion of Methane by Oxygen Enrichment and Depletion, *International Journal of Hydrogen Energy* 2004, vol. 29, pp. 1365-1370.

112. Dobrego, K. V., Shmelev, E. S., Koznacheev, I. A., and Suvorov, A. V., Water Purification of Organic Inclusions by the Method of Combustion within an Inert Porous Media, *International Journal of Heat and Mass Transfer* 2010, vol. 53, pp. 2484-2490.

113. Gintert, J. L., Ahmed, N., Santiago, R. M. de, and Shah, M., Senior Design Final Report: Porous Burner, Spring 2010-Fall 2010, University of Central Florida, College of Engineering and Computer Science.

114. Petrović, S., Rakić, V., Jovanović, D. M., Baričević, A. T., Oxidation of CO over Ru Containing Perovskie Type Oxides, *Applied Catalysis B: Environmental* 2006; 66: pp. 249-257.

115. Jennings, A. J., Shaw, C. K. M., Skinner, S. J., Electrical Conductivity of $La_xSr_{2-x}Fe_{1-y}Ru_yO_{4\pm\delta}$, *Materials Chemistry and Physics* 2005; 89: pp. 354-358.

116. Goldwasser, M. R., Rivas, M. E., Pietri, E., Pérez-Zurita, M. J., Cubeiro, M. L., Grivobal-Constant, A., and Leclercq, G., Perovskites as Catalysts Precursors: Synthesis and Characterization, *Journal of Molecular Catalysis A: Chemical* 2005; 228: pp. 325-331.

117. Zhao, S. and Gorte, R. J., The Effect of Oxide Dopants in Ceria on *n*-butane Oxidation, *Applied Catalysis A: General* 2003; 248: 9-18.

118. Marina, O. A. and Mogensen, M., High-temperature Conversion of Methane on a Composite Gadolina-doped Ceria-gold Electrode, *Applied Catalysis A: General* 1999; 189: pp. 117-126.

119. Tellurex, 2009-2011, "Frequently Asked Questions About Our Power Generation Technology", from http://www.tellurex.com/technology/seebeck-faq.php, retrieved 9/30/2011.